Estimation of Stochastic Degradation Models Using Uncertain Inspection Data

by

Lu Dongliang

A thesis
presented to the University of Waterloo
in fulfilment of the
thesis requirement for the degree of
Doctor of Philosophy
in
Civil Engineering

Waterloo, Ontario, Canada, 2012

Author's Declaration

I hereby declare that I am the sole author of this thesis. This is a true copy of the thesis, including any required final revisions, as accepted by my examiners.

I understand that my thesis may be made electronically available to the public.

Abstract

Modelling and forecasting the progress of corrosion and other degradation phenomena in engineering systems is an important element of reliability management programs. Because of the random nature of the degradation process, probabilistic models are mostly employed. Parameters of the probabilistic models are estimated using degradation data from in-service inspections. The estimated model parameters are then used for predicting future degradation growth or failure time of the components.

In the nuclear power plants, usually small samples of degradation data are collected using non-destructive examination (NDE) tools, which are not perfect in detecting degradation flaws and they also add random noise when measuring the size of the detected flaws. Ignoring these inspection uncertainties in the estimation of the degradation model would result in biased estimates and subsequently erroneous predictions of future degradation.

The main objective of the thesis is to develop methods for the accurate estimation of stochastic degradation models using uncertain inspection data. Three typical stochastic models are considered, namely, the random degradation rate model, the gamma process model and the Poisson process model. The random rate model and the gamma process model are used to model the flaw growth, and the Poisson process model is used to model the flaw generation. Likelihood functions of the three stochastic models from noisy and incomplete inspection data are derived.

The thesis also investigates Bayesian inference of the stochastic degradation models. The most notable advantage of Bayesian inference over classical point estimates is its ability to incorporate background information in the estimation process, which is especially useful when inspection data are scarce.

It is shown in the thesis that likelihood evaluation of the stochastic models using uncertain inspection data is a computationally challenging task as it often involves calculation of high dimensional integrals or large number of convolutions. The thesis develops efficient numerical methods to overcome this difficulty. For example, for the maximum likelihood estimation of the gamma process model, the Genz's transform and quasi-Monte Carlo simulation are adopted. The Markov Chain Monte Carlo simulation with sizing errors

as auxiliary variables is utilized in the Poisson flaw generation model. The approximate Bayesian computation (ABC) is explored for the Bayesian inference of the gamma process model subject to sizing error.

The practical applications of the proposed models are illustrated through the analysis of degradation data collected from nuclear power plant systems. These examples confirm the importance of consideration of inspection uncertainties in probabilistic analysis of degradation data.

Acknowledgments

I would like to express my great gratitude to my supervisor, Professor Mahesh D. Pandey, for his inspirational guidance and financial support throughout the doctorate program. Professor Mahesh D. Pandey has been a wonderful mentor. Without his helps, this work could have not been completed.

I would like to thank sincerely to my co-supervisor, Professor Wei-Chau Xie, for enlightening discussions and refreshing encouragement. At every stage of this research, Professor Wei-Chau Xie offered many valuable suggestions and insightful comments.

Many of the raw corrosion data were processed by Dr. Mikko Jyrkama, to whom I am very grateful. Without his excellent work, the data would have never been in useful form.

I would also like to thank Dr. Xianxun Yuan from Ryerson University, Toronto, with whom I had many informative discussions during the PhD program.

My special thanks are given to my wife and my parents for their great love, understanding, support and sacrifice.

Finally, I would like to thank my colleagues and friends: Tianjin Cheng, Shunhao Ni, Xunfang Zhang, Deyi Zhang, Bo Li, Zhaoliang Wang, Min Wang, Xianxun Yuan, Arun Veeramany, Anup Sahoo, Yusong Xue, and Xin Lu.

TO

My Family

Contents

List of Figures

List of Tables

Abbreviations and Notations

ABC	Approximate Bayesian computation
CANDU	CANada Deuterium Uranium reactor
CDF	Cumulative distribution function
CI	Confidence interval
COV	Coefficient of variation
EFPY	Effective full-power year
FAC	Flow-accelerated corrosion
GEV	Generalized extreme value (distributions)
GP	Gamma process
i.i.d.	Independent and identically distributed
ISI	In-service inspection
LDS	Low-discrepancy sequence
MCMC	Markov chain Monte Carlo
ML	Maximum likelihood
MoM	Method of moments
NDE	Non-destructive examination
NPP	Nuclear power plants
OLS	Ordinary least squares
PDF	Probability density function for continuous random variable
PMF	Probability mass function for discrete random variable
PoD	Probability of detection
QMC	Quasi-Monte Carlo
RMSE	Root mean squared error
RV	Random variable model
SD	Standard deviation of random variables

SG	Steam generator
$\mathsf{E}[X]$	Expectation of a random variable X
$\mathrm{COV}[X]$	Coefficient of variation of a random variable X
$\mathrm{Var}(X)$	Variance of a random variable X
$\mathrm{cov}(X, Y)$	Covariance of two random variables X and Y
$X \sim \mathsf{Ga}(a, b)$	X is gamma distributed with shape parameter a and scale parameter b
$X \sim \mathsf{Bino}(x; n, p)$	X is a binomial random variable generated by n trails with success probability p
$X \sim \mathsf{Pois}(\lambda)$	X is Poisson distributed with rate λ
$X \sim \mathsf{N}\left(\mu, \sigma^2\right)$	X is normally distributed with mean μ and variance σ^2
$X \sim \mathsf{U}(a, b)$	X is uniformly distributed between a and b
$f_X(x)$	PDF of a random variable X
$F_X(x)$	CDF of a random variable X
$f_{\mathrm{Ga}}(x; a, b)$	PDF of a gamma random variable with parameters a and b
$f_{\mathrm{Bino}}(x; n, p)$	PMF of a binomial random variable with parameter n and p
$F_{\mathrm{Ga}}(x; a, b)$	CDF of a gamma random variable parameters a and b
$f_{\mathrm{Pois}}(x; \lambda)$	PMF of a Poisson random variable with rate λ
$F_{\mathrm{Pois}}(x; \lambda)$	CMF of a Poisson random variable with rate λ
$\Phi(x)$	CDF of standard normal distribution (mean 0 and standard deviation of 1)
$\Gamma(z)$	Gamma function defined by $\Gamma(z) = \int_0^\infty u^{z-1} e^{-u} du$

CHAPTER 1

Introduction

1.1 Engineering background

Infrastructure and other large engineering systems, such as the road and highway networks, mass transport systems, power plants and electrical grids, are preconditions for a modern industrial society. Reliable and efficient operation of these systems is crucial to both daily lives of individuals and the prosperity and progress of the whole society. An important characteristic of these engineering systems is that they often consist of vast number of structures and components, which are likely to experience various degradation as service time increases.

Take the Canadian designed nuclear power plants (CANDU) as an example. As illustrated in Figure 1.1, a CANDU nuclear power plant consists of a number of subsystems, including the reactor core, the heat transport system (e.g. feeder pipes and steam generators), the electric generator turbine and other safety systems. The reactor core contains several hundreds pressure tubes, called fuel channels, where the nuclear fuel is stored and the fission reaction takes place. Heavy water coolant flows over the fuel channels and carries the heat produced by the fission reaction to the steam generators via feeder pipes. The steam generator consists of large number (3000-4000) of thin-wall tubes in which the heat in the hot coolant is transferred to the secondary side to produce pressurized steam. The steam then drives the turbine and produces electricity.

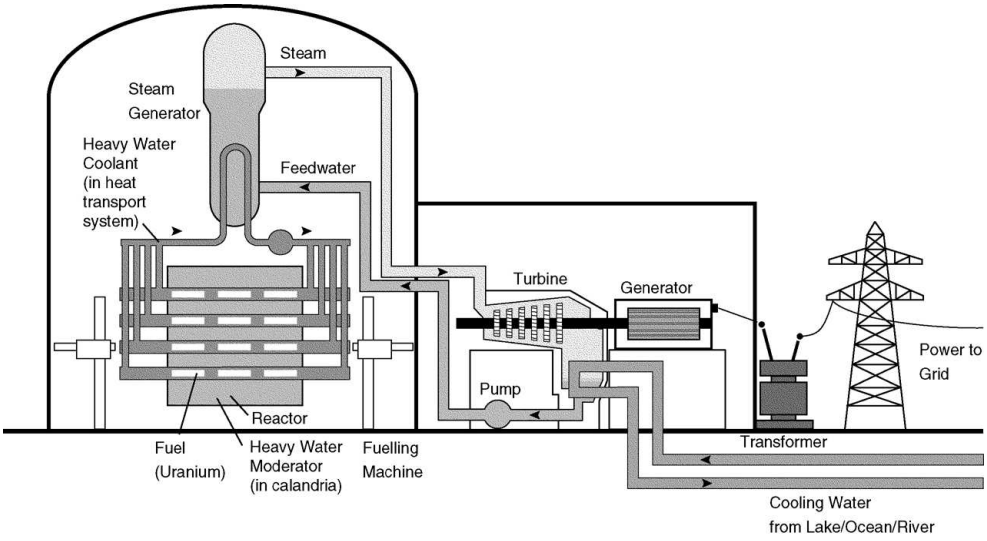

Figure 1.1 Layout of a CANDU nuclear power plant (from http://canteach.candu.org)

As can be seen, many of the nuclear power plant components work under extreme conditions of high temperature and high pressure, and therefore are likely to suffer from various types of degradation mechanisms. For instance, the fuel channels in CANDU reactors are known to be vulnerable to degradation mechanisms such as deformation and the delayed hydride cracking. The feeder pipes are found to experience flow-accelerated corrosion (FAC) and steam generator (SG) tubes are susceptible to corrosion and fretting wear. Degradation of the components in the nuclear power plant can deteriorate the efficiency of electricity generation, harm the structural integrity of the plant and may even cause severe failures including leakage of radioactive materials.

In general, degradation phenomena create localized changes in the geometry of the component, which are referred as flaws in this study. For example, common flaws that can be found in a nuclear power plant include pits caused by pitting corrosion, cracks caused by fatigue and localized wall thickness loss in feeder pipes by FAC. A component is said to reach its end of life and should not continue to service when the extent of the degradation, such as the number or the dimension of the flaws, is found to be beyond some given threshold (but not necessarily with a physical failure).

To ensure the reliability and performance, degradation of the structures and components needs to be properly managed. Heavily degraded components need to be correctly identified and replaced before reaching its end of life. In nuclear power industry, this is done through periodic in-service inspection (ISI) and maintenance activities. Every two or three years, inspections of the nuclear plant are carried out using non-destructive examination (NDE) probes. The extent of the degradation is then assessed using the inspection data and other relevant information, and heavily degraded components are repaired or removed from service. In order to lower the cost while keeping the required reliability level, many inspection and maintenance strategies are developed, in the aim of helping to determine the maximum acceptable degradation level, scope of the inspections, optimal inspection intervals, etc.

1.2 Maintenance decisions under uncertainties

1.2.1 Probabilistic approach

One of the main concerns in the inspection/maintenance optimization is that decisions must be made under various uncertainties. The uncertainties involved in a maintenance decision making process can be roughly categorized as the aleatory uncertainties and the epistemic uncertainties. The aleatory uncertainties mainly refer to the inherent randomness of the degradation phenomena. Due to the existence of aleatory uncertainties, future degradation or the failure time of a component cannot be predicted precisely. The epistemic uncertainties, on the other hand, are not inherent properties of the degradation but represent the state of lacking relevant information (Kiureghian and Ditlevsen, 2009). Two most important epistemic uncertainties in degradation assessment are the inspection uncertainties and the sampling uncertainties. The inspection uncertainties are the uncertainties introduced by imperfect inspection tools, such as the random noise added to the flaw size measurement or the inability in detecting small defects in the components. The sampling uncertainties are the uncertainties brought in by the incomplete inspection due to the limited inspection time or funds. Although the serviceability and failure time of a component depend only on the aleatory uncertainties of the degradation, they are masked by epistemic uncertainties.

Proper consideration of both the aleatory uncertainties and the epistemic uncertainties is necessary for optimal maintenance decisions.

Probabilistic models have long been regarded as effective tools to handle randomness and uncertainties. The most common probabilistic models used in practice are parametric models, which are probabilistic models with finite number of parameters. In the parametric modelling approach, aleatory uncertainties are represented by the probabilistic model itself with parameters inferred from inspection data and other relevant information; whereas epistemic uncertainties are summarized as the uncertainty associated with the estimates of the parameters (i.e., the parameter uncertainty). Since all models are only approximations of real world phenomena, the use of parametric models inevitably introduces an additional uncertainty, namely the model uncertainty, to the degradation assessment and prediction. Model selection and validation are also necessary, so that the selected models can be applied with confidence.

The basic procedures of typical degradation assessment and system maintenance activities using probabilistic modelling approach are illustrated in Figure 1.2. The first step is to select an appropriate probabilistic model for the degradation process based on inspection data, past experience or laboratory studies. Then, parameters of the selected model are estimated from inspection data and other relevant information. From the estimated parameters, predictions regarding the degradation of the components are obtained, based on which optimal maintenance decisions, such as when to perform the next inspection or whether a deteriorating component should be replaced, are made. The data collected from the scheduled maintenance activities are then used for further validation and calibration of the probabilistic model.

1.2.2 Stochastic models for degradation

The aleatory uncertainties of a degradation process can be characterized using various types of probabilistic models. Traditionally, the lifetime distribution model is used, in which the uncertainty of the degradation is described from the perspective of the uncertain failure time of the component. The lifetime distribution model is commonly applied in age-based maintenance strategies, where a component is replaced when its operation time reaches

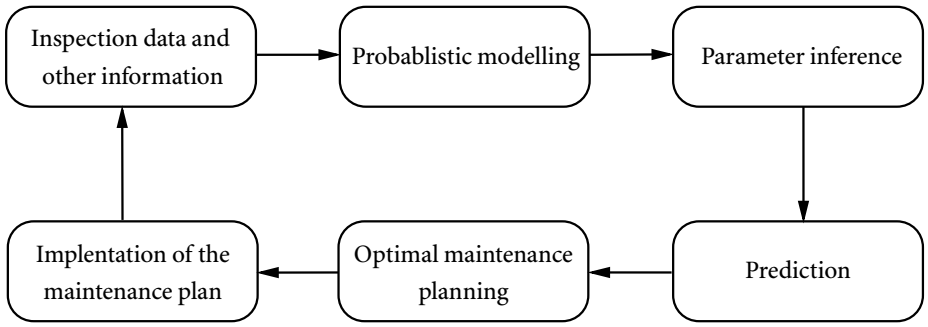

Figure 1.2 Procedures of a typical maintenance cycle using probabilistic modeling approach

certain threshold. When the inspection and replacement cost is prohibitively high, such as in the case of a nuclear power plant, age-based maintenance strategies are usually inefficient as inspection and replacement of a component are irrespective of its actual condition of degradation. In such cases, condition-based maintenance strategies are often employed, which require direct modelling of the degradation progress.

However, direct probabilistic modelling of the degradation process can be rather complicated. Generally speaking, the uncertainties in a degradation process can be classified into the unit-varying uncertainty and the time-varying uncertainty (Yuan, 2007). The unit-varying uncertainty, also called the sample uncertainty, characterizes the random effects of degradation across a group of components; whereas the time-varying uncertainty characterizes the temporal variation of the degradation process over time. Complex functional or probabilistic structures are often observed regarding both the unit-varying and time-varying uncertainties. Compared to some classical parametric models, such as the regression-based models, stochastic models are in general more flexible in modelling these complex structures of degradation process. For this reason, the use of stochastic models in degradation assessment and prediction has become increasingly popular in recent years.

1.2.3 Challenges imposed by inspection uncertainties

Due to the complexity of many stochastic models, accurate estimation of the model parameters is often not straightforward. Much effort has been spent in the past on developing formal estimation methods for various stochastic models from inspection data. However,

most of these methods use data collected in laboratory testings, in which the detection and measurement of the flaws are fairly accurate. Investigations on parameter estimation of stochastic models from uncertain field measurement are still very limited.

As mentioned earlier, inspection uncertainties are the uncertainties introduced by imperfect inspection tools, such as the random noise in flaw size measurement or inability in detecting small flaws in the components. There are two major challenges imposed by the inspection uncertainties on the parameter estimation of stochastic degradation models. Firstly, the inspection uncertainties may mask specific features of the true degradation process. For instance, due to the random sizing error, the measurement of a monotonically increasing degradation may show some extent of non-monotonicity, or the measured value of independent degradation growths may become correlated. Correct formulation of the stochastic models using the uncertain inspection data is not easy. Secondly, even if the stochastic models with inspection uncertainties are correctly formulated, they often turn out to be much more complicated than the original models. Specific numerical methods need to be developed for efficient parameter estimation of the stochastic models subject to inspection uncertainties.

1.3 Research Objectives

As illustrated in Figure 1.2, a complete optimal maintenance cycle has a number of aspects, including model selection and validation, parameter estimation, degradation prediction and optimal maintenance planning, etc. Each of these aspects contains a rich content for further discussions. In this thesis, we focus on the aspect of model formulation and parameter estimation. In particular, we will investigate problems arising from the likelihood deriviation and parameter estimation of stochastic models using uncertain field data. Most of the discussions in the thesis are presented with the in-service inspection of nuclear power plants as the engineering background. Some major problems addressed in the thesis are:

- What are the common inspection uncertainties in the field data and how can they be properly quantified?

- How should the likelihood functions of the stochastic degradation models be formulated using uncertain field data containing different types of inspection uncertainties? Three typical stochastic models, the random rate model, the gamma process model and the Poisson process model, are considered.

- How can one estimate the model parameters efficiently using uncertain inspection data? This includes both estimating the value of the parameters and quantifying the associated parameter uncertainty. In this thesis, maximum likelihood (ML) estimation and Bayesian inference are used. Advanced numerical methods are developed to overcome the computational difficulties in the estimation.

- Applications. Some practical examples from the in-service inspection of nuclear power plants are analyzed to demonstrate the use of the proposed methods.

To better focus on our main objective of likelihood formulation and parameter estimation, a simplified, data-driven modelling approach is adopted. Exploratory variables of the degradation, such as temperature or pressure of the working environment, are not included in the analysis. But the methods developed for the simplified models can be applied similarly to those more realistic stochastic models if necessary.

1.4 Organization

The thesis is organized as follows.

Chapter 2 presents a brief introduction of inspection uncertainties. Two different types of inspection uncertainties, probability of detection (PoD) and sizing error, are introduced. Probabilistic models for the two inspection uncertainties are introduced and their effects on degradation modelling are discussed.

Chapter 3 introduces three common stochastic degradation models, the random rate model, the gamma process model and the Poisson process model, among which the random rate model and the gamma process model are used to model the flaw growth, and the Poisson process model is used to model the flaw generation. Definitions, properties, and likelihood functions given accurate inspection data of the three models are discussed.

In Chapter 4, parameter estimation of the random rate model and the gamma process model using uncertain inspection data is discussed. The difference between the random rate model and the gamma process model is that the former one models the unit-varying uncertainty of flaw growth and the latter models the time-varying uncertainty. Likelihood functions given inspection data with sizing error are derived for both models. A numerical method using Genz's transform and quasi-Monte Carlo simulation is developed to overcome the computational difficulty in the ML estimation of the gamma process model.

Chapter 5 discusses the parameter estimation of the Poisson flaw generation model. In the chapter, first a simple flaw generation problem is investigated in which the size of the flaws are assumed to be irrelevant. The results are then generalized to a complete model considering both PoD and sizing error. It is found that the likelihood function of the complete model is numerically intractable for ML estimation using large data-sets. This computational difficulty is resolved later in Chapter 7 using a simulation-based Bayesian method.

Chapter 6 discusses the application of Bayesian inference in degradation modelling. Using the Bayesian method, information other than the inspection data can be included in the analysis. The use of Bayesian inference also provides a more natural way to present the parameter uncertainty associated with an estimate. The application of Bayesian inference in degradation assessment are then illustrated through two practical examples.

Chapter 7 investigates the computational aspect of Bayesian inference. Using some recently developed simulation techniques, Bayesian estimate of complicated stochastic models, such as the flaw generation model in Chapter 5, can be obtained. The application of these advanced Bayesian methods also provide an accurate quantification of the parameter uncertainty, which is not discussed in the ML analysis (Chapter 4 and 5) due to computational difficulties.

Finally, summary and recommendations for future research are given in Chapter 8.

CHAPTER 2

Inspection Uncertainties

2.1 Introduction

Periodic inspections of degradation are important to the reliability and efficiency of large engineering systems. For nuclear power plants, such inspections are usually conducted using non-destructive examination (NDE) probes, which are able to detect and measure the extent of degradation without affecting the future serviceability of the components. Common NDE probes used in the NPP in-service inspection include the eddy current bobbin probe (ET-probe), X-probe and ultrasonic probe (UT-probe). For example, the UT-probe measures the pipe wall thickness by sending pulses of ultrasonic energy into the component and then measuring the time delay of the returning echo pulse. The thickness of the pipe wall is then calculated by multiplying the measured time delay by the speed of sound in the steel and the structural integrity of the pipe wall is retained during the measurement (EPRI, 2009).

In addition to the ability of retaining the future serviceability of the components under inspection, NDE probes are also less expensive and usually take much less time to implement compared to other destructive examination methods, such as metallogiraphic examinations. However, along with the advantages, NDE inspections are usually not as accurate as the destructive examination methods. The inspection uncertainties of the NDE inspections have two aspects: (1) the ability of flaw detection, and (2) the accuracy of flaw sizing.

Because the inspection uncertainties are usually random in nature, they are specified using probabilistic models. The ability of flaw detection can be characterized in terms of probability of detection (PoD), which is defined as the probability that the inspection probe will detect a flaw of certain type and dimension. The accuracy of flaw sizing can be quantified using the true-versus-measured values of structural quantities of interest, such as the length and the depth of degradation (EPRI, 2006a).

Due to the existence of inspection uncertainties, the number of detected flaws and their measured size from an NDE inspection are different from the actual degradation. This uncertainty in inspection data can have adverse impacts on the quality of degradation assessment and also add extra difficulties to the degradation modelling and parameter estimation. In the remainder of this chapter, probabilistic models of PoD and sizing error are discussed. Performances of some typical NDE probes used in NPP in-service are presented. Following that, the effects of the NDE inspection uncertainties on the probabilistic modelling of degradation are discussed briefly through examples. Summary of the chapter is given in the end.

2.2 Inspection uncertainty models

2.2.1 Probability of detection (PoD)

The ability of flaw detection of an NDE probe can be affected by many factors, such as flaw type, flaw size, variability in material properties, environmental noise, personnel training, just to name a few. Repeated inspections of the same component therefore do not necessarily give consistent results in flaw detection, which is the major reason why the ability of flaw detection needs to be quantified statistically.

Among all the factors affecting the PoD performance of an NDE probe, the flaw type and flaw size are two most important ones, not only because they tend to have greater impact than other factors do, but also because they are directly related to the reliability of the component under inspection. For this reason, PoD of an NDE probe is usually described as a function of the flaw size for each specific type of flaws. As one might expect, flaws with larger sizes are easier to be detected. Typical PoD functions thus start from zero when the

flaw size is very small and becomes closer to 1 as the flaw size increases. A commonly used PoD function for many NDE probes is the log-logistic function which is defined as (EPRI, 2006a)

$$\text{PoD}(x) = \frac{1}{1 + e^{-(a+b\log x)}}, \tag{2.2.1}$$

where x is the flaw size, a and b are constants that need to be estimated from test data of the NDE probe. Cumulative density functions of normal or log-normal random variables are also used as PoD functions in some applications. Figure 2.1 illustrates the PoD performance of two different NDE probes used for steam generator tubing inspection in log-logistic functions. The flaw size in the PoD function is given as percentage of through wall thickness (% tw) of the tubes (EPRI, 2006b).

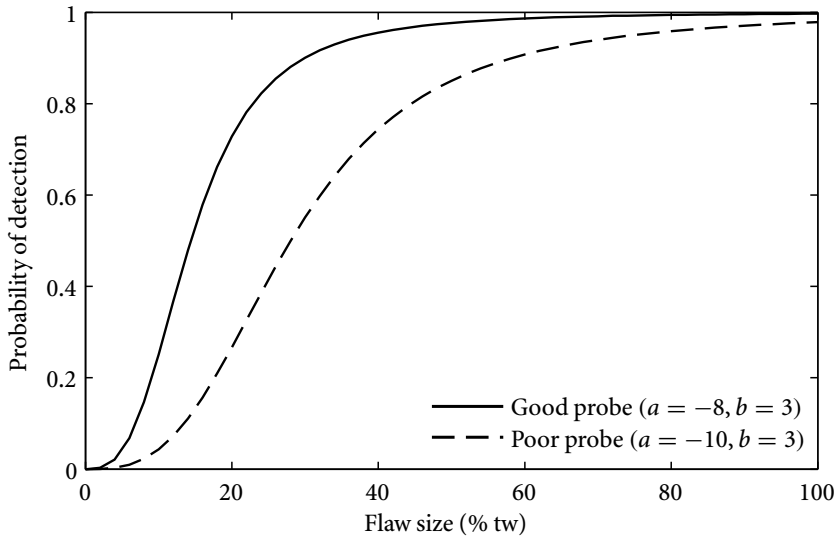

Figure 2.1 Log-logistic PoD of two NDE probes

In practice, the flaw detection data of NDE probes are recorded in one of the two following formats: the signal-response data and the hit-miss data. The signal-response data record the value of the actual readings from the inspection probe, such as the peak voltage of an ET-probe or the pulse delay time of an UT-probe. A detection threshold is then defined for the NDE readings by appropriately balancing the probability of detection and probability of false positive due to the background noise. Any reading greater than the threshold is considered as a indication of a flaw. PoD for flaws of certain size is then calculated as

the probability that the associated NDE readings of these flaws greater than the detection threshold, as illustrated in Figure 2.2. For detailed description of methodologies on developing PoD models based on signal response data, refer to HSE (2006) and Gandossi and Annis (2010).

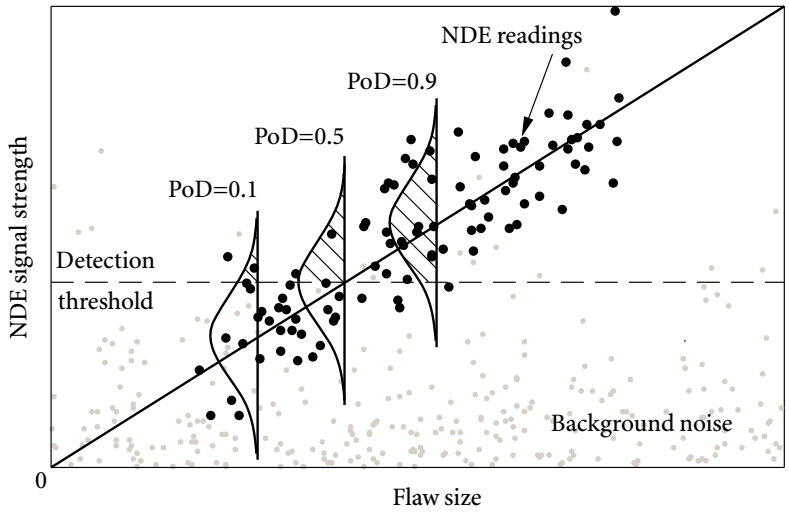

Figure 2.2 Illustration of the signal-response data from NDE inspection

In the hit-miss data, the result of an inspection is simply recorded as 0 or 1, indicating a detection or non-detection of a flaw. A simple method to estimate the PoD model parameters from the hit-miss data is the binomial modelling method (Gandossi and Annis, 2010). The main idea of the binomial modelling method is to group the flaws into intervals of flaw size (for example every 10% tw) and the PoD of each group is calculated as the ratio of detection within that group. Then, a curve fitting is conducted to produce the PoD function corresponding to the data (Figure 2.3).

The problem of the binomial modelling method is that: increasing the range of the size intervals to include a greater number of flaws will improve the accuracy in the detection ratio calculation, but this at the same time leads to fewer intervals and thus a poorer resolution in flaw size. Choosing a more narrow size range improves the size resolution, but at a cost of the accuracy in calculating the detection ratio (Gandossi and Annis, 2010). Statistical methods using maximum likelihood (ML) estimation or generalized linear regression are developed

for the calibration of the PoD model parameters. These methods are now recommended over the binomial modelling method because they are more accurate and are able to give the associated confidence intervals of the parameters. A good overview of these advanced methods is given by Gandossi and Annis (2010).

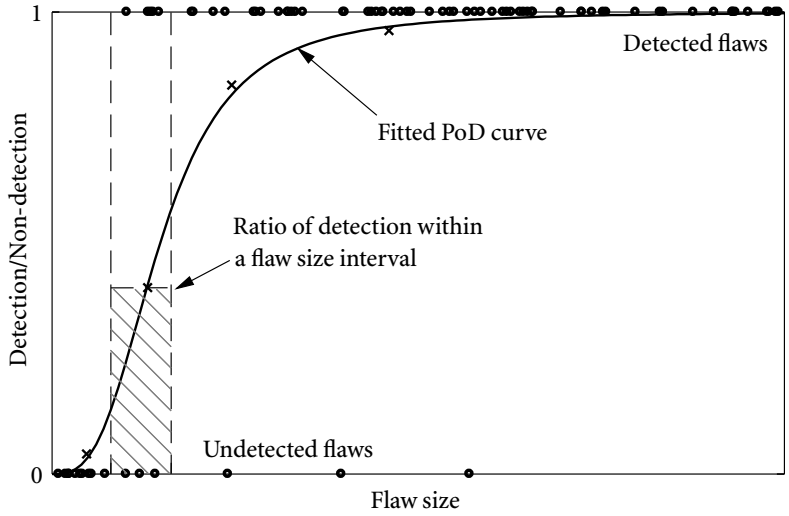

Figure 2.3 Illustrative plot of the hit-miss data and binomial method

For many degradation phenomena in nuclear power plants, a lowest acceptable PoD has been defined to ensure that the probability of missing large flaws is fairly small during any inspection. For example, for steam generator tube inspection, U.S. NRC (United States Nuclear Regulatory Commission) has defined the acceptable PoD performance as PoD $\geqslant$95% for flaws of size $\geqslant$75% tw and PoD $\geqslant$90% for flaws size $\geqslant$40% (as in shown Table 2.1). NDE probes that do not meet the requirement should not be used in the in-service inspection of nuclear power plants.

2.2.2 Sizing error

To characterize the sizing performance of an NDE probe, measured flaw sizes by the NDE probe are compared with the known sizes of the machined flaws in laboratory settings, or compared with the results from destructive metallographic examinations. A very effective way to present the measured-versus-true values from an NDE inspection is the scatter plot

Flaw depth (% tw)	Acceptable PoD
0	0.15
20	0.30
40	0.90
75	0.95
100	0.95

Table 2.1 Acceptable PoD performance for steam generator tubing inspection (Kurtz et al., 1996)

(dots in Figure 2.4). Usually, testing data in the scatter plot are analyzed statistically, mostly using the linear regression model, in which the sizing errors are regarded as normally distributed random variables.

Denote the actual size of a flaw as x. Due to the random sizing error, the measurement of the flaw is a random variable and is denoted as Y. Then the following linear regression model can be established as (Kurtz et al., 1996)

$$Y = c_1 + c_2 x + E, \tag{2.2.2}$$

where c_1 and c_2 are regression constants, and E is the normally distributed random error with mean 0 and standard deviation (SD) σ_E and is assumed to be independent from the true flaw size x. Using laboratory testing data, the regression equation (2.2.2) can be fitted using the standard least squares method, as illustrated by the solid line in Figure 2.4.

If the inspection is perfect, one has $c_1 = 0$, $c_2 = 1$ and $\sigma_E = 0$. A non-zero c_1 in equation (2.2.2) is called the offset error. The offset error will cause non-zero NDE readings when there is actually no flaw existence. The difference between c_2 and 1 is called the multiplier error, which means that the NDE reading changes either faster or slower than the actual flaw size does. The offset error and multiplier error are also called the systematic errors in general. The error due to E is called the random error and its magnitude is quantified by its standard deviation σ_E.

Unlike the random error, the systematic errors can be largely eliminated by calibration using test data of the NDE probe. After proper calibration, the only error left is the random error and the measurement of the NDE probe now can be characterized in the following

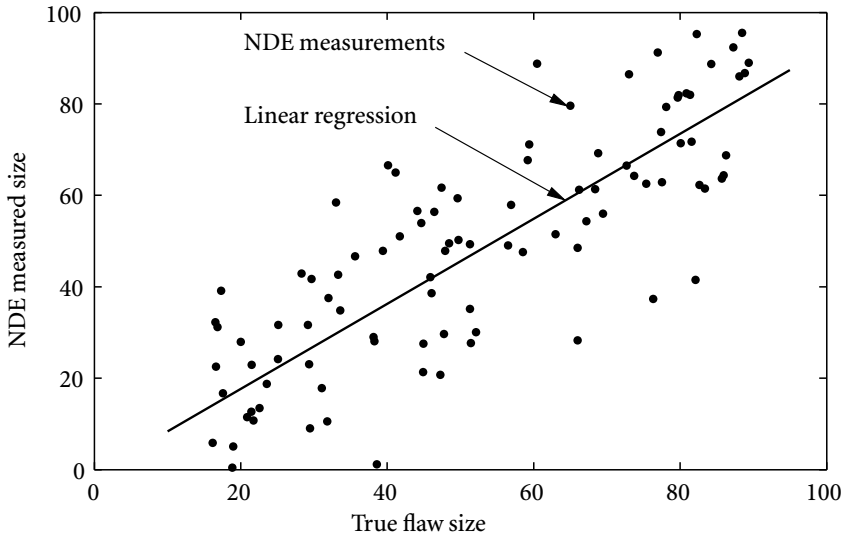

Figure 2.4 Regression method for determining the sizing performance of an NDE probe

simpler form as

$$Y = x + E. \tag{2.2.3}$$

Given equation (2.2.3), the measurement of a particular flaw by the NDE probe is normally distributed with mean as the actual flaw size and SD σ_E. Such calibration can simplify the degradation modelling when there is sizing error.

Sizing errors of typical NDE probes used in the in-service inspections of nuclear power plants are usually quite large due to the limits of the current techniques. For example, the standard deviation of the sizing error of the standard ET-probe in SG tubing inspection can be as large as 17% tw. The standard error of the more advanced X-probe is 6% tw, which is still pretty significant compared to the common repair limit of 40% tw in SG tube inspection.

2.3 Effects of uncertain inspection data

The NDE probes basically act like an uncertain filter when inspecting the flaws in the components. Because the PoD function of the probe is always less than 1, the probe can only detect part of the total flaws and the probability of missing smaller flaws is greater than

that of missing larger ones. On the other hand, due to the random sizing error, the reported flaw sizes by the inspection probes are also not accurate.

Consider the following example of the NDE inspection of flaws in SG tubes. The PoD of the inspection probe is assumed to be a log-logistic function with parameters $a = -8$ and $b = -3$ (i.e., the good probe in Figure 2.1). The sizing error of the probe is assumed to be normally distributed with mean zero and SD 6% tw. Figure 2.5 shows a simulated data-set using the above inspection uncertainty settings. The total number of the simulated flaws is 400 and the number of detected flaws is 301. As can be observed from Figure 2.5, the NDE inspection underestimates number of flaws especially smaller ones, and also adds additional dispersion to the flaw size distribution.

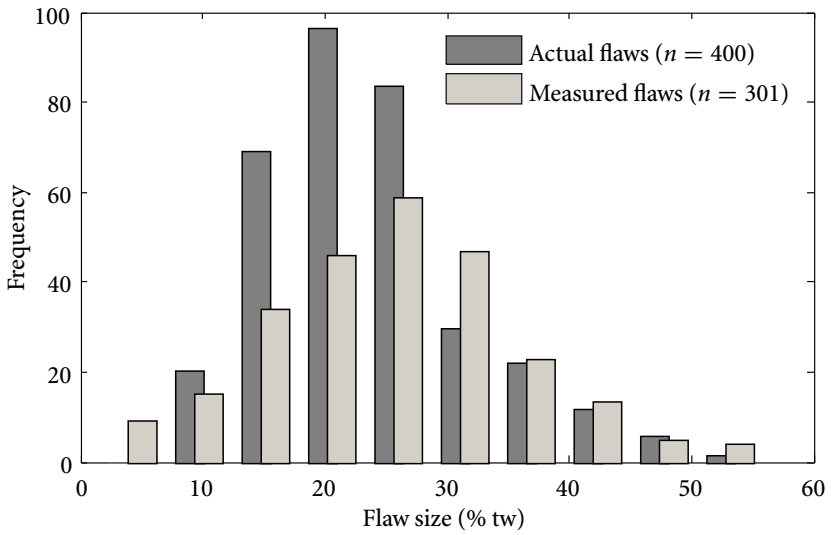

Figure 2.5 Illustration of uncertain inspection data from an NDE probe

The disparities between the measured degradation and the actual degradation as illustrated in Figure 2.5 can have profound implications on the probabilistic modelling of degradation. In the next, the effects of uncertain inspection data are discussed and the difficulties imposed by inspection uncertainties on degradation modelling are explained through two simple examples.

Example 1: effect of sizing error

First consider the following example. Suppose the size of the flaws in a structure is modelled as a random variable following some distribution with PDF $f_X(x;\theta)$, where θ is the parameter. To determine the value of parameter θ, inspections of the flaw sizes are conducted. If the inspection probes are perfect, i.e., with no sizing error or PoD, the value of the parameters can be obtained easily using standard statistical methods such as method of moments or ML method. For example, if it is found that there are n flaws in the structure and their flaw sizes are $x_1, x_2, \cdots, x_n$, the ML estimate of the model parameter θ can be calculated by maximizing the following model likelihood function

$$L(\theta \,|\, x_1, x_2, \cdots, x_n) = \prod_{i=1}^{n} f_X(x_i;\theta)$$

Now suppose the inspection probe has a normally distributed sizing error with mean zero and SD σ_E (assuming PoD is not an issue). The measured flaw size Y is then the sum of the true flaw size X and the random sizing error E, i.e., $Y = X + E$. If the sizing error is independent of the true flaw size, PDF of the measured flaw size can be obtained by calculating the following convolution

$$f_Y(y;\mu,\sigma) = \int_{-\infty}^{\infty} f_X(y-e;\mu,\sigma)\phi(e;0,\sigma_E)\mathrm{d}e, \tag{2.3.1}$$

where $\phi(e;0,\sigma_E)$ is the PDF of the normal sizing error. ML estimate of θ from n measured flaw size $y_1, y_2, \cdots, y_n$, can then be obtained by maximizing the following product

$$\begin{aligned} L(\theta \,|\, y_1, y_2, \cdots, y_n) &= \prod_{i=1}^{n} f_Y(y_i;\theta) \\ &= \prod_{i=1}^{n} \int_{-\infty}^{\infty} f_X(y_i-e;\theta)\phi(e;0,\sigma_E)\mathrm{d}e. \end{aligned} \tag{2.3.2}$$

Note that equation (2.3.2) does not have a closed form expression and has to be evaluated numerically. Compared to the likelihood without sizing error, it can be clearly seen that sizing error in the inspection data adds significant computational complexity to the probabilistic modelling of flaw size distribution.

Example 2: effect of sizing error and PoD

Let us now consider a slightly complicated case in which both sizing error and PoD are involved. The model is specified as follows:

- The number of flaws N in a component is assumed to follow some discrete distribution with PMF $f_N(n;\lambda)$, λ the parameter.
- The flaw size is a random variable with PDF $f_X(x;\theta)$, where θ is the parameter.
- The number of flaws and the flaw size are considered to be independent.
- The sizing error of the inspection probe is normally distributed with mean 0 and SD σ_E. To be simple, assume the PoD of the probe is a constant $p < 1$.

When there are no inspection uncertainties, the parameters can be estimated similarly using the maximum likelihood method as in the previous example. For instance, if there are n flaws with size $x_1, x_2, \cdots, x_n$, the model parameters can be estimated by maximizing the following product

$$L(\lambda, \theta \,|\, x_1, x_2, \cdots, x_n) = f_N(n;\lambda) \cdot \prod_{i=1}^{n} f_X(x_i;\theta).$$

However, when the inspection is conducted using an uncertain probe with both sizing error and PoD, probabilistic modelling of the inspection data becomes more complicated. As already shown in figure 2.5, both the number of detected flaws and their measured flaw size are inaccurate. Since the PoD is a constant p, given the total number of flaws $N = n$, the number of detected flaws, denoted in D, is a binomial distribution of n trials with success probability p. Using theorem of total probability, the unconditional PMF of the number of detected flaws is given as

$$f_D(d;\lambda) = \sum_{n=d}^{\infty} f_{\text{Bino}}(d;n,p) f_N(n;\lambda),$$

where $f_{\text{Bino}}(d;n,p)$ is the PMF of a binomial distribution with n trials and success probability p.

From the previous sizing error example, distribution of the measured size of the detected flaws is the convolution of the true flaw size distribution and the sizing error and is given

as equation (2.3.1). Since the flaw number and flaw size are independent, given d detected flaws with measured size $y_1, y_2, \cdots, y_d$, the model likelihood function is

$$\begin{aligned} L(\theta \,|\, y_1, y_2, \cdots, y_d) &= f_D(d;\lambda) \prod_{i=1}^{n} f_Y(y_i;\theta) \\ &= \sum_{n=d}^{\infty} f_{\text{Bino}}(d;n,p) f_N(n;\lambda) \prod_{i=1}^{d} \int_{-\infty}^{\infty} f_X(y_i - e;\theta)\phi(e;0,\sigma_E)\mathrm{d}e, \end{aligned}$$

which is much more complicated than the original likelihood function without inspection uncertainties.

Remarks

The above two examples are simple static models for degradation, in which the dynamics of flaw growth and flaw generation are not included. Yet, the additional modelling and estimation difficulties from inspection uncertainties are clearly exposed. For stochastic models considering the flaw growth and flaw generation, dealing with the inspection uncertainties can be more technically challenging, as will be shown in following chapters of the thesis.

2.4 Summary

In this chapter, two common inspection uncertainties, probability of detection (PoD) and sizing error, are introduced. Probabilistic models of the two inspection uncertainties and their calibration are discussed briefly.

A short discussion on the effects of the inspection uncertainties on degradation modelling is also presented in the chapter. Due to the existence of inspection uncertainties, the number of detected flaws and their measured sizes do not reflect the actual extent of the degradation accurately. The uncertain inspection data can have adverse impacts on the quality of degradation assessment and add extra difficulties to degradation modelling and parameter estimation.

CHAPTER 3

Stochastic Degradation Models

3.1 Introduction

3.1.1 Classical models and the stochastic models

Before discussing the stochastic models, we would like to first to examine some classical probabilistic degradation models.

Generally speaking, probabilistic degradation models can be divided into two broad categories: the flaw growth model and the flaw generation model. Traditionally, regression models are used the main probabilistic models for flaw growth. In regression models, the growth of a flaw is divided into two separate parts. First, a deterministic regression function is used to model the average growth path. Then, additional error terms, or more precisely speaking, the residual terms, are added to the regression function to account for the randomness in the flaw growth. The choice of the regression function is typically based on past experiences or expert judgment. In many cases, the regression function is simply chosen as a linear function of time. Parameter estimation of the regression models is usually performed using the least squares method or various maximum likelihood (ML) methods, depending on the assumed error structure of the model (Weisberg, 2005).

Although regression models are relatively easier to use for engineers, they do have important limitations. In addition to some common modelling difficulties such as the normality and the homoscedasticity requirement for the residual terms, the two most prominent short-

comings of the regression models are as follows. First, repeated measurements, although from the same flaw and therefore often dependent, are treated as independent observations in classical regression models (Yuan, 2007). Second, as reported by Pandey et al. (2006), regression methods cannot simulate the temporal uncertainties that are observed in many degradation phenomena. Although the first shortcoming regarding the repeated measurements can be partly fixed by applying the more advanced mixed-effects regression (Jiang, 2007), both the regression and the mixed-effects regression cannot handle temporal uncertainties in a proper manner. Therefore, regression models should not be applied when significant temporal variations in flaw growth are observed.

Compared to the flaw growth modelling, the full probabilistic modelling of flaw generation is usually more complicated, as it can involve both the number and the size of the flaws. A simplified strategy is to only model the maximum size of all the flaws in the component using extreme value analysis. For example, Gumbel distribution and other generalized extreme value (GEV) distributions have been widely used in predicting the maximum flaw size for pitting and other localized corrosion in various areas since 1950's (Gumbel and Lieblein, 1954; Aziz, 1956; Eldredge, 1957). Statistical analysis of the maximum flaw size based on extreme value theory are also reported in recent years using more advanced models. For example, Scarf et al. (1992) developed a method for estimating the extreme value distribution of the maximum pit depths using multiple deepest pit depth in one measurement area, rather than using only the maximum one. Martinsek (2003) developed an advanced statistical model which is able to include the correlation between neighboring flaws based on the extreme value theory and the beta auto-regression method. The extreme value method is also included in an ASTM (American Society for Testing and Materials) standard as a standard tool for the statistical analysis of various corrosion data (ASTM, 2010).

The extreme value analyses are effective in many cases. But they can only be used to predict the maximum flaw size. Detailed information on the total number of flaws and the associated flaw size distribution cannot be obtained. Furthermore, the static nature of the extreme value method limits its use in the analysis of the time-dependent probabilistic aspects of the degradation (Shibata, 1996).

To avoid some of the inherent limitations of these classical probabilistic models, stochastic based models are later introduced as alternative modelling tools for both flaw growth or flaw generation. Unlike the classical models, the stochastic models try to imitate the flaw growth path and flaw generation directly by using a collection of random variables indexed by time. Complex covariance structures of the flaw growth and flaw generation over time and across the population can thus be established using various stochastic models that are available in current statistical literature.

Early applications of the stochastic degradation models are mostly found in the fatigue of metal and other composite materials. For example, Birnbaum and Saunders (1958) investigated the fatigue damage of structures under dynamic loads using the renewal process model. Paris et al. (1961) utilized a non-linear general path model, known as the Paris-Erdogan law, to express the fatigue crack growth over time. Lately, applications of the stochastic models are extended to degradation phenomena from a much broader range of areas, such as bridge deck deterioration (Madanat et al., 1995; Madanat and Ibrahim, 1995), water pipe deterioration (Micevski et al., 2002), rock rubble displacement (Van Noortwijk et al., 1995), etc. Applications of the stochastic models in degradation related to nuclear power plants are also seen frequently. For example, the gamma process model is often used to model the flow accelerated corrosion (FAC) in feeder pipes in nuclear power plants (Yuan et al., 2008; Pandey et al., 2011; Cheng and Pandey, 2011). Camacho (2006) used a cumulative damage model with exponentially distributed annual increments to model the fretting wear of SG tubes in a nuclear power plant. Yuan et al. (2009) used a Poisson process model to predict the pitting flaws in SG tubes.

3.1.2 Organization

Due to the extremely rich content of the stochastic models, we are not going to cover all the related aspects in this chapter. Rather, we choose to introduce three typical stochastic models, namely, the random rate model, the gamma process model and the Poisson process model, among which the random rate model and the gamma process model are used to model the flaw growth, and the Poisson process model is for modelling the flaw generation. The remainder of this chapter is organized as follows. First, some basic concepts related

to the stochastic process are introduced. After that, definitions and properties of three stochastic models mentioned above are introduced. Parameter estimation of the model parameters given accurate measurements are derived. A summary of the chapter is given in the end.

3.2 Stochastic models in general

Unlike the classical probabilistic models, the stochastic models try to model the flaw growth and flaw generation directly using stochastic processes. A stochastic process, in short, is a family of random variables depending on an index set (Prabhu, 2007). We will use the notation $\{X(t) : t \in T\}$ to represent a stochastic process, where T is the index set, $X(t)$ is the actual distribution of the process at t. For the sake of conciseness, $X(t)$ is also used to indicate a stochastic process when it makes no confusion.

In degradation modelling, the index set T is normally taken as time. The set of the values taken by $X(t)$ is called the sample space of the process (Prabhu, 2007). Stochastic processes with two different types of sample spaces are mostly considered. To model the flaw size growth, such as crack length or volumetric wall thickness loss, $X(t)$ is usually taken as a positive real number. Examples of this types of stochastic models are the random rate model and the gamma process model. To model the number of new generated flaws in a component, such as number of pits in an SG tube, the sample space is taken as the natural number set $[0, 1, 2, \cdots]$. Examples of this types of stochastic processes are Poisson process and other general counting processes.

In practical applications, sometimes it is convenient to assume that the degradation starts from zero, i.e., $X(0)=0$. If a process $X(t)$ does not start from zero, a new process $Y(t)=X(t)-X(0)$ can always be defined, such that $Y(0)=0$. Therefore, there is no loss of generality by making such a simplification.

Suppose the degradation of a group of components follows a stochastic process $\{X(t) : t \in T\}$ with index set T the time. The degradation path of each individual component is then a deterministic function of time generated by the stochastic process. Let $X_k(t)$, $k=1, 2, \cdots, n$, be the degradation paths of n components from the group. $X_k(t)$ are called

realizations of the stochastic process $X(t)$. The random nature of the stochastic process is reflected in the fact that each realization of the process is generated separately and it is very unlikely to have two identical realizations from the same stochastic process. Following is a brief introduction of some basic concepts of the stochastic process based on Xie (2006).

Probability distribution functions

A stochastic process can be characterized using a series of probability distribution functions. For example, the first-order cumulative distribution function (CDF) of a stochastic process $\{X(t) : t \in T\}$ at time t is defined as

$$F_1(x,t) = \mathcal{P}\{X(t) \leqslant x\}.$$

Consider the example of the flaw growth of n components. Suppose at time t, the flaw size in k_1 out of n components is less than x. If n is sufficiently large, the first-order CDF of stochastic process $X(t)$ can be approximated by

$$F_1(x,t) \approx \frac{k_1}{n}.$$

The second-order CDF of the process of value x_1 and x_2 at time t_1 and t_2 is defined as the probability that $X(t_1) \leqslant x_1$ and $X(t_2) \leqslant x_2$ both hold, i.e.,

$$F_2(x_1,t_1;x_2,t_2) = \mathcal{P}\{X(t_1) \leqslant x_1, X(t_2) \leqslant x_2\}.$$

If the size of k_{12} out n flaws is smaller that x_1 at time t_1 *and* smaller than x_2 at time t_2, then

$$F_2(x_1,t_1;x_2,t_2) \approx \frac{k_{12}}{n}.$$

Similarly, the CDF of a stochastic process of order s, $s = 1, 2, \cdots$, is defined as

$$F_s(x_1,t_1;x_2,t_2;\cdots;x_s,t_s) = \mathcal{P}\{X(t_1) \leqslant x_1, X(t_2) \leqslant x_2, \cdots, X(t_s) \leqslant x_s\}.$$

The corresponding PDF of order s is then the derivation of the corresponding CDF functions (if they exist):

$$f_s(x_1, t_1; x_2, t_2; \cdots; x_s, t_s) = \frac{\partial^n F_n(x_1, t_1; x_2, t_2; \cdots; x_s, t_s)}{\partial x_1 \partial x_2 \cdots \partial x_s}.$$

A stochastic process is said to be completely described if its probability distribution functions of all orders are given. However, in practice it is often unnecessary to specify the probability distributions of all orders. Many common stochastic process models can be more clearly defined using their other specific properties, from which the probability distribution function of any order can be easily derived.

Mean and variance

In degradation assessment, it is important to know what is the average degradation in the component population as well as how far individual components are away from the average, i.e., the mean and variance of the degradation. Since at any time point, the value of a stochastic process is a random variable, the mean and variance of the process can be naturally defined as functions of time t, with their values at t being the mean and variance of random variable $X(t)$, respectively. Let the mean and variance of a stochastic process be $m(t)$ and $\sigma^2(t)$. One has

$$m(t) = \mathrm{E}[X(t)] = \int_{\Omega_X} x f_1(x, t) \mathrm{d}x,$$
$$\sigma^2(t) = \mathrm{Var}[X(t)] = \int_{\Omega_X} x^2 f_1(x, t) \mathrm{d}x - m^2(t),$$

where Ω_X is the sample space of the stochastic process and $f_1(x, t)$ is its 1st-order PDF. The square root of $\sigma^2(t)$, i.e., $\sigma(t)$, is called the standard deviation of the process and is also used for quantifying the dispersion of a stochastic process over time.

Stochastic Processes with stationary and independent increments

A special category of stochastic processes that are used extensively in degradation modelling is the process with stationary and independent increments. A stochastic process $X(t)$ is said to have stationary and independent increments if it has the following two properties (Prabhu, 2007):

- For any $0 \leqslant t_1 \leqslant \cdots \leqslant t_n$, random variables

$$X(t_1)-X(0),\ X(t_2)-X(t_1),\ \cdots,\ X(t_n)-X(t_{n-1}),$$

  are independent.

- For any $t \geqslant 0$ and $\tau > 0$, distribution of increment $X(t+\tau)-X(t)$ depends only on the time difference τ.

Suppose $X(t)$ is a stochastic process with stationary and independent increments and $X(0)=0$. One has

$$X(t+\tau) = X(t) + X^*(\tau), \tag{3.2.1}$$

where $X^*(\tau)$ has the same distribution as $X(\tau)$ and is independent of $X(t)$.

If the mean of the stochastic process $m(t)$ exists,

$$m(t+\tau) = m(t) + m(\tau). \tag{3.2.2}$$

The only bounded solution of equation (3.2.2) is known to be $m(t)=\mu t$, where μ is the expected degradation growth during unit time, i.e. $\mu = \mathrm{E}[X(1)]$ (Prabhu, 2007).

Similarly, calculating the variances of both sides in equation (3.2.1) gives

$$\sigma^2(t+\tau) = \sigma^2(t) + \sigma^2(\tau).$$

If the variance of the stochastic process exists and is finite, one has $\mathrm{Var}[X(t)]=\sigma^2 t$, where $\sigma^2 = \mathrm{Var}[X(1)]$. Thus, for stochastic processes with stationary and independent increments

$$\mathrm{E}[X(t)] = \mu t, \quad \mathrm{Var}[X(t)] = \sigma^2 t.$$

The coefficient of variation (COV) of the process, defined as $\mathrm{COV}[X(t)] = \sqrt{\mathrm{Var}[X(t)]}/\mathrm{E}[X(t)]$, is

$$\mathrm{COV}[X(t)] = \frac{\sigma}{\mu\sqrt{t}}. \tag{3.2.3}$$

Equation (3.2.3) implies that the sample paths of stochastic processes with stationary and independent increments will become relatively closer to the average as time increases, because its COV decreases over time.

Time transform of stochastic processes

Due to the mathematical tractability of stochastic processes with stationary and independent increments, they are widely used to model various types of degradation phenomena. Examples of stochastic processes with stationary and independent increments include the gamma process and Poisson process, both of which will be discussed in the next. However, an obvious limitation of these stochastic processes is that they can only model degradation phenomena that grow linearly over time. It is known that the propagation of some degradation phenomena, such as the fatigue crack growth, accelerates as the components ages (Bogdanoff and Kozin, 1985). In order to model the non-linear degradation, the following time transform of the stochastic processes can be applied.

Suppose $X(\tau)$ is a stochastic process with stationary and independent increments. The mean of $X(\tau)$ is $m_X(\tau)=\mu\tau$. Let $\tau=s(t)$, where $s(t)$ is a non-linear function of the real time t. Substituting $\tau=s(t)$ into the stochastic process $X(t)$ gives a new process $Y(t)$, $Y(t)=X(\tau)=X(s(t))$. The mean of $Y(t)$, denoted as $m_Y(t)$, is given as

$$m_Y(t) = m_X(s(t)) = \mu s(t).$$

$Y(t)$ is then a stochastic process with non-linear average $\mu s(t)$. In practice, the functional form of $s(t)$ can be determined either by laboratory research or by curve fitting using actual measured flaw growth. A popular choice of $s(t)$ is the exponential family where $s(t)=\alpha t^{\beta}$ with α and β to be some constants. Figure 3.1 shows an example of the time transform of a stochastic process using transform function $s(t)=2t^2$.

3.3 Random variable model

A random variable model (also referred as the general path model) is a stochastic process model that describes the flaw growth in a group of components using a deterministic function with random parameter and can be described using the following equation

$$X(t) = g(t;\Theta),$$

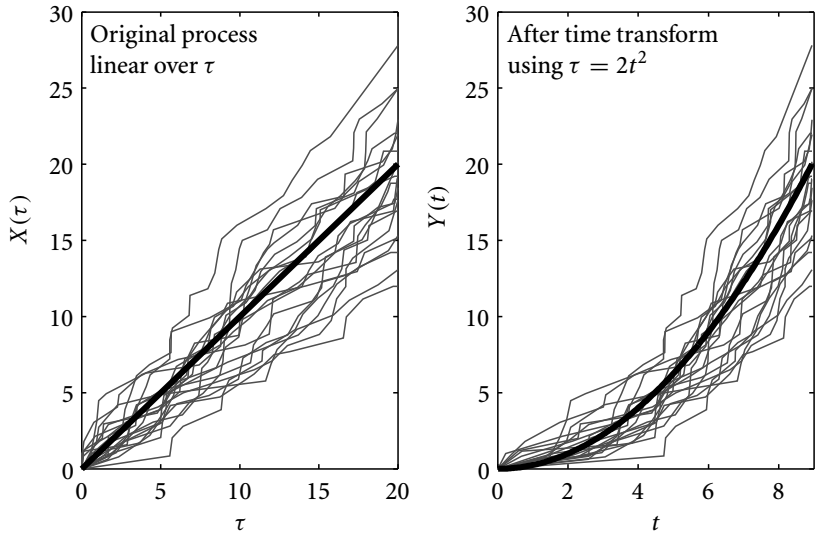

Figure 3.1 Time transform of a stochastic process

where g is a deterministic function of time t and random variable Θ is the parameter. The flaw growth of an individual component is then given by a *deterministic* function $g(t;\theta_k)$, with its parameter θ_k a sample drawn from random variable Θ. Once Θ is given, the distribution of the process at any time t, $X(t)$, can be calculated using transformation techniques for functions of random variables (Ang and Tang, 1975).

The random variable model is a very special case of the stochastic models and is widely applied to model various corrosion and wear phenomena (Fenyvesi et al., 2004; EPRI, 2006a; Huyse and van Roodselaar, 2010). In the random variable model, only sample uncertainty of the degradation is considered. Once the component is specified, its flaw growth is a deterministic function in which no temporal uncertainty is involved. The motivation of the random variable model comes from practice. For example, in the case of fretting wear degradation of SG tubes, as the working conditions, such as temperature and pressure, usually do not change, the flaw growth rate at a specific location is found to be quite stable. However, variations in the degradation rate can still be observed across the fleet of the SG tubes due to individual differences from imperfect manufacturing process or other sources (EPRI, 2009). This randomness in the individual differences across population is exactly what the random variable model tries to capture.

In this thesis, we mainly consider the following simple case of the random variable model called the random rate model, in which g is a linear function. Many other more complicated random variable models can be transformed into a linear random rate model using the time transform mentioned earlier. Without loss of generality, we assume the process starts from zero. One has

$$X(t) = Rt. \tag{3.3.1}$$

Suppose equation (3.3.1) is used to model the flaw growth in a group of components. At time t, the degradation of the components is distributed as Rt. We call R the population flaw growth rate, or simply the population rate. On the other hand, for a specific ith component, its flaw growth path $x_i(t)$ is a deterministic function of time t: $x_i(t) = r_i t$, where r_i is the component specific rate and is a fixed number sampled from the population rate R. Figure 3.2 shows several sample flaw growth paths from a typical random rate model.

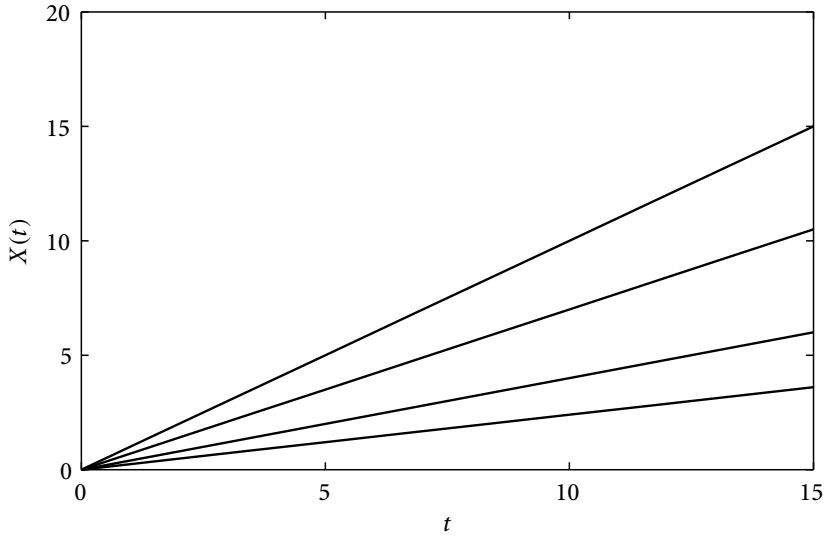

Figure 3.2 Sample paths from a random rate model

It is clear that for a group of components whose degradation follows the random rate model given by equation (3.3.1), the mean and variance of degradation for the population are

$$\mathrm{E}[X(t)] = t\mathrm{E}[R], \quad \mathrm{Var}[X(t)] = t^2\mathrm{Var}[R].$$

The COV of the degradation is $\sqrt{\text{Var}[R]}/\text{E}[R]$ and is a constant.

If inspection data are perfect, parameter estimation of the random rate model, and random variable model in general, is straightforward. Since the degradation growth of each component in the population is a deterministic function of known form, its component specific parameters can be calculated from a finite number of inspection results. A statistical fitting of random variable Θ using method of moments (MoM) or ML estimation can then be conducted using the collection of individual growth rates. However, when large inspection uncertainties are presented, parameter estimation of the random rate model is much more complicated since in such cases the component specific rate cannot be obtained precisely. Parameter estimation of random rate model considering inspection uncertainties will be discussed in details in the next chapter.

3.4 Gamma process model

The gamma process model is a stochastic process model which belongs to a broader category of degradation model called the cumulative damage model. The basic assumption of the cumulative damage model is that the degradation of a component is caused by a series of independent but random small damages. Suppose $X(t)$ is the total growth of a flaw within time interval $[0, t]$. $[0, t]$ is discretized into k sub-intervals as $0 \leqslant t_1 \leqslant t_2 \leqslant \cdots \leqslant t_k$. Denote the flaw growth within each sub-interval as X_i, $i = 1, 2, \cdots, k$. In the cumulative damage model, X_i are regarded as independent random variables, and the total flaw growth $X(t)$ is the sum of all X_i, i.e.,

$$X(t) = X_1 + X_2 + \cdots + X_k. \tag{3.4.1}$$

The PDF of $X(t)$ is then the convolution of the density functions of all X_i. Normally, evaluation of such convolution is difficult. However, when X_i is gamma distributed with properly chosen parameters, calculation of the convolution can be avoided, making the model much more practical in engineering applications.

3.4.1 Definition

Denote the gamma distributed random variable X with shape parameter $a>0$ and scale parameter $b>0$ as

$$X \sim \text{Ga}(a, b).$$

The PDF of X is

$$f_X(x) = f_{\text{Ga}}(x; a, b) = \frac{(x/b)^{a-1}}{b\Gamma(a)} \exp(-x/b), \quad \text{for } x>0,$$

where $\Gamma(a) = \int_0^\infty t^{a-1}e^{-t}\mathrm{d}t$ is the gamma function. Figure 3.3 shows density functions of several gamma random variables with different parameters. As can be seen from the figure, gamma distribution is a very flexible distribution that is able offer a good fit to different types of data-sets.

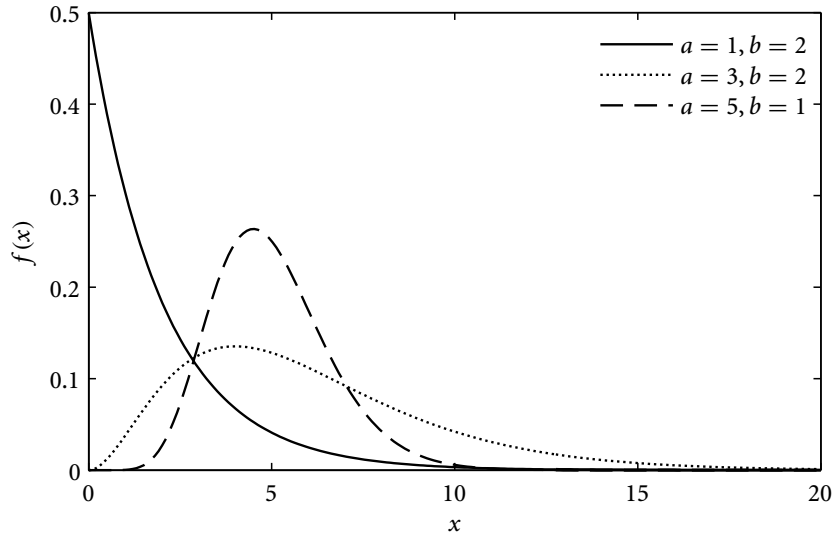

Figure 3.3 Probability density functions of gamma random variables with different parameters

An important property of the gamma distribution is that the sum of two independent gamma random variables with the same scale parameter b is still gamma distributed. Suppose X_1 and X_2 are two independent gamma random variables, $X_1 \sim \text{Ga}(a_1, b)$ and $X_2 \sim \text{Ga}(a_2, b)$. The sum of X_1 and X_2 is then a gamma random variable with shape

parameter a_1+a_2 and scale parameter b, i.e., $X_1+X_2 \sim \text{Ga}(a_1+a_2 b)$. Therefore, if X_i, $i=1,2,\cdots,k$, in equation (3.4.1) are all gamma distributed with the same scale parameter, the total degradation $X(t)$ is also gamma distributed and its parameters can be obtained directly without conducting the time-consuming convolutions.

Utilizing the above property of the gamma distribution, the gamma process model is defined as follows: a continuous-time stochastic process $\{X(t); t \geqslant 0\}$ with sample space $[0, +\infty)$ is called a gamma process with shape parameter α and scale parameter β ($\alpha, \beta > 0$) if (Singpurwalla, 1997):

- At time 0, $X(0) = 0$.
- For any $0 \leqslant t_1 \leqslant \cdots \leqslant t_n$, the random variables

$$X(t_1)-X(0),\ X(t_2)-X(t_1),\ \cdots,\ X(t_n)-X(t_{n-1}),$$

  are independent.
- For any $t \geqslant 0$ and $\tau > 0$, $X(t+\tau)-X(t)$ is gamma distributed with shape parameter $\alpha\tau$ and scale parameter β, i.e.,

$$X(t+\tau)-X(t) \sim \text{Ga}(x; \alpha\tau, \beta).$$

From the definition, it is can be concluded that gamma process is a monotonically increasing stochastic process with independent gamma distributed increments, and possesses all the general properties of the stochastic processes with stationary and independent increments, such as the linear mean and decreasing COV over time. The monotonically increasing property of the gamma process makes it ideal for modelling gradual damage that monotonically accumulates over time (Abdel-Hameed, 1975). Together with its other advantages, such as flexibility and mathematical tractability, gamma process has gained much interest in recent years and has been successfully applied in modelling a wide range of degradation phenomena, including wear, corrosion, erosion, and creep of materials (van Noortwijk, 2009).

Using the properties of the stochastic process with stationary and independent increments, the mean and variance of the gamma process are given as

$$\mathrm{E}[X(t)] = \alpha\beta t, \quad \mathrm{Var}[X(t)] = \alpha\beta^2 t.$$

The coefficient of variation (COV) of $X(t)$ is

$$\mathrm{COV}[X(t)] = \frac{\mathrm{E}[X(t)]}{\mathrm{Var}^{-1/2}[X(t)]} = \frac{1}{\sqrt{\alpha t}}.$$

Let $\mu = \alpha\beta$ and $\nu = 1/\sqrt{\alpha}$, one has $\mathrm{E}[X(t)] = \mu t$, $\mathrm{COV}[X(t)] = \nu/\sqrt{t}$. μ is called the average rate of the gamma process model and ν is the COV. μ and ν are sometimes used as an alternative set of the model parameters. The PDF of $X(t)$ in terms of μ and ν is given as

$$\begin{aligned} f_{X(t)} &= f_{\mathrm{Ga}}\left(x; t/\nu^2, \mu\nu^2\right) \\ &= \frac{\left[x/(\mu\nu^2)\right]^{t/\nu^2-1}}{\mu\nu^2\Gamma(t/\nu^2)} \exp\left[-x/(\mu\nu^2)\right]. \end{aligned}$$

Compared to the random rate model, the gamma process model is qualitatively different in the following two aspects: (1) in the random rate model, the flaw growth rate for a specific component; while in the gamma process model the flaw growth is modelled as the sum of a sequence of small independent random damages and thus the rate changes continually over time; (2) in the random rate model, flaw growth rates for different components vary across the population; whereas in the gamma process model, the future flaw growths of different component follow same distributions, regardless of their current flaw sizes. In short, random rate model and gamma process model are two extremes. The former one tries to capture the sample differences across the population while assuming there are no temporary uncertainties. And the latter one models the temporary uncertainties well but assumes the population is homogeneous in terms of future flaw growth distribution.

3.4.2 Simulation

Computer simulation of stochastic processes provides an effective way to numerically validate theories and methods developed for the stochastic models. A common approach

to simulate the sample paths of gamma process is to make use of its property of the independent and stationary gamma increments. To generate a sample path of a gamma process with parameter α and β from time 0 to t, the time is divided into n small intervals: $0 < t_1 < t_2 < \cdots < t_n = t$. Then, a random increment for each time interval is generated independently from a gamma distribution with shape parameter $\alpha \Delta t$ and scale parameter β, where Δt is the length of the corresponding time interval of the flaw growth. By adding up all the successive increments an approximate sample path of the gamma process can be obtained up to time t. When n is sufficiently large, this approximation can be very good (Yuan, 2007).

Figure 3.4 shows simulated sample paths of a gamma process with parameters $\alpha = 2$ and $\beta = 1$. Comparing Figure 3.2 and 3.4, the distinct characteristics of the random rate model and the gamma process model are clearly presented.

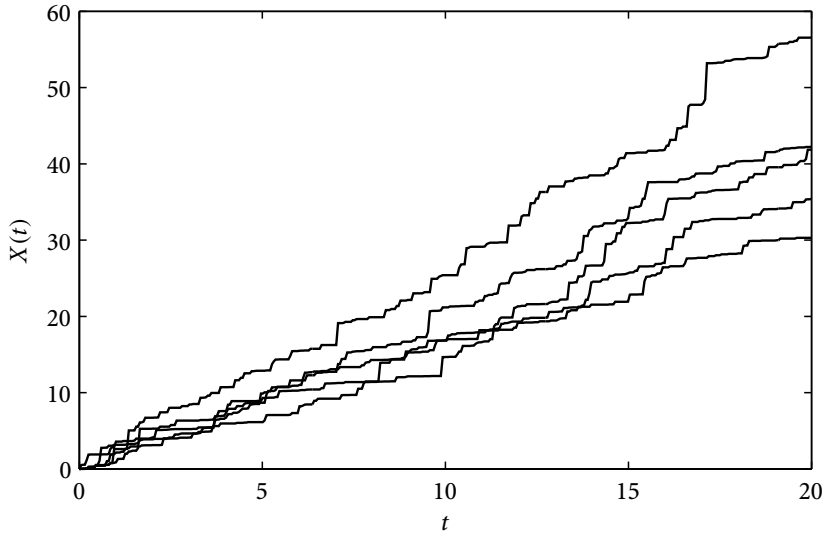

Figure 3.4 Simulated sample paths of a gamma process model

3.4.3 Parameter estimation

In practice, it is usually impossible to monitor the degradation process continuously. Rather, inspections are conducted at limited number of time instances. Suppose the flaw growth of a group of n components follows a gamma process with shape parameter α and scale

parameter β. For the ith component, at initial time t_{i0}, the flaw size is x_{i0}. The component is then inspected m_i times at $t_{i1}, t_{i2}, \cdots, t_{im_i}$. The measurement of the flaws is assumed to be perfect. Denote the actual flaw size of the ith component at time t_{ij} as x_{ij}. Let $\Delta t_{ij} = t_{ij} - t_{i,j-1}$ and $\Delta x_{ij} = x_{ij} - x_{i,j-1}, j = 1, 2, \cdots, m_i$. Δx_{ij} is then the flaw growth of the ith component over time interval Δt_{ij}.

For the sake of conciseness, the flaw growths of the ith component are written in vector form as $\Delta \mathbf{x}_i = \{\Delta x_{i1}, \Delta x_{i2}, \cdots, \Delta x_{im_i}\}$. From the definition of the gamma process, $\Delta \mathbf{x}_i$ is a realization of some random vector $\Delta \mathbf{X}_i$, where its elements, ΔX_{ij}, are independent and gamma distributed random variables. The PDF of ΔX_{ij} is

$$f_{\Delta X_{ij}}(\Delta x_{ij}; \alpha, \beta) = \frac{(\Delta x_{ij}/\beta)^{\alpha \Delta t_{ij} - 1}}{\beta \Gamma(\alpha \Delta t_{ij})} \exp(-\Delta x_{ij}/\beta).$$

Since ΔX_{ij} are independent, the likelihood function of α and β given flaw growths of the ith component $\Delta \mathbf{x}_i$ is simply the product of the probability density of each Δx_{ij}, i.e.,

$$L(\alpha, \beta \,|\, \Delta \mathbf{x}_i) = \prod_{j=2}^{m_i} f_{\Delta X_{ij}}(\alpha, \beta \,|\, \Delta x_{ij}) = \prod_{j=2}^{m_i} \frac{(\Delta x_{ij}/\beta)^{\alpha \Delta t_{ij} - 1}}{\beta \Gamma(\alpha \Delta t_{ij})} \exp(-\Delta x_{ij}/\beta).$$

When the degradation of each component is considered to be independent of others in the group, the likelihood function of the model parameters, given data from all the n components, can be written as the product of the likelihood for each individual component, i.e.,

$$L(\alpha, \beta | \Delta \mathbf{x}_1, \Delta \mathbf{x}_2, \cdots, \Delta \mathbf{x}_n) = \prod_{i=1}^{n} L_i(\alpha, \beta | \Delta \mathbf{x}_i). \tag{3.4.2}$$

Maximizing equation (3.4.2) gives the maximum likelihood estimation of the gamma process parameters α and β. The maximizing process is usually conducted numerically, using multivariate optimization algorithms, such as conjugate gradient algorithms or the simplex algorithm (Rao and Rao, 2009).

3.5 Poisson process model

In previous sections, the random rate model and the gamma process model are introduced. Both of these two models are defined on continuous sample spaces and are appropriate for modelling the flaw growth. In order to model the flaw generation, counting process models can be used, which are stochastic processes that count the number of occurrences over time. Therefore, sample space of a counting process is defined on the natural number set. Examples of counting processes include pure birth process, Bernoulli process and Poisson process. In this section, the Poisson process model is introduced, which is one of the most important counting process for the stochastic modelling of degradation.

3.5.1 Definition

Denote the Poisson distributed random variable X with parameter $\lambda > 0$ as

$$X \sim \text{Pois}(\lambda).$$

Here λ is also called the Poisson rate of the distribution. The probability mass function (PMF) of X is

$$f_X(x) = f_{\text{Pois}}(x;\lambda) = \frac{\lambda^x}{x!}\exp(-\lambda), \quad \lambda > 0 \text{ and } x = 0, 1, 2, \cdots .$$

Figure 3.5 shows the PMF of several Poisson random variables with different λ. Similar to the gamma distribution, the summation of two independent Poisson random variable with rate λ_1 and λ_2 is still a Poisson random variable, with rate $\lambda_1 + \lambda_2$. In addition, for the Poisson distribution, the converse of the above property, commonly known as Raikov's theorem, also holds, which is stated as: if the sum of two independent random variables is Poisson distributed, so is each of these two independent random variables (Gupta et al., 2010).

Based on the Poisson distribution, Poisson process is defined as follows: a continuous-time stochastic process, $X(t), t \geqslant 0$, is called a homogeneous Poisson process with rate λ, if it has the following properties (Prabhu, 2007):

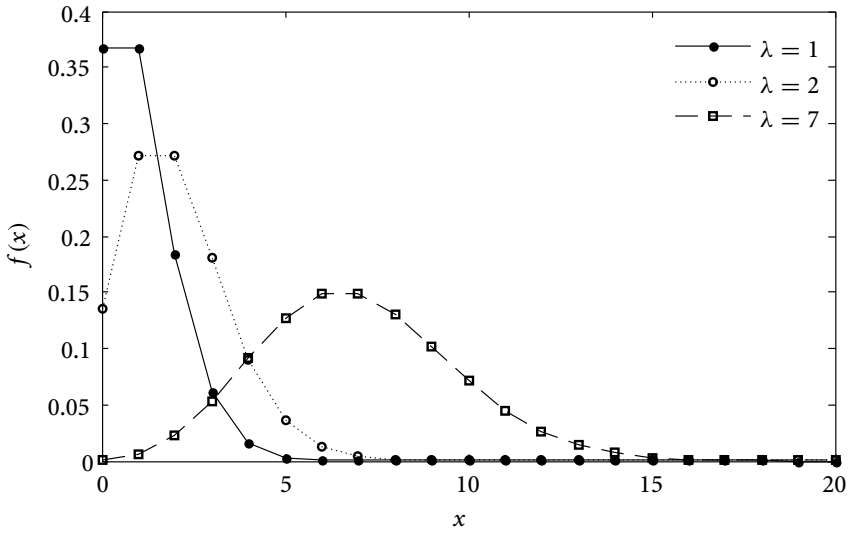

Figure 3.5 Probability mass functions of Poisson random variables with different parameters

- At time 0, $X(0) = 0$.
- For any $0 \leqslant t_1 \leqslant t_2 \leqslant \cdots \leqslant t_n$, random variables

$$X(t_1) - X(0),\ X(t_2) - X(t_1),\ \cdots,\ X(t_n) - X(t_{n-1})$$

  are independent.
- The number of occurrences between t and $t+\tau$, $X(t+\tau) - X(t)$, is Poisson distributed with rate $\lambda\tau$, for any $t \geqslant 0$ and $\tau > 0$, i.e.,

$$X(t+\tau) - X(t) \sim \text{Pois}(\lambda\tau).$$

From the definition, Poisson process is a stochastic process with stationary and independent increments. The mean and variance of Poisson process are

$$\text{E}[X(t)] = \lambda t, \quad \text{Var}[X(t)] = \lambda t.$$

The COV of the process is

$$\text{COV}[X(t)] = \frac{1}{\sqrt{\lambda t}}.$$

Obviously, parameter λ is simply the average number of occurrences per unit time.

3.5.2 Properties

Inter-arrival time distribution

The kth waiting time of a Poisson process, denoted as T_k, $k=0,1,\cdots$, is defined as the time of the kth occurrence of the process. Obviously, $T_0=0$. The difference between two successive waiting times, T_k and T_{k-1}, is called the inter-arrival time of the process and denoted as ΔT_k, $\Delta T_k = T_k - T_{k-1}$.

From the definition of Poisson process, CDF of first interval-arrival time ΔT_1 is

$$\begin{aligned} F_{\Delta T_1}(t) &= 1 - \bar{P}(\Delta T_1 > t) = 1 - \bar{P}(T_1 - T_0 > t) = 1 - \bar{P}(T_1 > t) \\ &= 1 - \bar{P}\{X(t)=0\} = 1 - \exp(-\lambda t). \end{aligned}$$

Thus, ΔT_1 is exponentially distributed with rate λ. To determine the distribution of ΔT_2, move the time origin of the Poisson process to T_1. The resulted process is then an identical Poisson process as the original one. ΔT_2 is therefore also an exponentially distributed random variable with the same rate parameter λ. In general, it can be shown that the inter-arrival time of the Poisson process, $\Delta T_1, \Delta T_2, \cdots$, are all independent and identically distributed (*i.i.d.*) random variables following exponential distribution with rate λ (Prabhu, 2007).

The property of *i.i.d.* inter-arrival time makes the computer simulation of the Poisson process very easy. One only needs to drawn a series of inter-arrival times from *i.i.d.* exponential distributions to simulate a sample path of a Poisson process. Figure 3.6 presents several sample paths of a Poisson process with $\lambda=1$ using this simulation method.

Superposition and splitting

The superposition of Poisson process states that the sum of several independent Poisson process is still a Poisson process and its rate is the summation of the rates of each individual Poisson process. Suppose $\{X_i(t), t \geqslant 0\}$, $i=1,2,\cdots,r$, are r independent Poisson processes with rates $\lambda_1, \lambda_2, \cdots, \lambda_r$. Let $X(t) = \sum_{i=1}^{r} X_i(t)$. From the superposition property, $X(t)$ is a Poisson process with rate $\lambda = \sum_{i=1}^{r} \lambda_i$ (Prabhu, 2007).

The splitting property of Poisson process is the inverse of the superposition property. Let $X(t)$ be a Poisson process with rate λ. Suppose the occurrences generated by $X(t)$ are split

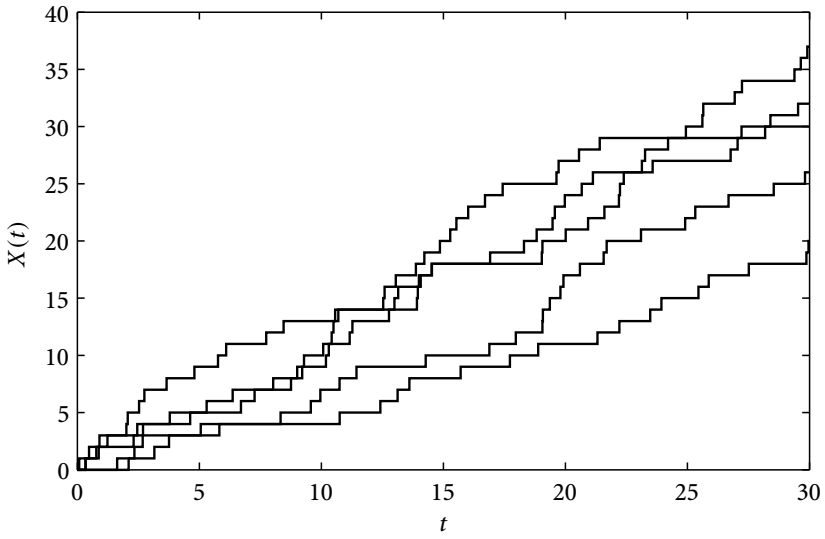

Figure 3.6 Simulated sample paths of a Poisson process model

randomly into k categories and the probability that an occurrence falls into the ith category is p_i, $\sum_{i=1}^{k} p_i = 1$. Let $X_i(t)$ be the number of occurrences in the ith category at time t. The splitting property then states that $X_i(t)$ are independent Poisson processes and the rate of $X_i(t)$ is simply $p_i\lambda, i = 1, 2, \cdots, k$ (Prabhu, 2007).

3.5.3 Parameter estimation

The derivation of the likelihood function of the Poisson process model is very similar to that of the gamma process model, since both are stochastic processes with stationary and independent increments. Suppose the number of flaws in a component follows a Poisson process with rate λ. At time t_0, the number of flaws is x_0. The component is then inspected for n times at $t_1, t_2, \cdots, t_n, t_0 < t_1 < t_2 \cdots < t_n$. The corresponding number of flaws at time t_i is x_i. In addition, we assume the inspection is perfect. Let $\Delta t_i = t_i - t_{i-1}$ and $\Delta x_i = x_i - x_{i-1}$. Δx_i is then the number of new generated flaws during time interval Δt_i.

According to the definition of the Poisson process, Δx_i are realizations of independent Poisson distributed random variables $\Delta X_i \sim \text{Pois}(\lambda \Delta t_i)$. The PDF of ΔX_i is

$$f_{\Delta X_i}(\Delta x_i) = \frac{(\lambda \Delta t_i)^{\Delta x_i}}{\Delta x_i!} \exp(-\lambda \Delta t_i), \quad i = 1, 2, \cdots, n.$$

Denote Δx_i in vector form as $\Delta \mathbf{x} = \{\Delta x_1, \Delta x_2, \cdots, \Delta x_n\}$. Since random variables ΔX_i, from which Δx_i are sampled, are independent, the likelihood function of the Poisson rate λ given $\Delta \mathbf{x}$ can be written as the product of the density of each Δx_i as

$$L(\lambda \,|\, \Delta \mathbf{x}) = \prod_{i=1}^{n} f_{\Delta X_i}(\Delta x_i) = \prod_{i=1}^{n} \frac{(\lambda \Delta t_i)^{\Delta x_i}}{\Delta x_i!} \exp\left(-\lambda \Delta t_i\right). \tag{3.5.1}$$

The corresponding log-likelihood function can be obtained by taking the logarithms of both sides of equation (3.5.1) as

$$\begin{aligned} l(\lambda \,|\, \Delta \mathbf{x}) &= \log L(\alpha, \beta \,|\, \Delta \mathbf{x}) \\ &= \sum_{i=1}^{n} \left[-\lambda \Delta t_i + \Delta x_i \log \lambda + \Delta x_i \log \Delta t_i - \log(\Delta x_i!)\right] \\ &= -\lambda \sum_{i=1}^{n} \Delta t_i + \log \lambda \cdot \sum_{i=1}^{n} \Delta x_i + \sum_{i=1}^{n} \left[\Delta x_i \log \Delta t_i - \log(\Delta x_i!)\right]. \end{aligned} \tag{3.5.2}$$

Maximum likelihood estimation can be obtained by differentiating equation (3.5.2) with respect to λ and letting the derivative be zero:

$$\frac{\partial l}{\partial \lambda} = -\sum_{i=1}^{n} \Delta t_i + \frac{1}{\lambda} \sum_{i=1}^{n} \Delta x_i = 0. \tag{3.5.3}$$

Solving equation (3.5.3) gives the maximum likelihood estimate of λ as

$$\lambda = \frac{\sum_{i=1}^{n} \Delta x_i}{\sum_{i=1}^{n} \Delta t_i},$$

which is simply the number of flaws generated per unit time.

3.6 Summary

Probabilistic modelling of degradation is important to reliable and efficient maintenance of large engineering systems. Traditionally, probabilistic modelling of degradation are carried

out using regression analysis and extreme value analysis. Although effective in many cases, these traditional approaches have their inherent limitations. Stochastic based models are therefore used as alternative modelling tools for some degradation phenomena.

This chapter introduces three common stochastic models, the random rate model, the gamma process model and the Poisson process model. The random rate model and the gamma process model are suitable for modelling flaw growth, and the Poisson process model are usually used for modelling flaw generation. Definitions and some properties of the three models are introduced. Likelihood functions of the models are also derived under the assumption that the inspection data are accurate. The derived likelihood function can then be used to estimate the model parameters when there are little or no inspection uncertainties. However, if large inspection uncertainties are presented, likelihood function considering the inspection uncertainties should be used, which will be discussed in following chapters.

CHAPTER 4

Estimation of Flaw Growth Model

4.1 Introduction

In the previous chapter, three typically stochastic models, namely, the random rate model, the gamma process model and the Poisson process model, are introduced. Likelihood functions of the models given accurate inspection data are derived, from which maximum likelihood (ML) estimates of the model parameters can be obtained either analytically or numerically. However, the assumption that the inspection data are accurate is usually unrealistic. In many practical applications, such as the in-service inspection of nuclear power plants, inspection uncertainties can be very significant, as discussed in Chapter 2. Large inspection uncertainties can mark the features of the degradation data, making the exploratory analysis difficult, and often lead to biased parameter estimates of the probabilistic models (Carroll, 2006).

As mentioned earlier, there are two types of degradation models: the flaw growth model and the flaw generation model. In this chapter, parameter estimation of the first category, the flaw growth model, is discussed. In particular, we will discuss the estimation of two specific flaw growth models, the random rate model and the gamma process model, using noisy inspection data with large sizing errors. Probability of detection is not considered in this chapter, as the analyses are based on repeated measurements from existing flaws.

The problem of noisy measurement in the estimation of classical regression models have been discussed extensively in the literature, as summarized by Fuller (1987) for linear regression models and Carroll (2006) for non-linear regression models. However, investigations of this problem in the settings of stochastic models remain limited. In practical applications, approximate methods are still widely used. For example, it is very common to first delete all the negative measured flaw growth from data since they are physically impossible, and then estimate the model parameters as if there is no sizing error (Camacho, 2006; EPRI, 2006a, 2009). For safety considerations, most of the approximate methods, especially those used for safety critical systems, are formulated in a way such that conservative estimates of the parameters are obtained. The problem of the approximate methods is that the extent of the conservativeness in the estimation can hardly be quantified and overly conservative estimates are common. Better statistical methods for the stochastic modelling of flaw growth are needed.

One of the most statistically sound methods for the parameter estimation of probabilistic models is the likelihood-based method. Denote the actual flaw growth as $X(t)$ and the measured flaw size at time t as $Y(t)$. $Y(t)$ is then the sum of the true flaw size $X(t)$ and the associated measurement error $E(t)$, i.e.,

$$Y(t) = X(t) + E(t)$$

Obviously, $Y(t)$ and $X(t)$ share the same set of model parameters. Therefore, parameters of the actual degradation model $X(t)$ can be estimated from the likelihood function of the measured flaw size $Y(t)$. This likelihood approach was originally developed for regression models, as discussed in details by Carroll (2006). The same approach was first applied in stochastic modelling of degradation by Whitmore (1995) for the parameter estimation of a Wiener diffusion process from observations with normal sizing errors, and a closed form estimate of the model parameters was obtained. Later, following the same idea, Kallen and van Noortwijk (2005) derived the likelihood function of the gamma process model subjected to normally distributed sizing errors, though effective method for the numerical evaluation of the likelihood function is not given. In this chapter, we will also use

this likelihood approach to develop the maximum likelihood estimates of stochastic flaw growth models using noisy field measurement.

The remainder of the chapter is organized as follows. Section 4.2 focuses on the parameter estimation of the random rate model subject to sizing error. Random rate models with both exact and uncertain initial conditions are investigated. A numerical simulation and a practical case study are presented to illustrate the effectiveness of the proposed method. Section 4.3 discusses the gamma process model with normally distributed sizing error. Based on the previous work by Kallen and van Noortwijk (2005), the complete form of the model likelihood function is derived. In order to overcome the computational difficulties in the ML estimation, a novel numerical method using the Genz's transform (Genz, 1992) and quasi-Monte Carlo (QMC) simulation is proposed. A case study on the flow-accelerated corrosion (FAC) is presented using the proposed method. Summary of the chapter is given in the last section.

4.2 Random rate model with sizing error

4.2.1 Problem statement

A very common assumption regarding the flaw growth in a group of components is that the flaw growth is linear over time and the growth rates (slopes of the flaw growth) of the components are constants following some probability distribution. As discussed in Section 3.3, this linear growth assumption is exactly the motivation of the random rate model, in which only sample uncertainty is considered and the temporal uncertainty is assumed to be minimal and therefore ignored.

If the flaw inspection is perfect, parameter estimation of the random rate model is easy. Suppose the flaw growth in a group of n components can be described using the following random rate model

$$X(t) = Rt,$$

where R is flaw rate distribution for the component population. The PDF of R is $f_R(r;\theta)$, where θ is parameter. The inspections of an ith component in the group are carried

out at times $t_{i1}, t_{i2}, \cdots, t_{im_i}$, and the corresponding actual flaw sizes are $x_{i1}, x_{i2}, \cdots, x_{im_i}$, respectively. From previous discussions, it follows the actual flaw growth rate of the ith component, r_i, can be determined from any two inspections as

$$r_i = \frac{x_{i2} - x_{i1}}{t_{i2} - t_{i1}} = \frac{x_{i3} - x_{i2}}{t_{i3} - t_{i2}} = \cdots = \frac{x_{im_i} - x_{i,m_i-1}}{t_{im_i} - t_{i,m_i-1}}.$$

The growth rate distribution R of the population can then be obtained by fitting the collection of all the component specific rates $r_i, i = 1, 2, \cdots, n$, using some appropriate probability distributions.

In reality, however, the inspection probe invariably adds random noise to the actual flaw size, such that the measurement of x_{ij} has to be conceptually treated as a random variable Y_{ij},

$$Y_{ij} = x_{ij} + E_{ij},$$

where E_{ij} is the sizing error of Y_{ij}. For simplicity, E_{ij} are assumed to be independent and normally distributed with mean 0 and some known SD σ_E. Any specific measured size y_{ij} of this flaw at time t_{ij} is a realization from distribution Y_{ij}. Suppose a series of measurements of the ith flaw were taken as $y_{i1}, y_{i2}, \cdots, y_{im_i}$, at times $t_{i1}, t_{i2}, \cdots, t_{im_i}$, respectively, as shown in Figure 4.1 in relation to the true flaw growth path. The measured growth rate $\tilde{r}_{ij}$ over any inspection interval $[t_{i,j-1}, t_{ij}]$ can be calculated as

$$\tilde{r}_{i2} = \frac{y_{i2} - y_{i1}}{t_{i2} - t_{i1}}, \tilde{r}_{i3} = \frac{y_{i3} - y_{i2}}{t_{i3} - t_{i2}}, \ldots, \tilde{r}_{im_i} = \frac{y_{im_i} - y_{i,m_i-1}}{t_{im_i} - t_{i,m_i-1}}$$

It is clear that the measured flaw growth rates, $\tilde{r}_{ij}$, are not equal to the actual rate r_i, and $\tilde{r}_{ij}$ are likely to fluctuate due to effect of random sizing error. Furthermore, the measured rates can also be negative, even though the underlying growth rate is always positive. The departure between the measured and actual rate will increase with the increase in variability associated with the sizing error E_{ij}.

The challenge is thus clear: how do we estimate the population flaw growth rate distribution R when the component specific rate cannot be obtained accurately. This population rate

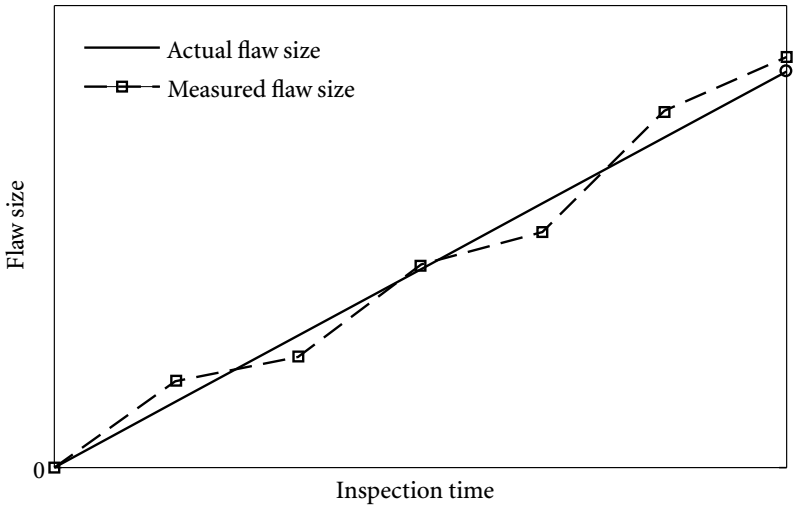

Figure 4.1 Illustration of an actual and measured linear degradation growth path for a specific component

distribution can be subsequently used in the reliability analysis of uninspected components, which are susceptible to the same degradation as the inspected components.

4.2.2 Current methods

The problem of estimating the flaw growth rate from noisy measurement has been discussed extensively in many areas under the random rate assumption (explicitly or implicitly), especially in the corrosion and wear assessment (Fenyvesi et al., 2004; EPRI, 2006a; Huyse and van Roodselaar, 2010), and various methods have been developed. A review on some of these methods are presented in the next. These methods are divided into three categories: method of moments, simulation method, and regression method, among which the first two are applicable when there are only two repeated measurements.

Method of moments

The method of moments is popularly used in the engineering literature due to its analytical and computational simplicity (Nessim et al., 2008; Huyse and van Roodselaar, 2010; Fenyvesi et al., 2004). While applying this method, the user should be clear about the nature of

degradation model being random rate or random process with independent increment. An ambiguity about this aspect would lead to incorrect results, as discussed below.

Suppose that two random samples of measured flaw sizes are available from inspection done at two separate times t_1 and t_2. While conducting inspection at t_2, it is not necessary to keep track of the flaws found and measured at t_1. Denote the actual flaw size distribution of the components at time t_1 and t_2 as X_1 and X_2. From the random rate assumption, the mean and SD of X_1 and X_2 are

$$\mu_{X_i} = \mu_R t_i \quad \text{and} \quad \sigma_{X_i} = \sigma_R t_i, \quad i=1,2.$$

Since the sizing error are assumed to be normally distributed with mean 0 and SD σ_E, the mean and variance of the corresponding measured flaw size, Y_1 and Y_2, can be given as

$$\mu_{Y_i} = \mu_{X_i} \quad \text{and} \quad \sigma^2_{Y_i} = \sigma^2_{X_i} + \sigma^2_E, \quad i=1,2.$$

In the method of moments, the flaw growth rate is then regarded as a difference between actual flaw sizes, X_2 and X_1, divided by the time interval $t_2 - t_1$. This estimate of the growth rate is denoted as Z to distinguish it from the actual growth rate R. One has

$$Z = \frac{X_2 - X_1}{t_2 - t_1}. \tag{4.2.1}$$

The mean and variance of Z are given as

$$\mu_Z = (\mu_{X2} - \mu_{X1})/(t_2 - t_1) = (\mu_{Y2} - \mu_{Y1})/(t_2 - t_1)$$
$$\sigma^2_Z = (\sigma^2_{X2} + \sigma^2_{X1})/(t_2 - t_1)^2 = (\sigma^2_{Y2} + \sigma^2_{Y1} - 2\sigma^2_E)/(t_2 - t_1)^2.$$

The parameters of the assumed rate distribution Z can then be evaluated by method of moments using the sample mean and sample variance of the measured flaw size Y_1 and Y_2.

However, it can be shown that the random variable Z is not equivalent to R by comparing the mean and SD of these two variables. To do this, mean and SD of X_2 and X_1, in terms of μ_R and σ_R, are substituted in equation (4.2.1), which leads to

$$\mu_Z = \mu_R \quad \text{and} \quad \sigma_Z = \sigma_R \frac{\sqrt{t_2^2 + t_1^2}}{(t_2 - t_1)} \quad \text{or} \quad \sigma_Z = k_R \sigma_R \quad (k_R > 1 \text{ for } t_2 > t_1). \tag{4.2.2}$$

Since $\mu_Z = \mu_R$, the mean of growth rate is correctly estimated as an unbiased quantity, but the estimated SD of Z turns out to an incorrect number. From equation (4.2.2), σ_Z will always be greater than the true value of σ_R, and depending on the inspection times, t_1 and t_2, it can be several times larger than σ_R. For example, if $t_1 = 5$ and $t_2 = 10$, then $\sigma_Z = 2.33\sigma_R$. The reason for this anomaly is an implicit assumption of X_1 and X_2 as two independent random variable as implied by equation (4.2.1), which they are not.

This anomaly continues in the prediction of flaw size at a future time t_3, which is typically based on the following relation

$$X_3 = X_2 + Z(t_3 - t_2), \tag{4.2.3}$$

where X_2 and Z are implicitly assumed to be independent.

From equation (4.2.3), the mean of X_3 can be correctly obtained as

$$\mu_{X3} = \mu_{X2} + \mu_Z(t_3 - t_2) = \mu_R t_3. \tag{4.2.4}$$

However, the SD of X_3 turns out to be much different from the correct value. In fact, the independence assumption of X_2 and Z in equation (4.2.3) is not only in conflict with the assumption of the random rate model, but also inconsistent with equation (4.2.1) from which Z is obtained, as obviously Z is correlated with X_2 according to equation (4.2.1).

To show the difference between the predictions by the method of moment and the true underlying random rate model, let's denote the standard deviation obtained from equation (4.2.4) as $\hat{\sigma}_3$ to distinguish it from the correct value $\sigma_{X3} = \sigma_R t_3$. One has

$$\begin{aligned} (\hat{\sigma}_3)^2 &= \sigma_{X2}^2 + \sigma_Z^2 (t_3 - t_2)^2 \\ &= \sigma_R^2 t_2^2 + \sigma_R^2 (t_3 - t_2)^2 \frac{t_2^2 + t_1^2}{(t_2 - t_1)^2}. \end{aligned} \tag{4.2.5}$$

Define the error factor of $\hat{\sigma}_3$ as $k_3 = \hat{\sigma}_3 / \sigma_{X3} = \hat{\sigma}_3 / (\sigma_R t_3)$, such that

$$k_3 = \frac{1}{t_3} \sqrt{t_2^2 + (t_3 - t_2)^2 \frac{t_2^2 + t_1^2}{(t_2 - t_1)^2}}.$$

Depending on the values of t_1, t_2 and t_3, k_3 can be greater than or less than or equal to one. To illustrate the error given by equation (4.2.5), consider a special case in which the time

interval between inspections and prediction is equal, i.e., $(t_2 - t_1) = (t_3 - t_2) = d$, and t_1 is increased from 1 to 25. Figure 4.2 shows that the error associated with varies from -15% to +20% for various combinations of t_1 and d.

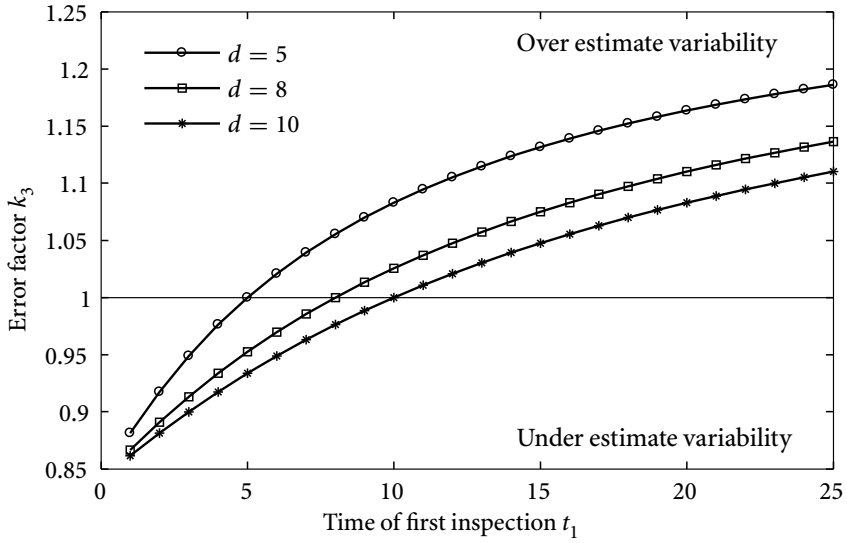

Figure 4.2 An illustration of error associated with the SD of flaw size predicted at a future time t_3 by the method of moments

In summary, the application of the method of moments in the literature is fraught with conceptual inconsistencies, as explained above. It is shown from the example that statistical inference without carefully specifying the underlying probabilistic model is likely to result in erroneous predictions.

Simulation method

In the context of wear of steam generator tubes in nuclear plants, a simulation based method was proposed to estimate the growth rate from noisy data (EPRI, 2006a). This method can be used only with flaw size data collected over two consecutive inspections.

Suppose a group of n components are inspected at time t_1 and t_2. The actual flaw size of the ith component at time t_1 and t_2 are x_{i1} and x_{i2}, and the measured flaw sizes are y_{i1} and y_{i2}. From the assumptions of the random rate model, it can be shown that the measured

rate of the component, $\tilde{r}_i$, is related to its actual rate r_i in the following manner

$$\tilde{r}_i = \frac{y_{i2} - y_{i1}}{t_2 - t_1} = \frac{x_{i2} - x_{i1}}{t_2 - t_1} + \frac{e_{i2} - e_{i1}}{t_2 - t_1} = r_i + \frac{e_{i2} - e_{i1}}{t_2 - t_1}, \tag{4.2.6}$$

where $e_{ij} = y_{ij} - x_{ij}, j = 1, 2$, are the associated sizing errors.

A log-normal distribution is then assumed for the actual growth rate and an unbiased normal distribution with SD σ_E is assumed for the sizing error. The first step of the simulation method is to compute the measured growth rates from the actual measurements. The mean of the actual rate μ_R is then equal to the sample mean of the measured rates, since the sizing error is unbiased.

The SD of the actual rate σ_R is estimated from a simulation-based approach. Assuming a value of σ_R, random samples of actual flaw growth rates are simulated from the log-normal distribution. Similarly, samples of sizing errors are simulated from the assumed normal distribution. These simulated values are then added as per equation (4.2.6) to obtain a simulated sample of measured rates. The cumulative distribution function (CDF) of the simulated measured rates is then visually compared with that obtained from the actual measurements. The value of σ_R is iteratively modified and simulations are repeated, until the simulated rate resembles the actual data.

This approach lacks a sound statistical foundation, since the comparison between simulated and actual rate is not based on a statistical test of goodness-of-fit. Also, flaw size data available from more than two inspections cannot be utilized, which is a waste of inspection data.

Regression method

Although with sizing error presented in data, the accurate values of the component specific rates cannot be known, they can indeed be estimated using the regression method, provided that there are sufficient number of repeated inspections. Suppose the flaw in the ith component in the population is measured as y_{ij} at multiple times t_{ij}. Then, a linear regression model, $y_{ij} = \beta_{i0} + \beta_{i1} t_{ij} + \epsilon_i$, can be fitted using the ordinary least-square (OLS) method. Here ϵ_i is the random error of the regression. The slope of regression, β_{i1}, can be interpreted as estimated the degradation growth rate of the ith component. The growth

rate distribution of the population can then be obtained by performing a statistical fitting on the estimated slopes from all the inspected components.

The problem of this linear regression approach is that sufficiently large number of component specific measurements are required to estimate regression coefficients with high confidence. If a component is expected to be inspected only 3-4 times over its service life, then data are not sufficient for the regression analysis.

In some studies, it is therefore suggested to pool the flaw size measurements of all the components into a single data-set and fitting an OLS regression model. However this is conceptually incorrect. The reason is that it assumes that flaw growth rate is same for all the components, which contradicts the basic assumption of the random rate model that the rate is a random variable across the population. The correct way to analyze pooled data is to use the linear mixed effect (LME) regression model, which treats the regression coefficients as random variables as

$$y = B_0 + B_1 t + \epsilon,$$

where $\mathbf{B} = [B_0, B_1]$ is a multivariate normal random variable. For the ith component, the model is given as $y_{ij} = b_{i0} + b_{i1} t_{ij} + \epsilon_i$, in which y_{ij} is the measured flaw size of the component at time t_{ij}, b_{i0} and b_{i1} are realizations of the joint distribution of B_0 and B_1.

Although LME regression is a feasible approach in theory, its practical application is often limited because the slope coefficient in the model, B_1, is required to be normally distributed, which may not be realistic in many cases. One way of applying the LME regression to flaw growth with non-normal rate distribution is to construct a transform of the flaw growth rate distribution to a normal distribution, as did by Lu and Meeker (1993). However, construction of such transform and the subsequent parameter estimate are usually extremely tedious, making the method not practical to engineers.

In summary, regression methods are currently the most sophisticated methods for estimating the flaw growth rate distribution from noisy measurement. However, both the linear regression and the mixed effect regression have their limitations, as explained above.

4.2.3 Proposed method

In this section, based on the simple idea that the measured value of the flaw size is the combined result of the underlying degradation model and the random sizing error, likelihood function of the random rate model given data with random sizing error is derived, from which ML estimate of model parameters can be obtained. The proposed method accounts the sizing error with a sound statistical basis and is able to handle flaw growth rate of arbitrary distributions. Two scenarios are considered: (1) initial degradation is zero, and (2) initial degradation is only known with uncertainty.

Zero Initial degradation

In many situations, the initial condition of the component is known exactly. For example, in some cases of wear degradation, there is no incubation time for the wear initiation. Therefore, if the components are degradation free when they are installed, the initial wear of the components are precisely known as zero.

Under the assumption of zero initial degradation, the actual flaw size of the ith component at its jth inspection at time t_{ij} is given as

$$x_{ij} = r_i t_{ij}.$$

Here r_i is the flaw growth rate of this specific component and is a sample of the population rate distribution $f_R(r;\theta)$. Due to the random sizing error, measurement of x_{ij} is a random variable, denoted as Y_{ij}. Any specific measured value of the flaw size in the inspection, denoted as y_{ij}, is then an observation of random variable Y_{ij}. From previous discussions, one has

$$Y_{ij} = x_{ij} + E_{ij} = r_i t_{ij} + E_{ij},$$

where E_{ij} is the independent normal sizing error with mean zero and SD σ_E. For a specified ith component, r_i and t_{ij} are fixed numbers, such that Y_{ij} are independent normal random

variables with mean $r_i t_{ij}$ and SD σ_E. The PDF of Y_{ij} is

$$\begin{aligned} f_{Y_{ij}}(y_{ij}; r_i) &= \phi(y_{ij}; r_i t_{ij}, \sigma_E^2) \\ &= \frac{1}{\sqrt{2\pi\sigma_E^2}} \exp\left[-\frac{(y_{ij} - r_i t_{ij})^2}{2\sigma_E^2}\right], \end{aligned}$$

where $\phi(x; \mu, \sigma^2)$ is the PDF of normal random variable with mean μ and SD σ.

Denote the distribution of all the m_i measured flaw size of the ith component in vector form as $\mathbf{Y}_i = \{Y_{i1}, Y_{i2}, \cdots, Y_{im_i}\}$. Since Y_{ij} are independent random variables, the joint PDF of $\mathbf{Y}_i$ is given as the product of the PDF of each Y_{ij}, i.e.,

$$\begin{aligned} f_{\mathbf{Y}_i}(\mathbf{y}_i; r_i) &= \prod_{j=1}^{m_i} f_{Y_{ij}}(y_{ij}; r_i) \\ &= \prod_{i=1}^{m_i} \frac{1}{\sqrt{2\pi\sigma_E^2}} \exp\left[-\frac{(y - r_i t_{ij})^2}{2\sigma_E^2}\right]. \end{aligned} \tag{4.2.7}$$

Since SD of the sizing error σ_E is known, the only parameter left for $\mathbf{Y}_i$ is the component specific rate r_i. Notice that r_i itself is a sample of the population rate distribution $f_R(r; \theta)$. Therefore, the measured flaw size of the component, $\mathbf{Y}_i$, actually follows a two-stage hierarchical model, with the component specific rate r_i be the low-level parameter and the population rate parameter θ be the hyper-parameter. Using theorem of total probability, the marginal likelihood of the hyper-parameter θ given inspection data of the ith component, $\mathbf{y}_i$, is

$$\begin{aligned} L_i(\theta \,|\, \mathbf{y}_i) &= \int_0^\infty f_{\mathbf{Y}_i}(\mathbf{y}_i; r_i) f_R(r_i; \theta) \mathrm{d}r_i \\ &= \int_0^\infty \prod_{i=1}^{m_i} \frac{1}{\sqrt{2\pi\sigma_E^2}} \exp\left[-\frac{(y - r_i t_{ij})^2}{2\sigma_E^2}\right] f_R(r_i; \theta) \mathrm{d}r_i. \end{aligned}$$

The likelihood of θ for a group of n components can be written as a product of the likelihood functions for the individual component and is given in following equation

$$L(\theta \,|\, \mathbf{y}_1, \mathbf{y}_2, \cdots, \mathbf{y}_n) = \prod_{i=1}^{n} L_i(\theta \,|\, \mathbf{y}_i). \tag{4.2.8}$$

The product can be written, because growth rate in each component is assumed to be independent of the other component.

Finally, a point estimate of parameters θ can be obtained by maximizing equation (4.2.8). Numerical evaluation of the likelihood function can be conducted using the classical quadrature rules as discussed in Davis and Rabinowitz (2007); and the maximum likelihood estimation can be obtained using the simplex method (Nelder and Mead, 1965) which does not require calculating the derivatives of the objective function.

Uncertain initial degradation

We have discussed the random rate model with sizing errors under the assumption that the initial degradation of components is known precisely as zero. However, in some other cases, the initial condition of the component may not be known exactly. An example of such case is the degradation of the wall thickness corrosion of SG tubes. The wall thickness loss of the SG tube is obtained by comparing the measured wall thickness at inspection times with the nominal wall thickness. Due to the imperfect manufacturing process, the initial wall thickness of the tubes is not a fixed number, but rather a random quantity following some distribution. The difference between the actual initial wall thickness and the nominal wall thickness can then be treated as the initial degradation for practical purposes.

Suppose the initial degradation of a group of n components is a random variable denoted as A. To be simple, here A is assumed to be normally distributed with zero mean and SD σ_A, but it can be any arbitrary distribution. For a specific ith component, its initial degradation a_i is a realization of A. The actual degradation of the ith component, x_{ij}, at its jth inspection is then

$$x_{ij} = a_i + r_i t_{ij},$$

where r_i is the component specific degradation rate and t_{ij} is the time of the jth inspection. Similar to the case of zero initial degradation, the measured value of x_{ij} is a random variable, denoted as Y_{ij}. Y_{ij} is given as

$$Y_{ij} = a_i + r_i t_{ij} + E_{ij},$$

where E_{ij} are *i.i.d.* sizing errors.

Because a_i, r_i and t_{ij} are all fixed numbers for the specific ith component, Y_{ij} are independent normal random variables with mean $a_i + r_i t_{ij}$ and SD σ_E. The PDF of Y_{ij} is

$$\begin{aligned} f_{Y_{ij}}(y_{ij}; a_i, r_i) &= \phi(y_{ij}; a_i + r_i t_{ij}, \sigma_E^2) \\ &= \frac{1}{\sqrt{2\pi\sigma_E^2}} \exp\left[-\frac{(y_{ij} - a_i - r_i t_{ij})^2}{2\sigma_E^2} \right]. \end{aligned} \tag{4.2.9}$$

Denote all m_i measured flaw sizes of the ith component as $\mathbf{Y}_i = \{Y_{i1}, Y_{i2}, \cdots, Y_{im_i}\}$. Because Y_{ij} are independent random variables, from equation (4.2.9), the joint PDF of $\mathbf{Y}_i$ is

$$\begin{aligned} f_{\mathbf{Y}_i}(\mathbf{y}_i; a_i, r_i) &= \prod_{j=1}^{m_i} f_{Y_{ij}}(y_{ij}; a_i, r_i) \\ &= \prod_{j=1}^{m_i} \phi(y_{ij}; a_i + r_i t_{ij}, \sigma_E^2) \\ &= \prod_{j=1}^{m_i} \frac{1}{\sqrt{2\pi\sigma_E^2}} \exp\left[-\frac{(y_{ij} - a_i - r_i t_{ij})^2}{2\sigma_E^2} \right]. \end{aligned} \tag{4.2.10}$$

Following the concept of hierarchical modelling, it can be seen that $\mathbf{Y}_i$ are normally distributed random variables with parameter a_i and r_i; while a_i and r_i are samples from random variables A and R, respectively. Suppose the initial wall thickness distribution A and the population flaw growth rate R are independent. Using the theorem of total probability, the marginal likelihood function of the model parameter θ given the inspection data of an ith component is

$$\begin{aligned} L_i(\theta \,|\, \mathbf{y}_i) &= \int_0^\infty \int_{-\infty}^\infty f_{\mathbf{Y}_i}(\mathbf{y}_i; a_i, r_i) \phi(a_i; 0, \sigma_A) f_R(r_i; \theta) \mathrm{d}a \mathrm{d}r_i \\ &= \int_0^\infty \int_{-\infty}^\infty \prod_{i=1}^{m_i} \frac{1}{\sqrt{2\pi\sigma_E^2}} \exp\left[-\frac{(y - r_i t_{ij})^2}{2\sigma_E^2} \right] \phi(a_i; 0, \sigma_A) f_R(r_i; \theta) \mathrm{d}a \mathrm{d}r_i. \end{aligned}$$

The likelihood of θ for a group of n components can be written as a product of the likelihood functions for the individual component and is given in following equation

$$L(\theta \,|\, \mathbf{y}_1, \mathbf{y}_2, \cdots, \mathbf{y}_n) = \prod_{i=1}^{n} L_i(\theta \,|\, \mathbf{y}_i),$$

from which the maximum likelihood estimation can be obtained using the quadratic rules for integration and the simplex method for the maximization.

4.2.4 Numerical validation

The accuracy of the proposed MLE method is illustrated through a simulation-based example. Consider a group of 100 components under degradation. At time 0, all the components are in good condition. The flaw growth rate of the components is modelled as a log-normal distribution with PDF

$$f_R(r;\mu,\sigma) = \frac{1}{r\sigma\sqrt{2\pi}} \exp\left\{-\frac{(\ln r - \ln \mu)^2}{2\sigma^2}\right\}, \quad \text{for } r>0, \tag{4.2.11}$$

where $\mu = -1$ and $\sigma = 0.5$ are the log-scale and shape parameters. The mean and SD of growth rate are 0.42 and 0.22 mm/year, respectively. The 95th percentile of the growth rate, often used as an upper bound rate, is calculated as 0.84 mm/year.

Suppose two inspections of the flaw sizes are conducted at time 2 and 4 years. The sizing error of the inspection is assumed to be normally distributed with mean zero and some standard deviation. Monte Carlo simulation method is used to quantify the bias and root mean squared error (RMSE) of the predicted mean and 95th percentile of the growth rate from simulated inspection data. The simulation involves following steps:

- A sample of 100 growth rates is simulated from the log-normal distribution. The true flaw sizes at inspection time are then calculated as $x_i(t) = r_i t$, where r_i is the simulated rate of the ith component.
- Simulate two values of sizing error from the normal distribution for flaw measurement. The measured flaw sizes are then obtained by adding the sizing errors to the simulated true flaw sizes. In total, the sample consists of 200 measurements, 2 measurements for each of the 100 flaws.
- The simulated flaw measurements are then analyzed using the proposed method and the estimated mean and 95th percentile of the growth rate distribution are calculated.

For the purpose of comparison, the simulated data are also analyzed using the linear regression method discussed previously. First, the growth rate of each flaw is calculated

Proposed method

SD of error	Estimated Mean		Estimated 95th percentile	
	Bias	RMSE	Bias	RMSE
0.1 mm	-0.06%	5.5%	-0.48%	7.1%
0.5 mm	-0.15%	6.5%	-0.84%	8.3%
1.0 mm	0.22%	8.5%	-2.2%	12%
1.5 mm	0.21%	11%	-3.6%	20%

Regression method

SD of error	Estimated Mean		Estimated 95th percentile	
	Bias	RMSE	Bias	RMSE
0.1 mm	-0.06%	5.8%	0.14%	7.2%
0.5 mm	-0.20%	6.8%	9.2%	12%
1.0 mm	0.27%	9.0%	32%	34%
1.5 mm	0.27%	12%	61%	62%

Table 4.1 Bias and RMSE of the estimated mean and 95th percentile of the growth rate by the proposed method and the regression method

from linear regression analysis. Then, parameters of the growth rate distribution are obtained using method of moments from the regressed component flaw growth rates.

The simulation was carried out for various SD of sizing error (σ_E) ranging from 0.1 mm to 1.5 mm. For each value of σ_E, the procedures are repeated for 500 times, and the corresponding bias and RMSE of the mean and 95th percentile of the estimated flaw growth rate by the two methods are calculated. For ease of comparison, the obtained bias and RMSE of the estimations are normalized with respect to the true average rate 0.42 mm/year. The results of the simulation are presented in Table 4.1.

It is shown in Table 4.1 that the proposed method and the linear regression method both give fairly accurate estimates for the mean growth rate. However, when the level of sizing error increases, the linear regression method tends to overestimate the right percentile of the flaw growth rate; whereas the estimate by the proposed approach remains unbiased. The RMSE performance of the proposed approach is also significantly better that the linear

regression method when sizing error is large. The RMSE of the 95th percentile by the proposed approach is about 1/3 of that by the linear regression method when SD of sizing error is greater than 1.0 mm. Overall, the proposed maximum likelihood method shows good statistical accuracy for the parameter estimation of the random rate model even when data contain significant sizing errors.

4.2.5 Example: fretting wear of SG tubes

Background

A practical example regarding the fretting wear of the steam generator (SG) tubes in a nuclear power plant is presented. Fretting wear is a wear damage in SG tubes caused by the flow-induced vibration and is usually found at the tube-to-support locations. In order to examine the extent of the wear damage in a nuclear power plant, two inspection campaigns were conducted in year 2005 and 2007. The inspection time is transformed to the equivalent operating time at the plants full capacity, or simply the effective full power year (EFPY), as 17.08 and 18.4 EFPY for the two inspections, respectively. Among all the tubes, 81 tubes were inspected only once either in 2005 or in 2007, and another 26 tubes were inspected in both years. The data-set consists of minimum wall thickness of each tube obtained from ET probes. The sizing error of the wall thickness measurement is a normal distribution with zero mean and SD $\sigma_E = 0.25$ mm. Due to the imperfect manufacturing process, the initial wall thickness of the SG tubes is random and is assumed as a normal random variable with mean 6.5 mm (the nominal wall thickness) and SD of 0.15 mm. For ease of the analysis, the difference between the nominal initial wall thickness and the actual initial wall thickness of the SG tubes is treated as the initial wall wear A. Obviously, A is a normal random variable with mean $\mu_A = 0$ and SD $\sigma_A = 0.15$ mm.

Parameter estimation

As the tubes were inspected only for once or twice, it is impractical examine whether there is significant temporal uncertainty in the degradation. We simply assume that the fretting wear follows the linear random rate model. Log-normal distribution with log-scale parameter μ

and shape parameter σ is assumed as the population rate distribution R. The PDF of the log-normal distribution can be found at equation (4.2.11).

Using the proposed method, ML estimates of the wear rate distribution are obtained. The estimated wear rate distribution is then compared with the result obtained using the linear regression method and the histogram of the measured wear rate, which is calculated as the difference between the nominal initial wall thickness and the last measured value divided by time. The results are given in Table 4.2 and Figure 4.3. From the results, the estimated average wear rates by both the proposed method and the linear regression method are close to the average measured rate. However, the estimated COV of the wear rate by the proposed method is smaller than the result by the linear regression and the COV of the measured rate. This is because the latter two did not consider the effects of sizing error and uncertainty of the initial wall thickness properly.

Method	Estimated parameters	mean (mm/EFPY)	COV
Proposed MLE	$\mu = -2.31, \sigma = 0.165$	0.10	0.166
Linear regression	$\mu = -2.36, \sigma = 0.247$	0.098	0.251
Measured rate	N.A.	0.097	0.236

Table 4.2 Estimated parameters of the wear rate distribution by the proposed method and the regression method

Time to failure analysis

From the estimated parameters, predictions regarding the future wall thickness loss or time to failure distribution of uninspected tubes can be obtained.

For a randomly selected tube from the uninspected population, its wall thickness loss at time t is a random variable, denoted as $X(t)$,

$$X(t) = A + Rt,$$

where A is the distribution of the initial wear (i.e., difference between the nominal wall thickness and the actual initial value), and R is the estimated wear rate distribution. Since the initial wall thickness loss A and wear rate R are independent, CDF of $X(t)$ is given as the

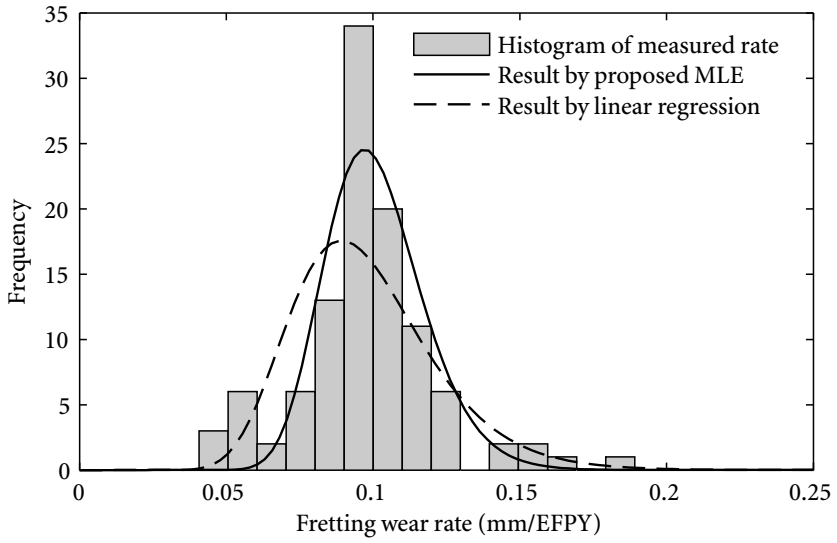

Figure 4.3 Estimated rate distribution compared with histogram of the measured rate

following convolution

$$F_{X(t)}(x) = \int_0^\infty F_A(x - rt) f_R(r) \mathrm{d}r,$$

where F_A is CDF of initial degradation A.

Suppose the maximum tolerable wall thickness loss with respect to the nominal initial wall thickness is x_{cr}. Tubes with wear greater than x_{cr} are considered to be failed units and should be replaced by new ones. The CDF of the failure time T of the uninspected tubes can then be calculated from $F_{X(t)}(x)$ using the following relation

$$\begin{aligned} F_T(t) &= \mathcal{P}[T \leqslant t] = \mathcal{P}[X(t) > x_{\mathrm{cr}}] \\ &= 1 - F_{X(t)}(x_{\mathrm{cr}}), \end{aligned}$$

The PDF of T can also be obtained by taking the derivatives of the corresponding CDF analytically or numerically.

The predicted wall thickness loss $X(t)$ and the remaining lifetime distribution T can be then used as input for the life cycle management of the SG tubes. Suppose in our case, the maximum acceptable wall thickness loss is $x_{\mathrm{cr}} = 3$ mm. PDF of the failure time distribution of the uninspected tubes are then calculated using parameters estimated from the proposed

method and the regression method, as plotted in Figure 4.4. The mean, SD and the 5% percentile of the time to failure distribution are also calculated as 30.4 EFPY, 5.5 EFPY and 22.7 EFPY using the proposed MLE, and 32.5 EFPY, 8.3 EFPY and 20.9 EFPY using the regression method. The predicted failure time by the linear regression has a larger SD and smaller 5% percentile. These differences will affect the optimal inspection and replacement planning of the SG tubes.

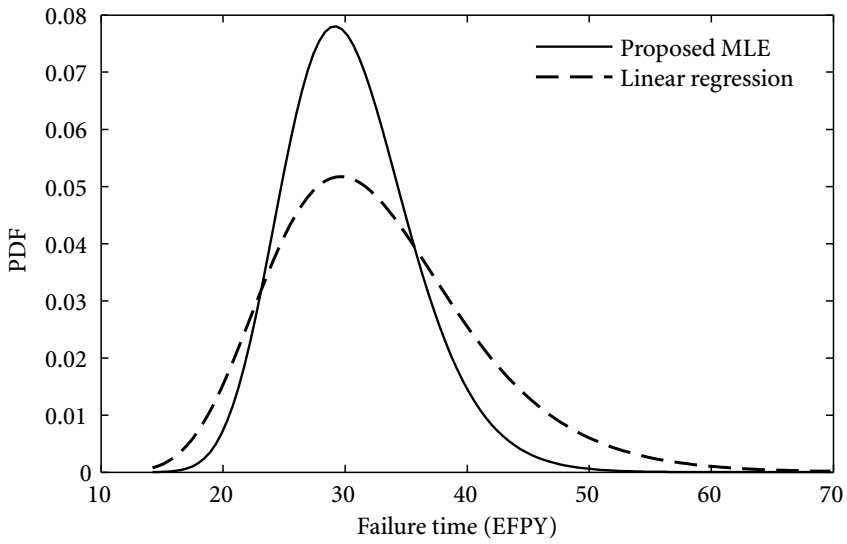

Figure 4.4 Failure time distribution of uninspected SG tubes by proposed method and linear regression

4.2.6 Remarks

In this section, an accurate ML method is developed for estimating flaw growth rate of arbitrary distribution from noisy measurements using the random rate model. This estimated growth rate distribution can then be used for reliability analysis of the uninspected components that suffer from the same degradation mechanism, as illustrated by the fretting wear example above.

For a more refined management of the degrading components, similar analysis should be conducted for each of the inspected components. However, due to the large sizing error and often limited number of repeated measurements, point estimate the component specific

rate cannot be obtained with high confidence. A better approach for the component specific analysis is to use Bayesian analysis, which is able to incorporate information from the flaw growth measurement of the component population. The component specific analysis of the random rate model will be discussed later in Chapter 6 when Bayesian method is introduced.

4.3 Gamma process model with sizing error

4.3.1 Problem statement

We now consider the likelihood formulation and parameter estimation of the gamma process model subject to normally distributed sizing errors. Unlike the random rate model, the gamma process model focuses on modelling the temporal fluctuation of the degradation process, while assuming that future flaw growths of different components follow the same gamma distribution.

When the flaw inspection is perfect, likelihood formulation of the gamma process model is simple. As discussed in Chapter 3, in the gamma process model, flaw growths over non-overlapped time intervals are independent random variables. Therefore, the model likelihood function is simply the product of the density functions of all flaw growth measurements. However, when the flaw measurement contains random sizing errors, this independence does not hold for the measured flaw growths anymore, despite the fact that the sizing errors themselves are usually assumed to be independent.

For example, suppose the flaw growths of a component over two adjacent time intervals $\Delta t_1 = t_2 - t_1$ and $\Delta t_2 = t_3 - t_2$ are given as ΔX_1 and ΔX_2. In gamma process model, ΔX_1 and ΔX_2 are two independent and gamma distributed random variables. When the flaw growths are measured using an uncertain inspection probe, random sizing errors are added to the data. Assume the sizing error at time t_i is E_i. $E_i \sim \mathrm{N}(0, \sigma_E^2)$ and are independent. The corresponding measured flaw growths of ΔX_1 and ΔX_2 can then be given as $\Delta Y_1 = \Delta X_1 + E_2 - E_1$ and $\Delta Y_2 = \Delta X_2 + E_3 - E_2$. Since ΔY_1 and ΔY_2 both contain term E_2, they are correlated. In fact, the covariance of ΔY_1 and ΔY_2 ($\mathrm{cov}(\Delta Y_1, \Delta Y_2)$) can be

calculated as

$$\begin{aligned}\operatorname{cov}(\Delta Y_1, \Delta Y_2) &= \operatorname{cov}(\Delta X_1 + E_2 - E_1, \Delta X_2 + E_3 - E_2) \\ &= \operatorname{cov}(\Delta X_1 - E_1, \Delta X_2 + E_3 - E_2) + \operatorname{cov}(E_2, \Delta X_2 + E_3 - E_2) \\ &= 0 - \operatorname{cov}(E_2, E_2) = -\sigma_E^2 \neq 0.\end{aligned} \tag{4.3.1}$$

In this case, the likelihood function of the model should not be written as the product of the density functions of ΔY_1 and ΔY_2. Instead, the joint PDF of ΔY_1 and ΔY_2 has to be used.

The correlation between the measured flaw growths makes the likelihood formulation and parameter estimation of the gamma process model much more difficult. Currently, approximate methods are mostly used. A common practice is to first delete the negative measured growths in the data and then estimating as if there is no sizing error (Camacho, 2006). Formal statistical analysis of gamma process model with sizing error included is still very limited. Kallen and van Noortwijk (2005) first gave the likelihood function of the gamma process model subjected to normally distributed sizing errors as a multidimensional integral. A crude Monte Carlo simulation is suggested for the numerical evaluation of the likelihood function. However, due to the computational difficulties of the crude Monte Carlo method, they assumed that the COV of the gamma process model is known and only estimated the average flaw growth rate.

In the next, following the work by Kallen and van Noortwijk (2005), the complete form of the likelihood function of the gamma process model with normally distributed sizing error is derived. To overcome the computational difficulty in the likelihood evaluation, a novel method combining the Genz's transform and quasi-Monte Carlo simulation is proposed. The effectiveness of the proposed numerical method is examined using Monte Carlo simulation. A practical case study on the flow-accelerated corrosion of SG tubes is presented.

4.3.2 Likelihood formulation

Suppose the degradation of a group of n components follows a gamma process model starting from zero and with shape parameter α and scale parameter β. The ith component is then inspected for m_i+1 times at time $t_{i0}, t_{i1}, t_{i2}, \cdots, t_{im_i}$. Using similar notations as in

the previous sections, denote the true degradation of the ith component at time t_{ij} as x_{ij} and the measured value of x_{ij} as y_{ij}. One has

$$y_{ij} = x_{ij} + e_{ij}, \quad i=1,2,\cdots,n, \quad j=0,1,2,\cdots,m_i,$$

where e_{ij} are the sizing errors associated with x_{ij}, and are realizations of *i.i.d.* normal random variables E_{ij} with mean zero and SD σ_E.

Let $\Delta t_{ij}=t_{ij}-t_{i,j-1}$, $\Delta x_{ij}=x_{ij}-x_{i,j-1}$, $\Delta y_{ij}=y_{ij}-y_{i,j-1}$ and $\Delta e_{ij}=e_{ij}-e_{i,j-1}$. Δx_{ij} are then the flaw growths during non-overlapped time intervals Δt_{ij}, Δy_{ij} are the measured values of Δx_{ij}, and Δe_{ij} are the associated error of Δy_{ij}. For sake of conciseness, let $\Delta\mathbf{x}_i$, $\Delta\mathbf{e}_i$ and $\Delta\mathbf{y}_i$ be the vectors consisting of all Δx_{ij}, Δe_{ij} and Δy_{ij}, $j=1,2,\cdots,m_i$, respectively. Obviously, one has $\Delta\mathbf{y}_i=\Delta\mathbf{x}_i+\Delta\mathbf{e}_i$

First, from previous discussions in Section 3.4.3, the actual degradation growth $\Delta\mathbf{x}_i$ is a sample from random vector $\Delta\mathbf{X}_i=\{\Delta X_{i1},\cdots,\Delta X_{im_i}\}$, whose elements ΔX_{ij} are independent and gamma distributed with shape parameter $\alpha\Delta t_{ij}$ and scale parameter β. The joint PDF of $\Delta\mathbf{X}_i$ is

$$f_{\Delta\mathbf{X}_i}(\Delta\mathbf{x}_i)=\prod_{i=1}^{m_i} f_{\Delta X_{ij}}(\Delta x_{ij})=\prod_{j=1}^{m_i}\frac{(\Delta x_{ij}/\beta)^{\alpha\Delta t_{ij}-1}}{\beta\Gamma(\alpha\Delta t_{ij})}\exp(-\Delta x_{ij}/\beta).$$

Now let us consider the probability density of $\Delta\mathbf{e}_i$. Clearly, $\Delta\mathbf{e}_i$ is a realization of some random vector $\Delta\mathbf{E}_i=\{\Delta E_{i1},\cdots,\Delta E_{im_i}\}$, where $\Delta E_{ij}=E_{ij}-E_{i,j-1}$, $j=1,\cdots,m_i$. Since E_{ij} are *i.i.d.* normal random variables with SD σ_E, ΔE_{ij} are also normal random variables. The mean and SD of ΔE_{ij} can be calculated as 0 and $\sqrt{2}\sigma_E$, respectively. However, only non-adjacent elements of $\Delta\mathbf{E}_i$ are independent. Adjacent elements, such as $\Delta E_{i,j-1}$ and ΔE_{ij}, are correlated and their covariance can be calculated as $\mathrm{COV}(\Delta E_{i,j-1},\Delta E_{ij})=-\sigma_E^2$ using steps similar to equation (4.3.1). Thus, $\Delta\mathbf{E}_i$ is a multivariate normal random vector. The mean of

$\Delta\mathbf{E}_i$ is $\{0, 0, \cdots, 0\}_{1\times m_i}$. The covariance matrix of $\Delta\mathbf{E}_i$, is a tridiagonal matrix given by

$$\Sigma_{\Delta\mathbf{E}_i} = 2\sigma_E^2 \begin{bmatrix} 1 & -1/2 & 0 & \cdots & 0 \\ -1/2 & 1 & -1/2 & \cdots & 0 \\ 0 & -1/2 & 1 & \cdots & 0 \\ \vdots & & \cdots & & \vdots \\ 0 & 0 & 0 & \cdots & 1 \end{bmatrix}_{m_i\times m_i}.$$

The joint PDF of $\Delta\mathbf{E}_i$ is

$$f_{\Delta\mathbf{E}_i}(\Delta\mathbf{e}_i) = \frac{1}{(2\pi)^{m_i/2}|\Sigma_{\Delta\mathbf{E}_i}|}\exp\left(-\frac{1}{2}\Delta\mathbf{e}_i\Sigma_{\Delta\mathbf{E}_i}^{-1}\Delta\mathbf{e}_i^T\right), \tag{4.3.2}$$

where $|\Sigma_{\Delta\mathbf{E}_i}|$ is the determinate of $\Sigma_{\Delta\mathbf{E}_i}$.

Because the measured degradation growth $\Delta\mathbf{y}_i = \Delta\mathbf{x}_i + \Delta\mathbf{e}_i$, it is thus clear that $\Delta\mathbf{y}_i$ is a sample from random vector $\Delta\mathbf{Y}_i = \{\Delta Y_{i1}, \Delta Y_{i2}, \cdots, Y_{im_i}\}$, and

$$\Delta\mathbf{Y}_i = \Delta\mathbf{X}_i + \Delta\mathbf{E}_i.$$

Because $\Delta\mathbf{X}_i$ and $\Delta\mathbf{E}_i$ are independent, the joint PDF of $\Delta\mathbf{Y}_i$, which is at the same time the likelihood function of the model parameters given measured flaw growth $\Delta\mathbf{y}_i$, is as the following convolution

$$\begin{aligned} L_i(\alpha,\beta|\Delta\mathbf{y}_i) &= f_{\Delta\mathbf{Y}_i}(\Delta\mathbf{y}_i) = \int_D f_{\Delta\mathbf{X}_i}(\Delta\mathbf{y}_i - \Delta\mathbf{e}_i) f_{\Delta\mathbf{E}_i}(\Delta\mathbf{e}_i)\mathrm{d}\Delta e_{i1}\cdots\Delta\mathrm{d}e_{im_i} \\ &= \int_{-\infty}^{\Delta y_{im_i}}\cdots\int_{-\infty}^{\Delta y_{i1}}\prod_{j=1}^{m_i} f_{\Delta X_i}(\Delta y_i - \Delta e_i) f_{\Delta\mathbf{E}_i}(\Delta e_{i1},\cdots,\Delta e_{im_i})\mathrm{d}\Delta e_{i1}\cdots\Delta\mathrm{d}e_{im_i}, \end{aligned} \tag{4.3.3}$$

where the region of integration D is defined by $\Delta y_{ij} - \Delta e_{ij} \geqslant 0$, $j = 1, 2, \cdots, m_i$.

The likelihood function, given measured flaw growth from a population of n components, can then be written as the product of the likelihood for each individual components as

$$L(\alpha,\beta \,|\, \Delta\mathbf{y}_1, \Delta\mathbf{y}_2, \cdots, \Delta\mathbf{y}_i) = \prod_{i=1}^{n} L_i(\alpha,\beta \,|\, \Delta\mathbf{y}_i). \tag{4.3.4}$$

4.3.3 Numerical evaluation of the likelihood

Crude Monte Carlo method

Equation (4.3.3) is a multi-dimension integral without closed form solutions and has to be evaluated numerically. For multi-dimension integrals, Monte Carlo method is generally preferable because its convergence rate $\mathcal{O}(N^{-1/2})$ is independent of the integration dimension s, compared to the convergence rate $\mathcal{O}(N^{-k/s})$ of the classical grid-based quadrature for an order k method (Caflisch, 1998).

Define the following function of $\Delta\mathbf{y}_i$ and $\Delta\mathbf{e}_i$ as

$$g(\Delta\mathbf{y}_i, \Delta\mathbf{e}_i) = \begin{cases} f_{\Delta\mathbf{X}_i}(\Delta\mathbf{y}_i - \Delta\mathbf{e}_i), & \Delta\mathbf{y}_i > \Delta\mathbf{e}_i, \\ 0, & \Delta\mathbf{y}_i \leqslant \Delta\mathbf{e}_i. \end{cases}$$

Likelihood function (4.3.3) can be rewritten as

$$\begin{aligned} f_{\Delta\mathbf{Y}_i}(\Delta\mathbf{y}_i) &= \int_D g(\Delta\mathbf{y}_i, \Delta\mathbf{e}_i) f_{\Delta\mathbf{E}_i}(\Delta\mathbf{e}_i) \mathrm{d}\Delta e_{i1} \cdots \Delta \mathrm{d}e_{im_i} \\ &= \int_{R^{m_i}} g(\Delta\mathbf{y}_i, \Delta\mathbf{e}_i) f_{\Delta\mathbf{E}_i}(\Delta\mathbf{e}_i) \mathrm{d}\Delta e_{i1} \cdots \Delta \mathrm{d}e_{im_i} \\ &= \mathsf{E}\left[g(\Delta\mathbf{y}_i, \Delta\mathbf{E}_i)\right], \end{aligned} \tag{4.3.5}$$

where $\mathsf{E}\left[g(\Delta\mathbf{y}_i, \Delta\mathbf{E}_i)\right]$ is the expectation of $g(\Delta\mathbf{y}_i, \Delta\mathbf{E}_i)$.

Equation (4.3.5) can be calculated using Monte Carlo method by generating sample points of $\Delta\mathbf{E}_i$ using the following steps:

- Generate N sets of independent and normally distributed sizing errors with mean zero and SD of σ_E as $\{e_{i0}^{(k)}, e_{i1}^{(k)}, \cdots, e_{im_i}^{(k)}\}, k = 1, 2, \cdots, N$.
- Calculate the corresponding sizing error differences $\Delta e_{ij}^{(k)} = e_{ij}^{(k)} - e_{i,j-1}^{(k)}, j = 1, 2, \cdots, m_i$.
- Let $\Delta\mathbf{e}_i^{(k)} = \{\Delta e_{i1}^{(k)}, \Delta e_{i2}^{(k)}, \cdots, \Delta e_{im_i}^{(k)}\}$. $\Delta\mathbf{e}_i^{(k)}, k = 1, 2, \cdots, N$, are N sets of samples of random vector $\Delta\mathbf{E}_i$.
- Equation (4.3.5) can then be approximately represented by the average of $g(\Delta\mathbf{y}_i, \Delta\mathbf{e}_i^{(k)})$ as

$$f_{\Delta\mathbf{Y}_i}(\Delta\mathbf{y}_i) \approx \frac{1}{N} \sum_{k=1}^{N} g(\Delta\mathbf{y}_i, \Delta\mathbf{e}_i^{(k)}),$$

where $\Delta\mathbf{y}_i = \{\Delta y_{i2}, \Delta y_{i3}, \cdots, \Delta y_{im_i}\}$ is the measured flaw growth of the ith component.

This method is suggested by Kallen and van Noortwijk (2005). Due to the computational difficulty of the method, they reduced the number of parameters of the gamma process model to one by fixing the coefficient of variation (COV) of the annual flaw growth and only estimate the average annual growth. We name this method as the crude Monte Carlo method.

The crude Monte Carlo method suffers from two important faults which would deteriorate its computational efficiency significantly, especially when used for ML estimation. Firstly, for components with several negative measured growths due to sizing error, only a small portion of the generated samples falls into the effective integration region D, where $g(\Delta\mathbf{y}_i, \Delta\mathbf{e}_i)$ has non-zero values. To grantee the accuracy of Monte Carlo simulation, more samples are required for such components. Secondly, the random nature of the Monte Carlo method leads to an unsmooth likelihood surface of the parameters α and β, which makes the convergence of the maximizing process difficult.

Proposed method

To overcome these deficiencies, an alternative method using the Genz's transform Genz (1992) and quasi-Monte Carlo (QMC) simulation is proposed for the ML estimation of the gamma process model. The method is described in details as follows.

(1) Genz's transform

Genz's transform is a sequence of transforms proposed by (Genz, 1992) for the numerical evaluation of multivariate normal probabilities. The main idea of Genz's transform is to covert the original multivariate normal integration into an integral over a unit hyper-cube but with a somewhat more complicated integrand.

Since the likelihood function of the gamma process model given by equation (4.3.3) has a multivariate normal density function as part of its integrand, Genz's transform can be applied similarly. After conducting the transform, the original likelihood function (4.3.3) is

converted into the following integral as

$$f_{\Delta \mathbf{Y}_i}(\Delta \mathbf{y}_i) = \int_0^1 \cdots \int_0^1 p(\mathbf{s}) \mathrm{d}\mathbf{s}, \tag{4.3.6}$$

where $\mathbf{s} = \{s_2, s_3, \cdots, s_{m_i}\}$ is the transformed variable of integration, $p(\mathbf{s})$ is the new integrand function calculated from the original integrand and be derived using the procedures given in Appendix A.1.

Sampling from the hyper-cubic region in integral (4.3.6) is equivalent to sampling directly in the effective integration region of the original likelihood function. Therefore, the transform reduces the required number of samples by not sampling from the ineffective integration region. Depending on the standard deviation of the sizing error, the number of repeated inspections, and the actual measured degradation growth, the number of samples required after applying the Genz's transform can ranges from less than 10% to about half of that required by an equivalent crude Monte Carlo integration.

(2) Quasi-Monte Carlo simulation

To further improve the computational efficiency, quasi-Monte Carlo (QMC) simulation can be used as a drop-in replacement of the Monte Carlo simulation for the numerical integration. Instead of drawing random (or pseudo-random) samples, QMC simulation uses carefully constructed deterministic sequences, called low discrepancy sequences (LDS), which are able to fill the integration region with better uniformity than a random sequence (Niederreiter, 1992). Common low discrepancy sequences used in QMC method include Halton sequence (Halton, 1964) and Sobol sequence (Sobol, 1967). Figure 4.5 shows the comparison between a Halton sequence and a random sequence over a unit region. It can be observed from the figure that the Halton sequence covers the region with better uniformly; whereas the random sequence shows gaps and clustering of points. For a general review on the construction of LDS, refer to Niederreiter (1992).

It is found that QMC simulation may outperform the Monte Carlo simulation in terms of convergence rate and required number of samples for having certain accuracy for a wide range of numerical problems (Niederreiter, 1992). The use of QMC simulation in the numerical integration of multivariate normal probabilities together with the Genz's transform was investigated by Beckers and Haegemans (1992) and showed to have better

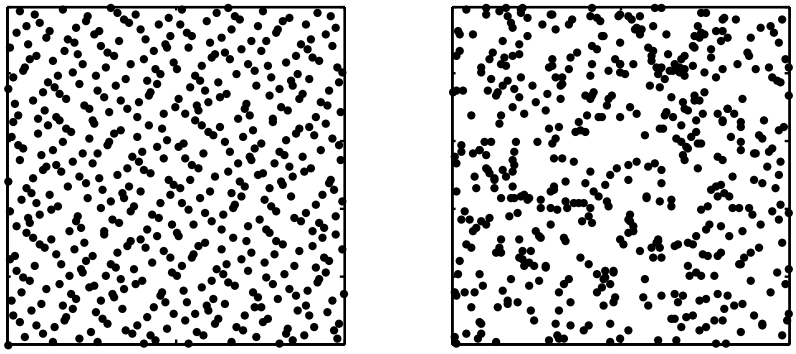

Figure 4.5 Comparison between the Halton sequence and random sequence

performance than using Monte Carlo simulation in high dimension cases. The combination of QMC and Genz's transform can be similarly applied to the numerical integration of the likelihood function of gamma process subject to normal sizing errors. As will be illustrated in a numerical example in the next, using the Genz's transform and QMC, the number of samples needed for having certain accuracy in the likelihood evaluation can be reduced by more than an order of magnitude compared to the crude Monte Carlo method. The detailed steps of the likelihood evaluation using Genz's transform and QMC are given as follows:

- Transform the original likelihood function (4.3.3) into equation (4.3.6) using Genz's transform.

- Construct an LDS of dimension m_i and length N over the unit-hyper cubic. Denote the constructed LDS as $\mathbf{s}_i^{(k)} = \{s_{i2}^{(N)}, s_{i3}^{(k)}, \cdots, s_{im_i}^{(k)}\}, k = 1, 2, \cdots, N$.

- Likelihood function $L_i(\alpha, \beta \mid \Delta\mathbf{y}_i)$ can then be approximated by the following sum as

$$f_{\Delta\mathbf{Y}_i}(\Delta\mathbf{y}_i) \approx \frac{1}{N}\sum_{k=2}^{N} p(\mathbf{s}_i^{(j)}),$$

  where $p(\mathbf{s}_i^{(j)})$ is the integrand of equation (4.3.6). Functional form of $p(\mathbf{s}_i^{(j)})$ is obtained using the procedures described in the Appendix A.1.

4.3.4 Comparison of computational efficiency

A numerical example with a small data-set is presented here to show the effectiveness of the proposed method. The data consist of the inspection data of the remaining wall thickness of 5 pipes in a steam generator as listed in Table 4.3. The pipes were inspected at most for 7 times, indicating the overall likelihood is a product of a number of integrals up to 6 dimensions. The time index for the wall thickness measurements is converted into the equivalent operating time at the plants full capacity, i.e., the effective full power year or EFPY. The standard deviation of sizing error is assumed to be 0.05 mm. Two comparisons between the crude Monte Carlo method and the proposed method are conducted: (1) the accuracy of likelihood evaluation with a given number of samples, and (2) the overall efficiency of maximum likelihood estimation.

	Inspection time (EFPY)						
	0	5.16	6.78	7.91	10.2	11.5	14.3
Pipe 1	6	5.74	5.56	5.48	5.31	5.19	4.90
Pipe 2			5.68		5.39	5.27	
Pipe 3	5.9	5.74	5.55	5.48		5.19	4.89
Pipe 4			5.70		5.3	5.25	
Pipe 5	5.8	5.74	5.57	5.47	5.28	5.18	4.94

Table 4.3 Measured wall thickness (in mm) of a group of pipes in a nuclear plant

Accuracy of likelihood evaluation

To examine the accuracy of the crude Monte Carlo method and the proposed method, the log-likelihood function of the 5 pipes is evaluated with parameters $\alpha = 4.8$, $\beta = 0.015$ (where the likelihood is close to the maximum) using both methods. Different number of samples, from 10^4 to 10^6, are used in the calculation and the results are compared to the reference value 25.47, which is calculated by the crude Monte Carlo method using very large sample size ($N = 10^8$). For the crude Monte Carlo method, for each number of samples, the calculation is repeated for 200 times and the standard error of the results is recorded. For the proposed method, Halton sequence is used. Because of the deterministic nature of

QMC, the likelihood evaluation using the same number of samples is always a fixed number. The error of the proposed method is thus compared with the standard error of the crude Monte Carlo method with the same number of samples.

The result of the simulation is presented in Figure 4.6. As can be observed from the figure, the proposed method already gives an accurate result at $N = 10^5$ while the crude Monte Carlo result still shows significant variability at $N = 10^6$. The proposed method shows better performance than the crude Monte Carlo over an order of magnitude in terms of required number of samples for having certain accuracy.

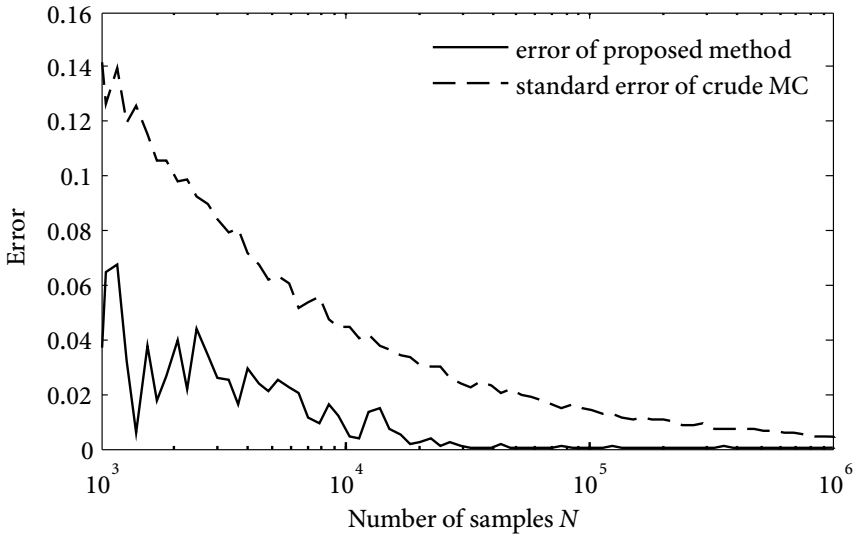

Figure 4.6 Comparison of the accuracy of likelihood evaluation using the crude Monte Carlo method and the proposed method

Overall efficiency of maximum likelihood estimation

By using the proposed method, the number of required samples for the likelihood evaluation can be reduced significantly. But this comes at a price of calculating a more computationally expensive integrand $p(\mathbf{s})$. For example, with both 10^5 samples, the numerical evaluation of the likelihood of the 5 pipes at parameters $\alpha = 4.8$ and $\beta = 0.015$ using the proposed method takes about 9 seconds; whereas the crude Monte Carlo method only takes about 1 second (CPU: Intel E2700).

However, if one's objective is to find the ML estimate of the model parameters, the numerical efficiency of the proposed method can be much better comparing to its efficiency in a single likelihood evaluation. There are two reasons. First, when conducting the ML estimation, the likelihood function needs to be evaluated repeatedly with respect to different values of model parameters. Because of the deterministic nature of the QMC method, the generated samples in each evaluation are identical. Therefore, much of the time consuming Genz's transform only needs to be conducted once in the first likelihood evaluation and the results can be stored for later use. Subsequent evaluations of the likelihood thus take about the same time as the crude Monte Carlo method with same number of samples. Secondly, unlike the crude Monte Carlo method, QMC gives a smooth likelihood surface because of the deterministic nature of LDS, making it easier for the maximization algorithm to converge.

ML estimation of parameters α and β given the measured data of the 5 pipes in Table 1 is conducted using both the proposed method and the crude Monte Carlo method. To have similar accuracy for both methods, the number of samples used in the proposed method is chosen as 10^5, and the number of samples for the crude Monte Carlo method is 10^6. Initial values of the maximization for both methods are $\alpha = 1$ and $\beta = 1$. The result and the time taken for the ML maximization are listed in Table 4.4.

4.3.5 Example: flow-accelerated corrosion of feeder pipes

Background

A case regarding the flow-accelerated corrosion (FAC) of feeder pipes in a nuclear power plant is presented here to illustrate the use of the proposed method with a larger practical data-set. The data-set contains wall thickness measurements of feeder pipes of a nuclear power plant during the period of ten years from 1999 to 2009. Because there are no reliable data on the initial wall thickness of these pipes, only pipes with more than one inspection are considered. In total, there are 50 feeder pipes in the data-set, with 26 pipes inspected twice, 13 inspected thrice, and the rest 11 inspected four or five times. The sizing error of the inspection probes is assumed to be normally distributed with mean 0 and SD of 0.05 mm. The first inspection conducted in 1999 is at EFPY of 5.16 and the last inspection in

	Proposed method	Crude Monte Carlo
Number of Samples	10^5	10^6
Initial value	$\alpha = 1, \beta = 1$	
1st likelihood evaluation	9.4 seconds	12.1 seconds
Subsequent evaluations	Average time: 0.8 seconds	Average time: 11 seconds
Total number of evaluations	26	34
Total time	$9.4 + 25 \times 0.8$ $= 29.4$ seconds	34×11 $= 374$ seconds
ML estimate	$\alpha = 4.77, \beta = 0.0155$	$\alpha = 4.71, \beta = 0.0157$

Table 4.4 ML estimation using the proposed method and the crude Monte Carlo method (CPU: Intel E2700)

2009 is at 14.3 EFPY. Figure 4.7 shows the wall thinning path of several typical feeders in the data-set, from which significant temporal variations can be observed. Therefore, the gamma process model is applied.

The objective of this case study is: (1) to apply the proposed method for ML estimation of the gamma process model; (2) to compare the differences between the ML estimations using the likelihood function with and without considering sizing errors.

Parameter estimation

Two maximum likelihood methods are applied for the analysis of the wall thickness data. The first method is to use the likelihood function (4.3.4) which considers the effects of the sizing errors. In the second method, one first deletes all the negative measured growth and then analyzes the remaining data using likelihood function (3.4.2) derived previously in Chapter 3, which does not consider sizing error. In total, there are 87 measured growths, 4 of which are negative and are deleted in the second method.

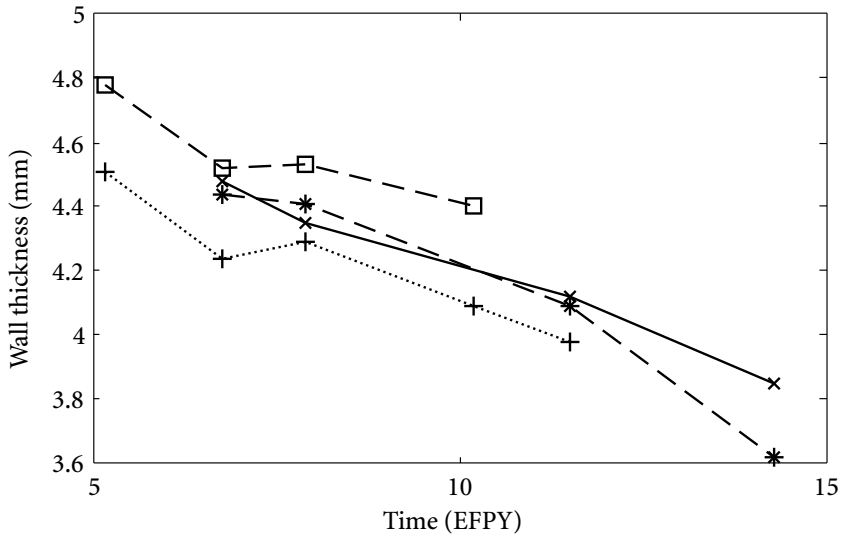

Figure 4.7 Variation of measured wall thickness of some feeder pipe over time

Numerical evaluation of the likelihood function with sizing error is conducted using the proposed method with Genz's transform and QMC simulation with sample size $N = 2 \times 10^5$. The first evaluation of the likelihood function with sizing error takes about 3 minutes and the following evaluations each takes about 15 seconds using a desktop computer. The likelihood function without sizing error is given in analytic form and therefore its numerical evaluation is straightforward.

Simplex algorithm (Rao and Rao, 2009) is used to find the maximum value of the likelihood, which does not require the derivative of the likelihood functions. With properly selected initial value of the parameters, number of likelihood evaluations needed in the maximization process is typically less than 50. Therefore, the whole ML estimation using the proposed method can be finished in less than 20 minutes.

The results of the parameter estimation using the two likelihood functions are listed in Table 4.5. From the results, it can be observed that the two maximum likelihood methods give similar estimations on the average thinning rate, with only 3% difference between the two; whereas the estimated COV of the annual thinning using likelihood without sizing error is about 29% higher that the estimation using the accurate likelihood function.

Method	Estimated parameters	Annual wall thinning
Likelihood with sizing error	$\alpha = 4.89$ $\beta = 0.015$	mean: $\mu = 0.071$, COV: $\nu = 0.45$ 95th upper bound: 0.13
Likelihood without sizing error	$\alpha = 2.93$ $\beta = 0.025$	mean: $\mu = 0.073$, COV: $\nu = 0.58$ 95th upper bound: 0.16

Table 4.5 ML estimate of the model parameters using likelihood function with and without considering the sizing errors

Goodness of fitting

To examine the goodness of fitting of the estimated parameters, one would like to compare the fitted model with the actual data. Because the recorded data by inspection probe contain random sizing errors, it is not appropriate to conduct this comparison directly. Instead, the random sizing error should be added to predicted thinning from the fitted model. Denote the predicted wall thinning of the pipes during time interval $[t, t+\tau]$ from the fitted model as $X_G(\tau)$. According the definition of the gamma process, $X_G(\tau)$ is gamma random variable with shape parameter $\alpha\tau$ and scale parameter β, where α and β are the fitted model parameters. The predicted measured value of $X_G(\tau)$, denoted as $X_{MG}(\tau)$, is given as follows

$$X_{MG}(\tau) = X_G(\tau) + E_2 - E_1,$$

where E_1 and E_2 are the normally distributed sizing errors at the beginning and the end of the time interval. Upper and lower bound of $X_{MG}(\tau)$ can then be used to compare with the actual NDE measured growth to test the goodness of the estimated parameters.

Figure 4.8 plots the 5% and 95% bound of $X_{MG}(\tau)$ from both method. It is shown that 4 out of total 87 measured data points is beyond the 95% upper bound calculated with likelihood function considering sizing error. The ratio is 4.6%, which matches the chosen upper bound well. On the contrary, only 1 measured data point is beyond the 95% upper bound calculated using the parameters calculated without consider sizing error and the ratio is 1.1%.

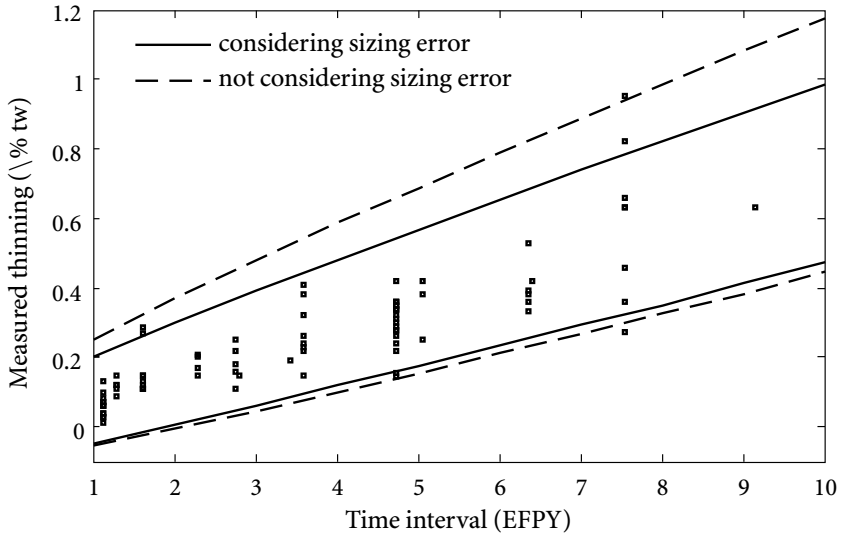

Figure 4.8 5% and 95% percentile of the measured thinning since first inspection by fitted models versus actual readings

Time to failure analysis

In the gamma process model, since the flaw growth of the components is independent of the current degradation and follows the same distribution across the population, the future flaw size and the failure time distribution can be obtained similarly for both inspected and uninspected components.

In our example of feeder thinning, suppose the measured wall thickness of a feeder at time t_m is y_m. A practical estimation of the remaining wall thickness at a future time t, denoted as $X(t)$, can be given as

$$X(t) = y_m - E - \Delta X(t - t_m),$$

where $E \sim N(0, \sigma_E^2)$ is the random variable for sizing error, $\Delta X(t-t_m)$ is the predicted flaw growth between time t_m and t and is a gamma random variable with parameter $\alpha(t-t_m)$ and β. Since the flaw growth $\Delta X(t-t_m)$ and sizing error E are independent, CDF of $X(t)$ is

given

$$\begin{aligned} F_{X(t)}(x) &= \bar{\mathcal{P}}\left(y_m - E - \Delta X(t-t_m) \leqslant x\right) \\ &= \bar{\mathcal{P}}\left(E + X(t-t_m) \geqslant y_m - x\right) \\ &= 1 - \int_{-\infty}^{\infty} F_{\mathrm{Ga}}(y_m - x - e; \alpha(t-t_m), \beta)\phi(e; 0, \sigma_E^2)\mathrm{d}e. \end{aligned}$$

Given the minimum wall thickness requirement as x_{cr}, CDF of the failure time distribution of the component is

$$\begin{aligned} F_T(t) &= \bar{\mathcal{P}}\left(T \leqslant t\right) = \bar{\mathcal{P}}\left(X(t) \leqslant x_{\mathrm{cr}}\right) \\ &= F_{X(t)}(x). \end{aligned} \tag{4.3.7}$$

From the estimated model parameters, CDF of the predicted failure time of all the feeders can be calculated. Take one feeder from the data-set as an example. The latest inspection of the feeder is at 11.5 EFPY and the measured wall thickness is 4.15 mm. The minimum wall thickness requirement of the feeders is given as $x_{\mathrm{cr}} = 3.1$ mm. CDF of the predicted failure time distributions using the estimated parameters considering and not considering sizing error are calculated and plotted in Figure 4.9. If considering the sizing error, the mean, SD and the 5% percentile of the time to failure distribution are 25.9 EFPY, 1.8 EFPY and 23.0 EFPY, respectively. If not considering the sizing error, the corresponding predictions are 26.0 EFPY, 2.4 EFPY and 22.3 EFPY.

4.4 Summary

In this chapter, estimation of flaw growth models from noisy measurement is discussed. Two specific models, the random rate model and the gamma process model, are considered.

For the random rate model, first some current methods, including method of moments, simulation method and regression method, are reviewed and their limitations are summarized. After that, likelihood function of the random rate model is derived for noisy measurements in the setting of a two-stage hierarchical model. ML estimate of the model parameters can then be obtained using well established numerical methods. The proposed ML method is more accurate than the current methods, and can handle repeated inspection

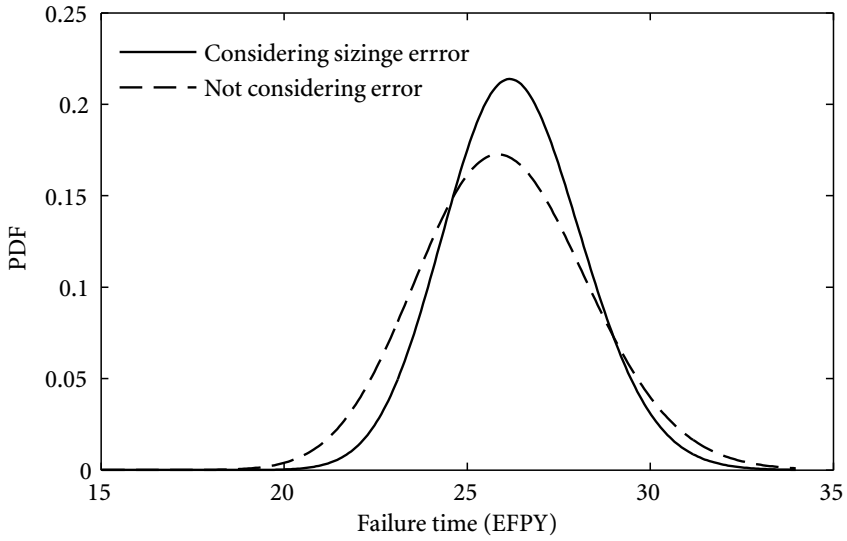

Figure 4.9 Time to failure distribution of a selected feeder with latest measured wall thickness 4.15 mm at 11.5 EFPY

data, arbitrary rate distribution and uncertain initial degradation in a statistically sound manner.

For the gamma process model, following the work by Kallen and van Noortwijk (2005), the complete form of the likelihood function given measurements with normally distributed sizing error is derived. A novel numerical method combining the Genz's transform and quasi-Monte Carlo method is proposed to overcome the computational difficulties in the likelihood evaluation. It is shown from a simulation study that the proposed method is able to improve the numerical efficiency of the crude Monte Carlo method by an order of magnitude.

CHAPTER 5

Estimation of Flaw Generation Model

5.1 Introduction

5.1.1 Literature review

This chapter discusses parameter estimation of flaw generation model using uncertain inspection data. The flaw generation models are often used to predict the initiation of localized corrosion in a steel structure, or the generation of new cracks on a concrete surface. Predicting the occurrence of defective individuals among a large group of identical components can also be regarded as an application of flaw generation models.

Stochastic models have long been used to model various flaw generation processes. One of the most widely used stochastic process for modelling flaw generation is the Poisson process, as can be seen at Hong (1999); van Noortwijk and Klatter (1999); Nicolai et al. (2007); Valor et al. (2007). However, most of these applications use data obtained from well-controlled laboratory testings, where the detection and measurement of the flaws are fairly accurate. Investigations on the parameter estimation of stochastic flaw generation model using uncertain field data are still limited.

An important fact about the stochastic modelling of flaw generation with uncertain inspection data is that when the flaw detection is not perfect, statistical inferences regarding the flaw generation and the flaw size are often closely interrelated even if the generation process and flaw size themselves are assumed to be independent. This is because when PoD

is involved, the detection of the flaws depends on the distribution of the flaw size; while at the same time the flaw size distribution itself cannot be precisely determined due to the sizing error and the undetected flaws. Because of the complexity of the problem, many approximate methods are developed. For example, Rodriguez (1989) considered the issue of PoD by dividing the detected flaws into a number of groups according to the flaw size. Then, the actual number of flaws for each group is calculated as the number of detected flaws in each group divided by the averaged PoD of that group. The effect of sizing error is not included in Rodriguez's analysis. Datla et al. (2008) worked around the issue of PoD and sizing error by considering only larger flaws on which the inspection uncertainties have relatively little impact.

Only a handful papers, including Yuan et al. (2009) and Kuniewski and van Noortwijk (2009), that considered the inspection uncertainties in the estimation of flaw generation model in a formal manner. Yuan et al. (2009) developed a stochastic model for the pitting flaws in the steam generator tubes using field data. In their model, the pitting initiation is simulated using a non-homogeneous Poisson process and the pit depth is considered to be stable (i.e., flaw size does not change over time) and follows a Weibull distribution. Both PoD and sizing error are considered. Kuniewski and van Noortwijk (2009) developed a general stochastic model for localized degradation from a single inspection. In Kuniewski and van Noortwijk's model, the flaw initiation is simulated using a non-homogeneous Poisson process; whereas the flaw growth is modelled using a stationary gamma process. However, only PoD is included in their analysis and flaw sizing is considered to be accurate.

It is worth noting that when repeated inspections are presented, accurate stochastic modelling of the flaw generation can be affected greatly by the inspection tools and maintenance strategies. For example, it is often the case that the detected flaws are not tracked across repeated inspections, or a previously detected flaw may not be detected in subsequent inspections, or certain detected flaws are required to be repaired or eliminated before the next inspection. Specific considerations of these factors must be taken when analyzing the flaw generation data. In the Poisson flaw generation model by Yuan et al. (2009), the difficulties regarding the repeated inspections are avoided by assuming that the inspection probe is able to report only new generated flaws in each inspection. With this assumption, previously

detected *and* undetected flaws are both excluded from the analysis of future inspections, and repeated inspections are therefore simplified to a series independent single inspections.

5.1.2 "Repair-on-detection" strategy

In this chapter, we consider the flaw generation problem with repeated inspections using the Poisson process model, under the so-called "repair-on-detection" maintenance strategy that is commonly employed in many safety-critical systems. The "repair-on-detection" maintenance strategy simply says that all the detected flaws should be repaired or eliminated before continuing the operation of the system (EPRI, 2006a). Therefore, previously detected flaws need not to be considered in subsequent inspections. The difference between the "repair-on-detection" strategy and the assumption that the probe is able to report only new generated flaws (Yuan et al., 2009) is that, by the latter assumption, previously undetected flaws are always ignored; whereas under the "repair-on-detection" strategy, the undetected flaws left from previous inspections may still be detected in future and therefore should be taken into account in the analysis.

5.1.3 Organization

The chapter is organized as follows. First, in Section 5.2, a simplified version of the Poisson flaw generation model is formulated, where the flaw size is irrelevant and the PoD is a constant. Likelihood function of the simplified model is derived and the accuracy of the likelihood function is validated by a numerical simulation. Based on the results of the simplified model, the complete flaw generation model under "repair-on-detection" strategy is investigated in Section 5.3. Likelihood function of repeated inspection data contaminated with both PoD and sizing error are derived, which turns out to be a very complicate function with a large number of convolution calculations. Computational issue and approximated likelihood functions are discussed. A numerical simulation is conducted and the accuracy of the complete likelihood and approximate likelihood functions is examined. Finally, summary of the chapter is given in the end as Section 5.4.

5.2 Poisson process model with PoD

In this section, we first consider a simplified version of the Poisson flaw generation model in which the size of the flaw is irrelevant. That is to say that: (1) probability of detection is assumed to be a constant regardless the flaw size; (2) only the number of flaws is of our concern.

5.2.1 Problem statement

Suppose the flaw initiation in a structure follows a homogeneous Poisson process with an unknown rate λ. At time zero, there are no flaws. In total, n inspections are performed at times $t_1, t_2, \cdots, t_n$, to determine the number of flaws in the structure. PoD of the inspection probe is a constant p regardless the flaw size. The "repair-on-detection" strategy is employed. Thus, all the detected flaws are repaired or removed immediately after the inspection so that no flaws will be detected twice.

Denote the number of actual flaws in the structure at the ith inspection as m_i and the number of detected flaws in m_i as d_i. According to the random nature of the Poisson process, m_i and d_i are both realizations of some random variables, denoted as M_i and D_i, respectively. For the convenience of discussion, M_i and D_i are also used to indicate the collection of all flaws and the detected flaws at the ith inspection, respectively. For example, when saying that a flaw is in D_i, it means that this specific flaw is one of the D_i detected flaws in the ith inspection. Our objective is to derive the joint distribution of $\mathbf{D} = \{D_1, D_2, \cdots, D_n\}$, from which the ML estimate of the Poisson rate λ can be obtained.

The derivation of the model likelihood is divided into three steps:

- Derive the likelihood function for the first inspection. Since at time zero there is no flaw in the structure, the likelihood given the first inspection data does not need to consider previously undetected flaws. This step is given in Section 5.2.2.
- Derive the likelihood function for subsequent inspections. The major difficulty for the subsequent inspections is how to handle the previously undetected flaws properly. In our derivation, this is done by dividing actual number of flaws in the structure at the ith inspection, M_i, into i subsets: $M_{1i}, M_{2i}, \cdots, M_{ii}$, where M_{ji} is the set of flaws

that initiated during time interval $(t_{j-1}, t_j]$ but remain undetected before time the ith inspection at t_i. This step is described in Section 5.2.3

- According to the splitting property of Poisson process, it can be shown that flaw detection data at different inspections are independent. Therefore, the overall model likelihood function is the product of the likelihood of each single inspection. A simulation study on the bias and RMSE of the ML estimate using the obtained likelihood function is presented in Section 5.2.4, which validates the accuracy of the derived likelihood function.

5.2.2 First inspection

Let $t_0 = 0$ and $\Delta t_i = t_i - t_{i-1}, i = 1, 2, \cdots, n$. Δt_i are then the time intervals between successive inspections. We start from the 1st inspection at time t_1. From the definition of Poisson process, the actual number of flaws at time t_1, M_1, is a Poisson distributed random variable with rate $\lambda \Delta t_1$, i.e.,

$$M_1 \sim \text{Pois}(\lambda \Delta t_1).$$

For a random selected flaw in M_1, it will either be detected in the first inspection with probability p, or left as undetected with probability $1-p$. According to the splitting property of Poisson process, the number of detected flaws in the first inspection, D_1, is a Poisson random variable with rate $p\lambda \Delta t_1$ and is independent of M_1, i.e.,

$$D_1 \sim \text{Pois}(p\lambda \Delta t_1).$$

The likelihood function of λ given number of detection $D_1 = d_1$ is then the probability mass function (PMF) of D_1 and is given as

$$L(\lambda \,|\, d_1) = f_{D_1}(d_1) = \frac{(p\lambda \Delta t_1)^{d_1}}{d_1!} \exp(-p\lambda \Delta t_1).$$

5.2.3 Repeated inspections

We now consider the repeated inspections for the flaw generation process. Suppose at the 2nd inspection at time t_2, there are in total M_2 flaws. Since all the detected flaws in the 1st

inspection were eliminated, flaws in M_2 can only come from two sources: the undetected flaws in the 1st inspection and the new generated flaws during time t_1 and t_2. Denote the former category as M_{12} and the latter as M_{22}. An illustrative plot of the number of detected and undetected flaws in the 1st and 2nd inspections is given in Figure 5.1.

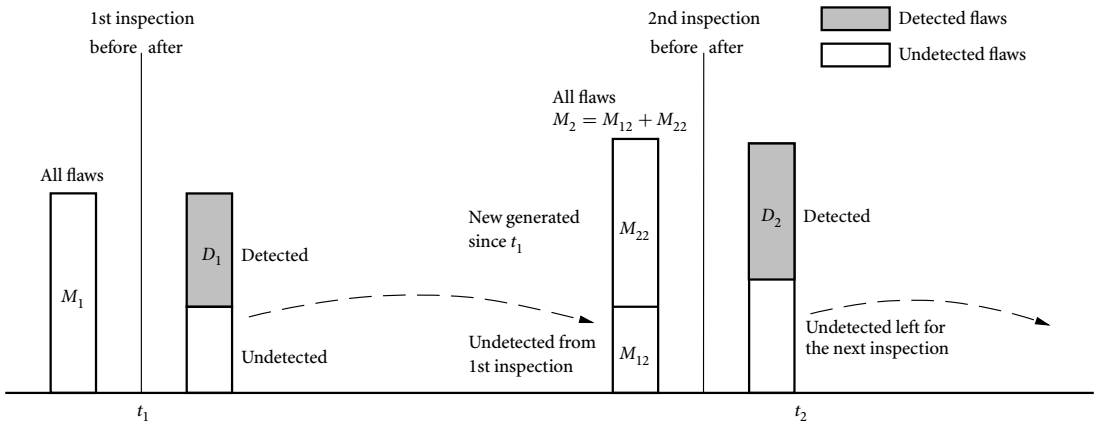

Figure 5.1 Illustration of number of detected and undetected flaws in the 1st and 2nd inspections

Since M_{12} are the undetected flaws in the first inspection, according to the Poisson splitting property, M_{12} is a Poisson distributed random variable with rate $(1-p)\lambda\Delta t_1$ and is independent of D_1. From the definition of Poisson process, M_{22} is Poisson distributed with rate $\lambda\Delta t_2$ as is independent of M_1, D_1 and M_{12}. Therefore, the total number of flaws at time t_2, M_2, which is the sum of M_{12} and M_{22}, is Poisson distributed with rate $(1-p)\lambda\Delta t_1+\lambda\Delta t_2$, i.e.,

$$M_2 \sim \text{Pois}(\lambda\Delta t_2+(1-p)\lambda\Delta t_1) \tag{5.2.1}$$

The number of detected flaws in the second inspection, D_2, is then a Poisson random variable given as

$$D_2 \sim \text{Pois}(p\lambda\Delta t_2+p(1-p)\lambda\Delta t_1).$$

Obviously, D_2 and D_1 are independent.

In general, flaws at the ith inspection, M_i, can be divided into i independent categories as $M_{1i}, M_{2i}, \cdots, M_{ii}$, where $M_{ji}, j=1,2,\cdots,i$, stands for the flaws that initiated during time interval $(t_{j-1}, t_j]$ but remain undetected before the ith inspection at time t_i. Since flaws in M_{ji}

remain undetected after a total of $i-j$ independent inspections with PoD p, using Poisson splitting property, M_{ji} is a Poisson distributed with rate $\lambda(1-p)^{i-j}$. The total number of flaws M_i, as the sum of all M_{ji} is therefore Poisson distributed as

$$M_i \sim \text{Pois}\left(\lambda \sum_{j=1}^{i} (1-p)^{i-j} \Delta t_j\right).$$

The number of detected flaws in M_i, i.e., D_i, is Poisson distributed as

$$D_i \sim \text{Pois}\left(p\lambda \sum_{j=1}^{i} (1-p)^{i-j} \Delta t_j\right).$$

The PMF of D_i is

$$f_{D_i}(d_i;\lambda) = \frac{(\lambda_i)^{d_i}}{d_i!} \exp(-\lambda_i),$$

where $\lambda_i = p\lambda\left(\sum_{j=1}^{i}(1-p)^{i-j}\Delta t_j\right)$. Denote the number of detected flaws in all the inspections in the vector form as $\mathbf{d} = \{d_1, d_2, \cdots, d_n\}$. According to the properties of Poisson process, D_i are all independent, and the likelihood function of the Poisson rate λ given $\mathbf{d}$ is the following product

$$L(\lambda \,|\, \mathbf{d}) = \prod_{i=1}^{n} f_{D_i}(d_i;\lambda). \tag{5.2.2}$$

5.2.4 Numerical validation

A Monte Carlo simulation of the flaw generation and detection is conducted in order to numerically validate the likelihood function derived above. In the simulation, the actual number of flaws are generated using a homogeneous Poisson process with rate $\lambda = 2$ flaws/year. Three inspections are performed to the generated data at 4, 8 and 12 years using an imaginary inspection probe with a constant PoD p. After each inspection, all detected flaws are removed from the data-set to simulate the "repair-on-detection" maintenance strategy. ML estimation of the Poisson rate is then obtained by maximizing likelihood function (5.2.2) using the generated inspection data. The above procedures are repeated for 500 times and the bias and RMSE of the estimated λ are examined.

Parameter estimation using the generated inspection data is also conducted using an approximate method similar to the method used by Yuan et al. (2009), in which all previously undetected flaws are ignored. In the approximate method, the detected flaws in the ith inspection, D_i, are assumed to come only from the new generated M_{ii} flaws, which is Poisson distributed with rate $\lambda\Delta t_i$. Therefore, in the approximate method, D_i is a Poisson random variable with rate $p\lambda\Delta t_i$. The approximate likelihood function of λ is given as

$$L(\lambda \,|\, \mathbf{d}) = \prod_{i=1}^{n} \frac{(p\lambda\Delta t_i)^{d_i}}{d_i!} \exp(-p\lambda\Delta t_i),$$

The simulation is carried out for different values of PoD p, ranging from 0.1 to 1. The bias and RMSE of the ML estimation using both likelihood functions are obtained and the results are plotted in Figure 5.2 and 5.3, respectively. From the results, it can be seen that the likelihood function we derived gives unbiased estimates of the Poisson rate λ for any value of PoD; whereas the approximate method over-estimates λ. The difference between the two estimates becomes insignificant only when PoD of the inspection probe is over 0.9.

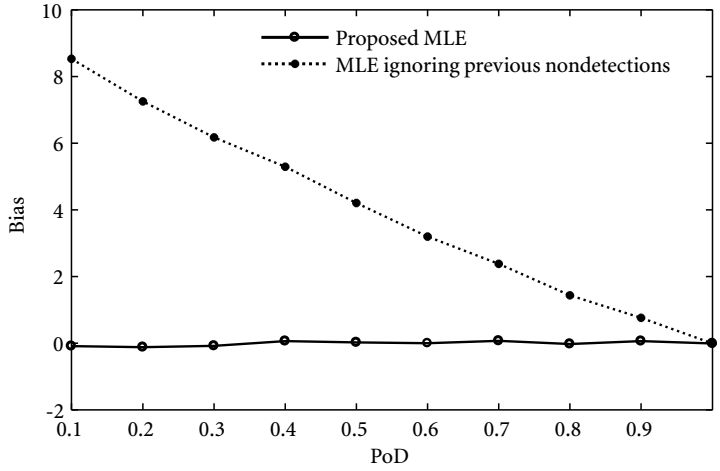

Figure 5.2 Bias of the estimated flaw generation rate using the accurate likelihood function and the approximate likelihood function

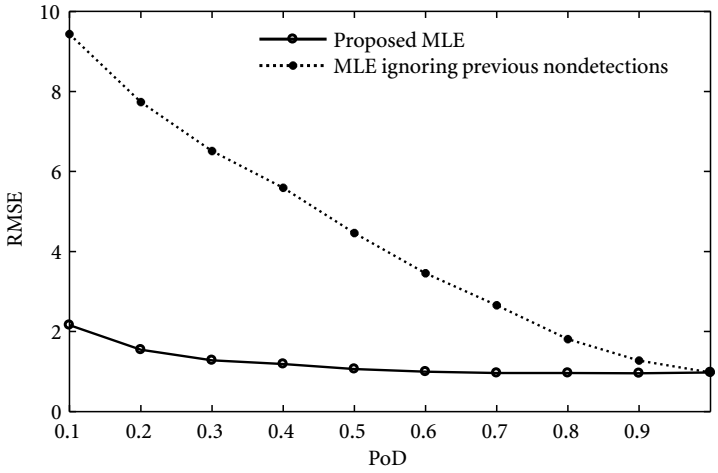

Figure 5.3 RMSE of the estimated flaw generation rate using the accurate likelihood function and the approximate likelihood function

5.3 Poisson process model with PoD and sizing error

5.3.1 Problem statement

In this section, based on the results of the simplified model discussed in the previous section, a complete Poisson flaw generation model with both PoD and sizing error investigated, still using the "repair-on-detection" maintenance strategy. In the complete model, the flaw generation is still assumed to follow a homogeneous Poisson process with rate λ. The flaw size, on the other hand, is assumed to be stable and follows some positively defined probability distribution $f_X(x;\theta)$, where θ is the distribution parameter and is often omitted in the derivation for the sake of conciseness. In addition, the flaw size and flaw generation are considered to be independent.

Suppose at time $t_0 = 0$, there are no flaws presented. The inspections of the flaws are conducted at time $t_1, t_2, \cdots, t_n$. PoD of the inspection probe is a function of the flaw size and is denoted as $p(x)$. The sizing error of the inspection probe, E, is assumed to be independent and normally distributed with mean zero and SD σ_E. To be simple, we also assume that PoD and sizing error are two separate properties of the inspection probe. That

is in the inspection the probe first detects certain flaws and then reports its measured flaw size.

In the inspection, both the number of detected flaws and their measured sizes are reported. Denote the inspection result in the ith inspection as $\mathbf{y}_i = \{y_1, y_2, \cdots, y_{d_i}\}$, where d_i is the total number detected flaws in the ith inspection. Obviously, d_i, y_{ij} are all realizations of their corresponding random variables, denoted as D_i and Y_{ij}. The objective is to derive the joint distribution functions of all D_i and Y_{ij}, from which the parameters of the flaw generation and flaw size can be estimated.

The discussion is divided into the following 5 steps:

- First, a basic problem of flaw detection and measurement for a group of flaws with some known size distribution is investigated. The average probability of detection and the size distributions of the detected and undetected flaws are obtained. The results then serve as basic blocks for the following likelihood derivations. This step is given in Section 5.3.2.

- Derive the likelihood function for the 1st inspection. As there are no flaws at time zero, this step is relatively easy, as described in Section 5.3.3.

- Derive the likelihood function for the 2nd inspection. Similarly to the previous simplified model, the actual flaws at the 2nd inspection can be separated into two subsets: the undetected flaws left from the 1st inspection and the new generated flaws. Numbers and flaw size distributions of the detected and undetected flaws from the two subsets are obtained. This step is described in details in Section 5.3.4.

- The likelihood function for the second inspection is generalized to all subsequent inspections. The overall likelihood is then the product of the likelihood functions of all the inspections. This step is given in Section 5.3.5.

- The computational issue and approximate likelihood functions of the model are discussed. A simulation study is presented and the ML estimates using the accurate likelihood and the approximate likelihood functions are compared. These are presented in Section 5.3.6 and Section 5.3.7.

5.3.2 Flaw inspection considering PoD and sizing error

Before starting to analyze the Poisson flaw generation model, let us first consider the following basic problem. Suppose there are in total m flaws in a structure. The flaw size X follows a probability distribution with PDF $f_X(x)$. An inspection of the flaws is conducted using an uncertain probe. The PoD of the probe is given as $p(x)$, where x is the actual flaw size. The sizing error of the inspection probe, E, is a normal random variable with mean zero and SD σ_E. Our objective is to determine the average probability of detection and the size distributions of the detected and undetected flaws.

First, consider the average PoD for flaws with size distribution X, which is defined the probability of detecting a random selected flaw with size distribution X. Clearly, when the PoD function $p(x)$ is given, this probability depends only on the distribution of flaw size X and therefore can be written as P_X. Using the total probability theorem, P_X is given as the following integral

$$P_X = \int_0^\infty p(x) f_X(x) \mathrm{d}x. \tag{5.3.1}$$

Let the detection of a flaw be event I, the actual size distribution (error-free size) of the detected flaws can then be written as the following conditional probability as $f_{X|I}(x)$. Using Bayesian theorem, $f_{X|I}(x)$ is

$$f_{X|I}(x) = \frac{\bar{P}(I|x) f_X(x)}{\int_0^\infty \bar{P}(I|x) f_X(x) \mathrm{d}x} = \frac{1}{P_X} p(x) f_X(x),$$

where $\bar{P}(I|x)$ is the probability of detecting flaws with actual size x, which is exactly how the PoD function $p(x)$ is defined. For ease of presentation, denote the actual size of the detected flaws from flaws with size distribution X as $\mathcal{D}X$. The PDF of $\mathcal{D}X$ is then given as

$$f_{\mathcal{D}X}(x) = f_{X|I}(x|I) = \frac{1}{P_X} p(x) f_X(x).$$

Similarly, let actual size distribution of the undetected flaws be $\mathcal{U}X$. PDF of $\mathcal{U}X$ is

$$f_{\mathcal{U}X}(x) = f_{X|\bar{I}}(x) = \frac{\big(1-p(x)\big) f_X(x)}{\int_0^\infty \big(1-p(x)\big) f_X(x) \mathrm{d}x} = \frac{1}{1-P_X} \big(1-p(x)\big) f_X(x). \tag{5.3.2}$$

Since the sizing error E is independent of the actual size x, PDF of the measured size of the detected flaws, Y, can be written in the following convolution as

$$f_Y(y) = \int_{-\infty}^{\infty} f_{\mathcal{D}X}(y-e) f_E(e) \mathrm{d}e = \frac{1}{P_X} \int_{-\infty}^{\infty} p(y-e) f_X(y-e) f_E(e) \mathrm{d}e,$$

where $f_E(e)$ is the distribution of sizing error E.

5.3.3 First inspection

Let $t_0 = 0$ and $\Delta t_i = t_i - t_{i-1}, i = 1, 2, \cdots, n$. Δt_i are the time intervals between successive inspections. We first consider the inspection at time t_1. According to the model assumptions, at the first inspection time t_1, the actual number of flaws, M_1, is a Poisson random variable with rate $\lambda \Delta t_1$. Since at time zero there are no flaws, the actual flaws size distribution for M_1, denoted as $f_{X_1}(x)$, is the same as the size distribution of new generated flaws, $f_X(x;\theta)$.

From equation (5.3.1), for a randomly selected flaw in M_1, its probability of being detected can be written as $P_X(\theta) = \int_0^{\infty} p(x) f_X(x;\theta) \mathrm{d}x$. Using the Poisson splitting property, the number of detected flaws in M_1, denoted as D_1, is independent of M_1 and is Poisson distributed with rate $P_X(\theta)\lambda\Delta t_1$, i.e.,

$$D_1 \sim \text{Pois}\left(P_X(\theta)\lambda\Delta t_1\right).$$

The PMF of D_1 is

$$f_{D_1}(d_1;\lambda,\theta) = \frac{\left(P_X(\theta)\lambda\Delta t_1\right)^{d_1}}{d_1!} \exp\left(-P_X(\theta)\lambda\Delta t_1\right). \tag{5.3.3}$$

The distribution of the actual size of flaws in D_1 is given as

$$f_{\mathcal{D}X_1}(x;\theta) = \frac{1}{P_X(\theta)} p(x) f_X(x;\theta). \tag{5.3.4}$$

The measured size of flaws in D_1, denoted as Y_1, is then given by the following convolution as

$$f_{Y_1}(y;\theta) = \int_{-\infty}^{\infty} f_{\mathcal{D}X_1}(y-e;\theta) f_E(e) \mathrm{d}e = \frac{1}{P_X(\theta)} \int_{-\infty}^{\infty} p(y-e) f_X(y-e;\theta) f_E(e) \mathrm{d}e. \tag{5.3.5}$$

From equation (5.3.3) and (5.3.5), it is clear that for a given inspection probe, the number of detected flaws D_1 in the 1st inspection is affected by both the Poisson rate λ of the flaw generation and the parameter θ of the flaw size distribution; whereas the measured size distribution of the detected flaws is only affected by θ.

Since the flaw generation and the flaw size are independent, the likelihood function of the model parameter λ and θ can be given as

$$L_1(\lambda, \theta | \mathbf{y}_1) = f_{D_1}(d_1; \lambda, \theta) \prod_{j=1}^{d_1} f_{Y_1}(y_{1j}; \theta), \tag{5.3.6}$$

where $\mathbf{y}_1 = \{y_{11}, y_{12}, \cdots, y_{1d_1}\}$ are the measured sizes of the d_1 detected flaws in the first inspection, f_{D_1} and f_{Y_1} are the PMF or PDF of the number of detected flaws and their measured size given by equation (5.3.3) and (5.3.5), respectively.

When no flaws are detected, i.e., $d_1 = 0$ and $\mathbf{y}_1$ is an empty set, a special case equation (5.3.6) is given as

$$L_1(\lambda, \theta \,|\, d_1 = 0) = f_{D_1}(0; \lambda, \theta) = \exp\left(P_X(\theta)\lambda \Delta t_1\right).$$

5.3.4 Second inspection

We can now consider the second inspection at time t_2. Similar to the previous simple case with only PoD, we denote the actual flaws at time t_2 as M_2. M_2 can be separated into two independent categories: the undetected flaws left from the first inspection, denoted as M_{12}, and the new generated flaws between time t_1 and t_2, denoted as M_{22}. The derivation of the likelihood then utilizes the independence of M_{12} and M_{22}. An illustration of the number and size distribution of the detected and undetected flaws in the first few inspections is given in Figure 5.4.

Number and size distribution of flaws in M_{12} and M_{22}

Flaws in M_{12} are the undetected flaws from the first inspection. From previous discussions, the probability of detecting a randomly selected flaw in the first inspection is $P_X(\theta)$, or simply written as P_X by omitting parameter θ. According to the Poisson splitting property, the number of undetected flaws in the 1st inspection, M_{12}, is Poisson distributed with rate

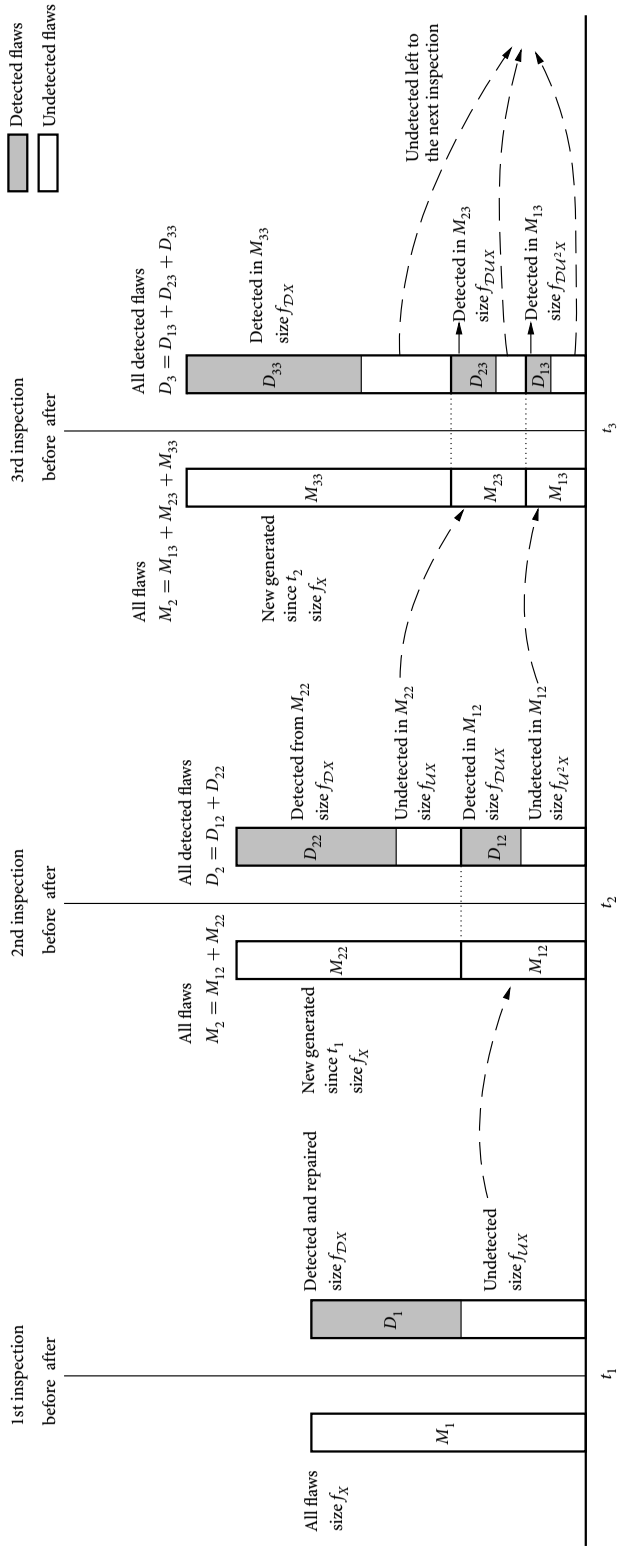

Figure 5.4 Illustration of number and size of the detected and undetected flaws in the first 3 inspections

$(1-P_X)\lambda\Delta t_1$ and is independent of D_1. The size distribution of the flaws in M_{12}, denoted as $f_{X_{12}}(x)$, is $f_{\mathcal{U}X}(x)$ given by equation (5.3.2).

Flaws in M_{22} are the new generated flaws between time t_1 and t_2. Therefore, M_{22} is Poisson distributed with rate $\lambda\Delta t_2$ and is independent of M_1 and D_2. The size distribution of flaws in M_{22}, $f_{X_{22}}(x)$ is equal to $f_X(x)$.

Number of the detected flaws

Let D_{12} and D_{22} be the detected flaws from M_{12} and M_{22}, respectively. The total number of detection in the 2nd inspection is $D_2 = D_{12} + D_{22}$.

From the above discussion, the size distributions of M_{12} and M_{22} are $f_{\mathcal{U}X}(x)$ and $f_X(x)$. Thus, the probability of detecting a randomly selected flaw from M_{12} and M_{22} are $P_{\mathcal{U}X}$ and P_X, respectively. Since M_{12} and M_{22} are independent Poisson random variables with rate $(1-P_X)\lambda\Delta t_1$ and $\lambda\Delta t_2$, using the Poisson splitting property, D_{12} and D_{22} are also independent and Poisson distributed. And one has

$$
\begin{aligned}
D_{12} &\sim \text{Pois}\left(P_{\mathcal{U}X}(1-P_X)\lambda\Delta t_1\right), \\
D_{22} &\sim \text{Pois}(P_X\lambda\Delta t_2).
\end{aligned}
$$

The total number of detected flaws in the second inspection, D_2, is then a Poisson random variable given as

$$
D_2 = D_{12} + D_{22} \sim \text{Pois}\left(P_{\mathcal{U}X}(1-P_X)\lambda\Delta t_1 + P_X\lambda\Delta t_2\right). \tag{5.3.7}
$$

Size distribution of the detected flaws

Since M_{12} and M_{22} are independent Poisson random variables with rate $\left(1-P_X\right)\lambda\Delta t_1$ and $\lambda\Delta t_2$, according to the properties of the Poisson distribution, for a randomly selected flaw from $M_2 = M_{12} + M_{22}$, the probability that it is from M_{12} (or M_{22}) is equal to the Poisson rate of M_{12} (or M_{22}) divided by the Poisson rate of M_2.

Using the theorem of total probability, the size distribution of a randomly selected flaw in M_2 is given as

$$\begin{aligned} f_{X_2}(x) &= \frac{(1-P_X)\lambda\Delta t_1}{(1-P_X)\lambda\Delta t_1+\lambda\Delta t_2} f_{X_{12}}(x) + \frac{\lambda\Delta t_2}{(1-P_X)\lambda\Delta t_1+\lambda\Delta t_2} f_{X_{22}}(x) \\ &= \frac{(1-P_X)\Delta t_1}{(1-P_X)\Delta t_1+\Delta t_2} f_{\mathcal{U}X}(x) + \frac{\Delta t_2}{(1-P_X)\Delta t_1+\Delta t_2} f_X(x). \end{aligned} \tag{5.3.8}$$

Likelihood function

From the discussions in Section 5.3.2, PDF of the actual size of the detected flaws in M_2, i.e., D_2, is

$$f_{\mathcal{D}X_2}(x) = \frac{1}{P_{X_2}} p(x) f_{X_2}(x),$$

where $P_{X_2} = \int_0^\infty p(x) f_{X_2}(x)\mathrm{d}x$ and $f_{X_2}(x)$ is given by equation (5.3.8).

PDF of the measured size of the flaws in D_2 is then the convolution of $f_{\mathcal{D}X_2}(x)$ and the sizing error distribution $f_E(e)$ given as

$$f_{Y_2}(y) = \int_{-\infty}^{\infty} f_{\mathcal{D}X_2}(y-e) f_E(e)\mathrm{d}e. \tag{5.3.9}$$

The likelihood function of the model parameters given measured flaws in second inspection, $\mathbf{y}_2 = \{y_{21}, y_{22}, \cdots, y_{2d_2}\}$

$$L_2(\lambda, \theta \,|\, \mathbf{y}_2) = f_{D_2}(d_2) \prod_{j=1}^{d_2} f_{Y_2}(y_{2j}), \tag{5.3.10}$$

where $f_{D_2}(d_2)$ is the PMF of the Poisson random variable D_2 and can be given from equation (5.3.7), $f_{Y_2}(y)$ is the PDF of Y_2 given by equation (5.3.9). Here parameters λ and θ in $f_{D_2}(d_2)$ and $f_{Y_2}(y)$ are omitted for sake of conciseness. A special case of equation (5.3.10) when $d_2 = 0$ is given as

$$L_2(\lambda, \theta \,|\, d_2 = 0) = f_{D_2}(0) = \exp\left(P_{\mathcal{U}X}\left(1-P_X\right)\lambda\Delta t_1 + P_X\lambda\Delta t_2\right).$$

5.3.5 Overall likelihood function

In general, in the ith inspection at time t_i, the actual number of flaws M_i can be separated into i independent categories as $M_{1i}, M_{2i}, \cdots, M_{ii}$, where M_{ji} are flaws that initiated during time interval $(t_{j-1}, t_j]$ but remain undetected before the ith inspection at time t_i (or equivalently, remain undetected after the $(i-1)$th inspection). In particular, M_{ii} are the new generated flaws during time $(t_{i-1}, t_i]$. Obviously, M_{ii} is Poisson distributed with rate $\lambda\Delta t_i$ and the actual size of the flaws in M_{ii} is distributed with PDF $f_X(x)$.

When $j < i$, M_{ji} consists of flaws that are generated during time $(t_{j-1}, t_j]$ but remain undetected before the ith inspection. Clearly, M_{ji} is a subset of M_{jj} which represents all the flaws that are generated during time interval $(t_{j-1}, t_j]$. After the jth inspection at time t_j, the undetected flaws in M_{jj} are left as $M_{j,j+1}$. From previous discussions in Section 5.3.4, the number and the actual size of flaws in $M_{j,j+1}$ are given as

$$M_{j,j+1} \sim \text{Pois}\left((1-P_X)\lambda\Delta t_j\right),$$
$$f_{X_{j,j+1}}(x) = f_{\mathcal{U}X}(x),$$

where $f_{X_{j,j+1}}(x)$ is the PDF of the actual size of the flaws in $M_{j,j+1}$.

Following the convention for the subscript of M, the flaws that were initiated during time interval $(t_{j-1}, t_j]$ but remained undetected before the $(j+2)$th inspection are dented as $M_{j,j+2}$. Obviously, $M_{j,j+2}$ is actually the undetected flaws left from $M_{j,j+1}$ in the $(j+1)$th inspection. Therefore, one has

$$M_{j,j+2} \sim \text{Pois}\left((1-P_{\mathcal{U}X})(1-P_X)\lambda\Delta t_j\right),$$
$$f_{X_{j,j+2}}(x) = f_{\mathcal{U}\mathcal{U}X}(x) = f_{\mathcal{U}^2X}(x),$$

where $f_{\mathcal{U}\mathcal{U}X}(x) = f_{\mathcal{U}^2X}(x)$ are the size distribution of the remaining undetected flaws after two inspections, from flaws originally with a size distribution $f_X(x)$, and can be calculated recursively from equation (5.3.2).

Continuing the above procedures, it can be inferred that M_{ji} is a Poisson random variable given as

$$M_{ji} \sim \text{Pois}(\lambda_{ji}),$$

where $\lambda_{ji} = \lambda \Delta t_j \prod_{k=1}^{i-j}(1 - P_{\mathcal{U}^{k-1}X}), j = 1, 2, \cdots, i-1$. The size distribution of the flaws in M_{ji} is

$$f_{X_{ji}}(x) = f_{\mathcal{U}^{i-j}X}(x).$$

To be consistent in notations, let $f_{\mathcal{U}^0 X}(x) = f_X(x)$ and the Poisson rate of M_{ii} be λ_{ii}, $\lambda_{ii} = \lambda \Delta t_i$. The total number of flaws at the ith inspection, M_i, as the sum of $M_{1i}, M_{2i}, \cdots, M_{ii}$, is therefore a Poisson random variable given as

$$M_i = \sum_{j=1}^{i} M_{ji} \sim \text{Pois}\left(\sum_{j=1}^{i} \lambda_{ji}\right).$$

Let $\lambda_i = \sum_{j=1}^{i} \lambda_{ji}$, M_i is a Poisson random variable with rate λ_i. Using theorem of total probability, the actual size of flaw in M_i is distributed as

$$f_{X_i}(x) = \sum_{j=1}^{i} \frac{\lambda_{ji}}{\sum_{j=1}^{i} \lambda_{ji}} f_{X_{ji}}(x) = \sum_{j=1}^{i} \frac{\lambda_{ji}}{\lambda_i} f_{\mathcal{U}^{i-j}X}(x). \tag{5.3.11}$$

From the previous discussions in Section 5.3.2, the number of detected flaws in the ith inspection, denoted as D_i, is then Poisson distributed as

$$D_i \sim \text{Pois}(P_{X_i} \lambda_i),$$

where $P_{X_i} = \int_0^\infty p(x) f_{X_i}(x) \mathrm{d}x$ is the average PoD of flaws in M_i. The actual size of the detected flaws in M_i is distributed as

$$f_{\mathcal{D}X_i}(y) = \frac{1}{P_{X_i}} p(x) f_{X_i}(x).$$

The corresponding measured size distribution of the detected flaws is

$$f_{Y_i}(y) = \int_{-\infty}^{\infty} f_{\mathcal{D}X_i}(y - e) f_E(e) \mathrm{d}e.$$

The likelihood function of the model parameters given measured flaws in the ith inspection, $\mathbf{y}_i = \{y_{i1}, y_{i2}, \cdots, y_{id_i}\}$, is

$$L_i(\lambda, \theta \,|\, \mathbf{y}_i) = f_{D_i}(d_i) \prod_{j=1}^{d_i} f_{Y_i}(y_{ij}),$$

where parameters λ and θ are omitted in $f_{D_i}(d_i)$ and $f_{Y_i}(y_{ij})$. A special case of the likelihood for no flaw detection is

$$L_i(\lambda, \theta \,|\, d_i = 0) = f_{D_i}(0).$$

Since the detected flaws in each inspection are independent, the overall likelihood function is simply the product of all L_i, i.e.,

$$L(\lambda, \theta \,|\, \mathbf{y}_1, \mathbf{y}_2, \cdots, \mathbf{y}_n) = \prod_{i=1}^{n} L_i(\lambda, \theta \,|\, \mathbf{y}_i). \tag{5.3.12}$$

5.3.6 Computational difficulties and approximate likelihood

The derivation of likelihood function (5.3.12) clearly shows the complexity of the stochastic modelling of flaw generation subject to both PoD and sizing error. Two types of numerical integrals need to be calculated when evaluating the likelihood function: the average probability of detection, and the measured flaw size distribution.

From the derivation of equation (5.3.12), it can be observed that, in order to evaluate the model likelihood function from n repeated inspections, only the following n average PoD need to be calculated, regardless the number of total detected flaws. They are $P_X, P_{\mathcal{U}X}, \cdots, P_{\mathcal{U}^{n-1}X}$. Therefore, the computational burden brought in by calculating average PoD is not very significant, since the number of repeated inspections is usually quite limited.

However, for each single detected flaw, calculation of its measured flaw size distribution $f_{Y_i}(y_{ij})$ has to the conducted, which is a convolution over infinite region. For example, for a data-set consisting of 100 detected flaws, which is not a very large data-set for repeated inspections over years, 100 convolution calculations are required for each evaluation of the model likelihood, and this can be extremely time-consuming since the actual size

distribution of the detected flaws $f_{\mathcal{D}X_i}(x)$ is already very complicated. Therefore, directly ML estimation using equation (5.3.12) can be only conducted for small data-sets. To avoid calculating the convolution in $f_{Y_i}(y_{ij})$, advanced Bayesian simulation using Markov Chain Monte Carlo (MCMC) and auxiliary variable method can be applied, which will be discussed in Chapters 7.

An obvious fact about the flaw detection is that after several inspections, the undetected portion of a group of flaws will decrease quickly and the size of the remaining flaws also tends to be smaller. Therefore, to simply the analysis, approximate likelihood can be obtained, by neglecting the remaining undetected flaws after their kth inspection. We call this approximation the kth order approximate of likelihood function (5.3.12). For example, in the 2nd order approximation, when deriving the likelihood of the ith inspection, one only considers M_{ii} and $M_{i-1,i}$ and assume all other $M_{ji}, j=1,2,\cdots,i-2$, to be zero. In particular, the 1st order approximate of (5.3.12) is same as the one used by Yuan et al. (2009), in which only the new generated flaws since last inspection are considered.

5.3.7 Numerical validation

A numerical simulation is presented to validate the likelihood function derived in this section. In the simulation, the flaw initiation is simulated using a homogeneous Poisson process with rate $\lambda=2$. The size of the generated flaws is considered to be stable and follows a log-normal distribution with log-scale $\mu=3.5$ and shape parameter $\sigma=0.4$ (average size 35.9 with standard deviation 14.9). Four inspections of the generated flaws are conducted at time 4, 8, 12, and 16 years, respectively, using an uncertain probe with PoD $p(x)$ and normal sizing error $E \sim \mathrm{N}(0,\sigma_E^2)$. All the detected flaws in each inspection are removed from the simulated flaws to mimic the "repair-on-detection" maintenance strategy. The measured size of the detected flaws are generated by adding the actual size with a generated normal sizing error. The number of the detected flaws and their measured sizes then form the generated data-set. Detailed procedures for generating the data-set is given in the Appendix A.2.

Two inspection probes are assumed in the simulation. Probe 1 has a better performance in probability of detection. The PoD function of Probe 1 is a log-logistic function given by

equation (2.2.1), with parameters $a=-8$ and $b=3$. Probe 2 has a relatively inferior PoD performance with PoD curve given as a log-logistic function with parameters $a=-10$ and $b=3$. Standard deviation of the sizing errors of both inspection probes are both assumed to be $\sigma_E=6$. Figure 5.5 shows the PDF of the assumed flaw size distribution and the PoD functions of both inspection probes.

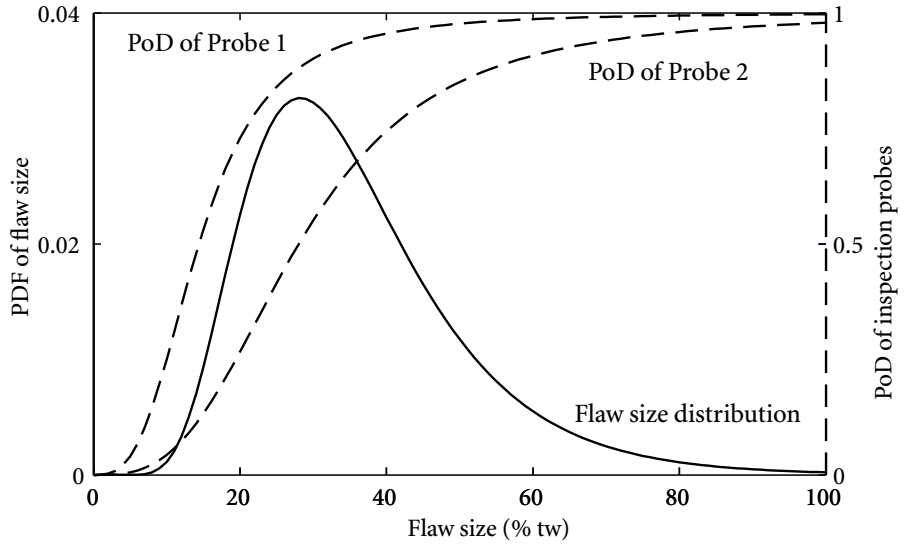

Figure 5.5 Flaw size distribution (solid line) and PoD curves of the two inspection probes (dashed lines)

ML estimates of the Poisson rate λ of flaw generation and the parameters of flaw size distribution are calculated by maximizing likelihood function (5.3.12) using the generated data-sets from the two inspection probes. The data simulation and ML estimation are repeated for 500 times. Bias and RMSE of the estimates are examined. The results are also compared with the estimates using kth order approximate of the likelihood function (5.3.12) to illustrate the effects of the approximation. The results are presented in Table 5.1.

From the results, it can be shown that the complete likelihood function (5.3.12) correctly gives unbiased estimates of both the Poisson rate λ and the parameters of flaw size distribution. The approximated likelihood functions also give fairly good estimates on the parameters of the flaw size distribution. However, approximated likelihood functions tend to over-estimate the flaw generation rate, because they do not handle previously undetected

For Probe 1 (with good PoD)

		Accurate likelihood	3rd order approx.	2nd order approx.	1st order approx.
λ	Bias	-0.002	0.003	0.018	0.166
	RMSE	0.35	0.37	0.38	0.44
μ	Bias	0.006	-0.005	-0.014	-0.047
	RMSE	0.089	0.089	0.093	0.106
σ	Bias	-0.002	-0.007	-0.002	-0.002
	RMSE	0.070	0.075	0.074	0.080

For Probe 2 (with poor PoD)

		Accurate likelihood	3rd order approx.	2nd order approx.	1st order approx.
λ	Bias	0.019	0.072	0.23	0.94
	RMSE	0.44	0.46	0.58	1.22
μ	Bias	0.001	-0.012	-0.030	-0.090
	RMSE	0.11	0.12	0.14	0.18
σ	Bias	-0.018	-0.008	-0.009	-0.006
	RMSE	0.085	0.089	0.089	0.090

Table 5.1 Bias and RMSE of estimated model parameters using the accurate likelihood and approximate likelihood functions (true value: $\lambda = 2$, $\mu = 3.5$, $\sigma = 0.4$)

flaws properly. The accuracy of the approximate likelihood functions becomes better as the order of approximation increases (i.e., more previously undetected flaws are considered) and the PoD performance of the probe improves.

For Probe 1 which has a better PoD performance, the bias of the estimates of λ from the 1st order approximate likelihood function is about 8% of the true value, and the bias obtained using the 2nd order approximate likelihood is less than 1%. The 2nd order approximation already gives very good estimation of λ. For Probe 2, the bias of the estimated λ using the 1st order, 2nd order, and 3rd order likelihood are 47%, 12% and 3.5% of the true value of λ, respectively. To have an reasonably accurate estimate of the flaw generation rate using data from Probe 2, the 3rd order approximation should be used.

5.4 Summary

In this chapter, parameter estimation of the Poisson flaw generation model using noisy and incomplete inspection data from repeated inspections is investigated under the "repair-on-detection" assumption.

First, likelihood function of a simple flaw generation problem considering only PoD is derived. The major difficulty in formulating the model likelihood function comes from the undetected flaws of previous inspections, which need to be accounted carefully when analyzing subsequent inspections.

Based on the results of the simple problem, the complete Poisson flaw generation model is investigated. Both PoD and sizing error are included in the model. Although PoD and sizing error are assumed to be two separated characteristics of the inspection probe, they are found to be closely interrelated in the parameter estimation, and the complete likelihood function turns out to be very complicated. The computational issue and the approximate likelihood functions are discussed briefly. The calculation of the convolution for the measured flaw size distribution is identified as the major computational difficulty. This computational difficulty can be resolved using Markov chain Monte Carlo simulation method, which will be discussed later in Chapter 7.

CHAPTER 6

Bayesian Inference for Degradation Models

This chapter introduces Bayesian parameter inference in the context of degradation modelling. We start with a brief discussion on the differences between the classical and Bayesian parameter inference. The concept of subjective probability is introduced, based on which Bayesian method is formulated. Although being conceptually different, the procedure of Bayesian inference can be regarded as a natural generalization of the classical maximum likelihood method by incorporating the prior distribution in the estimation process. Informative and non-informative prior distributions for Bayesian inference are discussed. Two practical applications are presented to illustrate the use of Bayesian inference in degradation assessment.

6.1 Classical and Bayesian parameter inference

Classical parameter inference

In previous chapters, parameter estimation of stochastic models for flaw growth and flaw generation using uncertain inspection data is discussed. Likelihood functions of stochastic models given error contaminated data are derived, from which ML estimates of the model parameters are obtained.

The ML method we discussed before is based on the classical statistical inference, in which the model parameters are assumed to be fixed (but unknown) constants. Estimation of the model parameters in the classical statistical inference is then regarded as a formal process that yields numerical estimates of the unknown parameters from observed samples (Benjamin and Cornell, 1970). Since the observations are random samples from the probabilistic model, the result of the parameter estimation process, as a function of the observations, is also random and is called an estimator of the model parameters defined by this specific estimation process. The actual estimate of the parameters from some specific observed data is then a realization of the estimator.

To better explain the classical approach of parameter inference, consider the following example. Suppose X is a normal random variable with mean μ and known SD of 1. In order to estimate the value of μ, n random samples, $X_1, X_2, \cdots, X_n$, are drawn from random variable X independently. The corresponding sample mean $\bar{X} = \frac{1}{n}\sum_{i=1}^{n} X_i$ is then an estimator of the unknown parameter μ. For a particular observed data-set $x_1, x_2, \cdots, x_n$, the corresponding realization of the sample mean $\bar{X}$, denoted as $\bar{x} = \frac{1}{n}\sum_{i=1}^{n} x_i$, is the estimate of μ from data-set $x_1, x_2, \cdots, x_n$, using the sample mean estimator.

The goodness of a parameter estimation method can be quantified using the distribution of its corresponding estimators. For example, with the help of some simple statistical calculation, the sample mean estimator $\bar{X}$ in the above example is found to be normally distributed with mean μ and SD $1/\sqrt{n}$. Therefore, when the estimation process (drawing n random samples and calculating the sample mean) is repeated, the expected value of the estimates is equal to the true value of μ, indicating that this sample mean estimation is unbiased. Furthermore, as the sample size n increases, SD of the estimator becomes smaller, which means the estimates from larger data-sets are more likely to be close to the true value of μ than estimates from small data-sets.

In general, the distribution of the estimators cannot be obtained analytically, except for some simple cases. For many parameter estimation methods, especially complicated ones, Monte Carlo simulation is needed in order to validate the goodness of the estimation, as we did in previous chapters for the validation of our proposed ML methods.

The uncertainty associated with an estimate of the model parameter from some specific observed data-set is expressed in terms of confidence intervals in classic parameter inference. A confidence interval (CI) is an observational interval (i.e., a function of the observed data) over which the true value of the parameter may lie (Ang and Tang, 1975). Take the above sample mean estimation of normal random variable as an example. Since the estimator $\bar{X}$ from n random samples is a normal random variable with mean μ and SD $1/\sqrt{n}$, one has

$$P\left[\bar{X} - 1.96/\sqrt{n} \leqslant \mu \leqslant \bar{X} + 1.96\sqrt{n}\right] = 0.95. \tag{6.1.1}$$

From equation (6.1.1), given n observations, $x_1, x_2, \cdots, x_n$, there is a 95% percent chance that interval $[\bar{x} - 1.96/\sqrt{n}, \bar{x} + 1.96/\sqrt{n}]$ contains the true value of the parameter μ, where $\bar{x} = \sum_{i=1}^{n} x_i$. $[\bar{x} - 1.96/\sqrt{n}, \bar{x} + 1.96/\sqrt{n}]$ is called a 95% confidence interval associated with the estimate $\bar{x}$ and can be used to quantify the parameter uncertainty associated with the estimate $\bar{x}$.

In the degradation assessment of nuclear power plants, the parameter uncertainty associated with an estimate is usually quite significant, due to the small sample size and the large inspection uncertainties. A proper consideration of parameter uncertainty is important to the safety of the plant operation. If the parameter uncertainty is found to be very large, the prediction of degradation will be unreliable. In such cases, additional data collection or more conservative predictions (say predictions using the upper bound of the 95% CI instead of the point estimate of the parameter) are needed, both of which could be very costly.

To improve the quality of the parameter estimation and reduce the parameter uncertainty, information from sources other than the inspection data, such as plant design, expert judgment and/or past operation experiences of similar plants, should be utilized, especially when inspection data are scarce. However, with the classical approach, there is no formal way for combining such information in the parameter estimation process.

Another difficulty regarding the parameter uncertainty in the classical approach is that constructing confidence intervals for estimates of complex statistical models is usually not easy. For the ML estimation, numerically expensive manipulations of the likelihood function are often needed. For example, to determine the asymptotic confidence interval

of a ML estimate, the second derivative of the likelihood function needs to be evaluated (Benjamin and Cornell, 1970), which is computationally prohibitive for models such as the gamma process model with sizing error that we discussed before.

Bayesian parameter inference

Bayesian inference is a conceptually different method for the parameter estimation, that is based on the subjective interpretation of probability. In the subjective interpretation, probability is regarded as a mathematical expression of our degree of belief with respect to a certain proposition (Box and Tiao, 1992). For example, one may conclude, from all the available information, that the chance of having heads when tossing a coin is somewhere between 30% and 70%, with any value in between being equally possible. From a Bayesian perspective, this actually assigns a uniform distribution over interval [30%, 70%] to the chance of having heads in the experiment, despite the fact that the actual chance is a fixed number.

It has been shown that in order to avoid inconsistency, probability, as a subjective degree of belief, is both necessary and sufficient to follow the classical probability calculus (Lindley, 1965; Savage, 1972). For instance, the degree of belief about a certain event is always 1, and the degree of belief on event A being true is always smaller than the belief on event B being true, given $A \subset B$.

With the subjective interpretation of probability, our degree of belief regarding certain propositions can be updated formally as new information becomes available, through Bayes' theorem. Suppose A and B are two propositions. In Bayesian statistics, $\bar{\mathcal{P}}(A)$ and $\bar{\mathcal{P}}(B)$ are, respectively, our degree of believes on that A and B are true, based on our background knowledge M, where M is usually omitted. The conditional probability $\bar{\mathcal{P}}(A \,|\, B)$ is then interpreted as the updated degree of belief of A being true when we know that B is true. Using Bayes' theorem, the updated degree of belief is given as

$$\bar{\mathcal{P}}(A \,|\, B) = \frac{\bar{\mathcal{P}}(B \,|\, A)\bar{\mathcal{P}}(A)}{\bar{\mathcal{P}}(B)},$$

$\bar{\mathcal{P}}(A)$ is then called the prior probability of A given the background knowledge M. $\bar{\mathcal{P}}(A \,|\, B)$ is called the posterior probability of A given B.

Using the concept of subjective probability and Bayes' theorem, Bayesian inference of model parameters can be formulated as follows. Suppose the PDF of the observation X from a probabilistic model is given as $f_X(x;\theta)$ with θ as the unknown parameter. First, a prior distribution on values of θ, denoted as $\pi(\theta)$, is assigned based on the background information. Bayesian inference of θ given an actual observation x is then simply the posterior distribution of θ given x, or $\pi(\theta \,|\, x)$. According to Bayes' theorem, one has

$$\pi(\theta \,|\, x) = \frac{f_X(x;\theta)\pi(\theta)}{\int f_X(x;\theta)\pi(\theta)\mathrm{d}\theta} = CL(\theta \,|\, x)\pi(\theta), \tag{6.1.2}$$

where $C = \left[\int f_X(x;\theta)\pi(\theta)\mathrm{d}\theta\right]^{-1}$ is the normalization constant, $L(\theta \,|\, x) = f_X(x;\theta)$ is the same likelihood function that is used in ML analysis. $L(\theta \,|\, x)$ is written in such form only to indicate that it is a function not of actual observation x but of the model parameter θ.

Compared to the classical parameter inference, Bayesian inference is able to incorporate information from sources other than the observed data in a formal way through Bayes' theorem and the prior distribution. The subjective interpretation in Bayesian inference also provides a more natural way for expressing the parameter uncertainty of the estimation using the posterior distribution of the parameter.

In the following sections of this chapter, Bayesian inference is discussed through some relatively simple examples, to illustrate its application in degradation assessment. Discussions on the computational aspects of Bayesian inference of some more complicated models are left for the next chapter.

6.2 Prior distribution

A complete Bayesian inference includes two parts. The first part is the likelihood function $L(\theta \,|\, x)$, which represents the chosen probabilistic model and the information from observed data. The likelihood formulation of stochastic models has been discussed extensively in previous chapters. The second part, which is not seen in the ML analysis, is the prior distribution $\pi(\theta)$, which represents all other information that is known or assumed about the model parameter θ other than observed data. The prior information can be any relevant information regarding the model parameters, such as engineering design data, expert judgment, data from other similar systems, or even lack of information.

In Bayesian inference, the prior distribution does not necessarily needs to be a proper distribution function, as long as the resulted posterior distribution is proper. A prior distribution $\pi(\theta)$ is called an improper prior if

$$\int_{\Theta} \pi(\theta) \mathrm{d}\theta = \infty,$$

where the integration region is the admissible range of θ. A typical example of the improper prior the uniform prior over an infinite region such as $(-\infty, \infty)$ or $[0, \infty)$.

Prior distributions used in Bayesian inference can be divided in two categories: the non-informative prior and the informative prior. The non-informative prior, also called the prior of ignorance, applies when there is relatively little subjective information compared to the observed data; and therefore, the posterior distribution is "dominated" by the likelihood function (Box and Tiao, 1992). On the other hand, the informative prior contains enough information that is comparable to the information from the observational data and the posterior distribution is affected heavily by both the prior distribution and the likelihood function. Further discussions on the prior distribution are presented in the next.

6.2.1 Non-informative prior

As pointed out by Box and Tiao (1992), an analyst may never in be a state of *complete* ignorance and the statement of non-informative can only mean relative to the information provided by the observed data. Therefore, in practice, the term non-informative should be interpreted as "not very informative".

Uniform prior

The simplest non-informative prior for Bayesian inference is uniform prior over the possible region of the parameter. The use of the uniform distribution is based on the "principle of indifference", that all the possible values of the parameter are of the same weight. From equation (6.1.2), it is clear that if the uniform prior is applied, the posterior distribution is equal to the likelihood function up to a constant factor. Therefore, ML estimation of the model can be obtained by simply finding the value of the parameter where the maximum posterior distribution is reached.

The uniform prior is usually not invariant under parameter transformation. For example, suppose the prior distribution for the standard deviation σ of a normal random variable is assumed to be uniformly distributed over $[0, \infty)$, i.e.,

$$\pi(\sigma) \propto 1, \quad \sigma \geqslant 0.$$

Its variance σ^2 is then distributed as

$$\pi(\sigma^2) \propto 1 \cdot \left| \frac{\mathrm{d}\sqrt{\sigma}}{\mathrm{d}\sigma} \right| = \frac{1}{2(\sigma^2)^{1/4}}.$$

That is more weight is assigned to smaller values for the variance in the prior.

Although the fact that uniform prior is not invariant under reparameterization may cause theoretical difficulties, it is widely used in practice due to its extreme simplicity.

Jeffreys prior

Jeffreys prior is a particular non-informative prior distribution proposed by Jeffreys (1961). Suppose $\boldsymbol{\theta} = \{\theta_1, \theta_2, \cdots, \theta\}$ is the n-dimension parameter of a probabilistic model $f_X(x; \boldsymbol{\theta})$. The Jeffreys non-informative prior is defined as

$$\pi(\boldsymbol{\theta}) \propto [\det(I(\boldsymbol{\theta}))]^{1/2}, \tag{6.2.1}$$

where $I(\boldsymbol{\theta})$ is the Fisher's information matrix and $\det(I(\boldsymbol{\theta}))$ is the determinant of $I(\boldsymbol{\theta})$. $I(\boldsymbol{\theta})$ is a $n \times n$ matrix with the following elements:

$$I_{ij}(\boldsymbol{\theta}) = \mathrm{E}\left[\frac{\partial \log f_X(X; \boldsymbol{\theta})}{\partial \theta_i} \frac{\partial \log f_X(X; \boldsymbol{\theta})}{\partial \theta_j} \right] \quad i, j = 1, 2, \cdots, n,$$

provided that the second-order partial derivatives of $\log f_X(X; \boldsymbol{\theta})$ exist.

A key feature of the Jeffreys prior is that it is invariant under reparameterization. Take the one-dimension case as an example. Let θ be the one-dimension parameter of probabilistic model $f_X(x; \theta)$. From equation (6.2.1), the Jeffreys prior for parameter θ is

$$\pi(\theta) = \sqrt{\mathrm{E}\left[\left(\frac{\mathrm{d} \log f_X(x; \theta)}{\mathrm{d}\theta} \right)^2 \right]}.$$

Suppose $\phi = g(\theta)$ is an 1-1 reparameterization of θ. The equivalent prior in parameter ϕ can be calculated as

$$p(\phi) = \pi(\theta)\left|\frac{\mathrm{d}\theta}{\mathrm{d}\phi}\right| \propto \sqrt{\mathrm{E}\left[\left(\frac{\mathrm{d}\log f_X(x;\theta)}{\mathrm{d}\theta}\right)^2\right]\left(\frac{\mathrm{d}\theta}{\mathrm{d}\phi}\right)}$$
$$= \sqrt{\mathrm{E}\left[\left(\frac{\mathrm{d}\log f_X(x;\theta)}{\mathrm{d}\theta}\frac{\mathrm{d}\theta}{\mathrm{d}\phi}\right)^2\right]} = \sqrt{\mathrm{E}\left[\left(\frac{\mathrm{d}\log f_X(x;g^{-1}(\phi))}{\mathrm{d}\phi}\right)\right]}.$$

Thus, $p(\phi)$ is the Jeffreys prior for ϕ.

Besides the uniform prior and Jeffreys prior, many other non-informative priors with different characteristics have also been developed. For example, Jaynes (1968) proposed a non-informative prior by maximizing its Shannon entropy. Bernardo (1979) proposed a non-informative by maximizing the expected Kullback-Leibler divergence of the posterior distribution with respect to the prior. For detailed discussions on various non-informative priors, one may refer to Kass and Wasserman (1996).

6.2.2 Informative prior

When substantial prior information is available, informative prior distribution should be used. An informative prior is a prior distribution that express specific and definite information regarding the parameters of a probabilistic model.

In some cases, the prior information is provided in the form of probability distribution and can be readily used in Bayesian inference. An example of such case is the component specific analysis in the random rate model. Since the flaw growth rate of a specific component is a constant sampled from the population rate distribution, it is natural to take the population rate distribution as the prior distribution. The growth rate estimation of each single component is then the posterior distribution updated from the population rate distribution using the component specific flaw size measurements. This case will be further discussed later in Section 6.4 as an example of practical application of Bayesian inference in degradation assessment.

However, in many other cases, the prior information is often provided in imprecise forms, such as personal experiences or expert judgments. For example, a piping engineer

may suggest that the wall thinning of a pipe is around 0.5 mm per year. It is often not feasible to ask an engineering to assess the probability density function of this thinning rate. Instead, the use of simple discrete density is suggested. The range of the degradation rate may be divided into four intervals: below 0.2 mm per year, between 0.2 mm and 0.4 mm per year, between 0.4 mm and 0.6 mm per year and above 0.6 mm per year. An engineer is then asked to assess a probability for each interval. The assessment from the engineer can then be fitted using an appropriate distribution function. Figure 6.1 shows a possible assessment of the probabilities from an engineer and the corresponding log-normal fit.

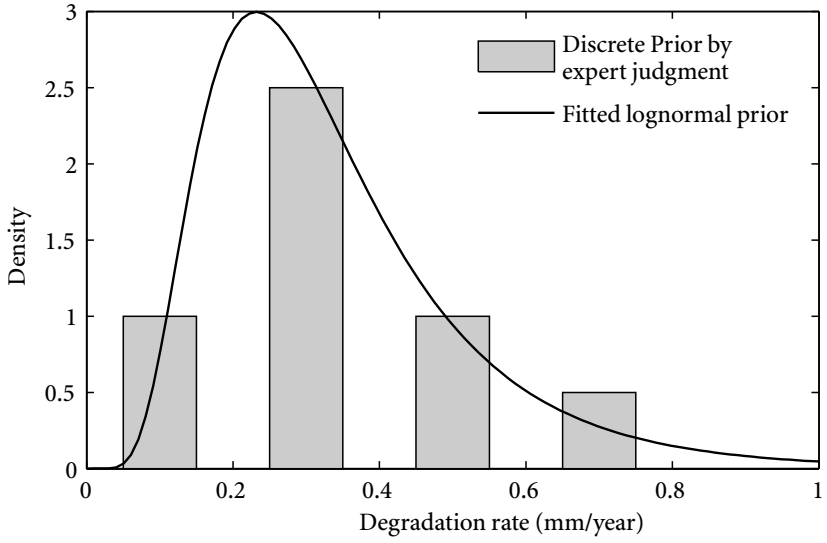

Figure 6.1 Discrete prior from an engineer and the corresponding log-normal fit

6.3 Example I: predicting probability of feeder cracking

An example of survival analysis of feeder cracking is presented here to illustrate the ability of Bayesian inference to incorporate additional judgmental information when there are little observed data. The problem is to predict the probability of cracking of feeders at a nuclear power plant given that 178 feeders are inspected and no cracks are found.

Likelihood Function

This is a binomial sampling problem. Denote the probability of feeder cracking as $\theta, 0<\theta<1$. Given θ, PMF of finding x cracks in n feeders is given by

$$f(x;\theta) = \binom{n}{x}\theta^x(1-\theta)^{n-x}, \quad x=0,1,\cdots,n.$$

With inspection result as 0 cracks found in 178 feeders, the likelihood function is

$$L(\theta \,|\, x=0) = \binom{178}{0}\theta^0(1-\theta)^{178-0} = (1-\theta)^{178}. \tag{6.3.1}$$

From equation (6.3.1), it is obvious that the maximum likelihood estimate of θ is 0. This result cannot be used directly for meaningful degradation assessment since it simply says there will be no cracks in future, which is inconsistent with the fact that cracks have been previously observed in other plants.

Prior distribution

Given the model likelihood function, the next task in Bayesian inference is to choose a proper prior distribution based on the information available. According to a previous inspection in a similar plant, no cracks were found in the 97 inspected feeders. Therefore, one may expect the mean of the cracking frequency to be less than 1/97. In addition, from engineering experiences the probability of feeder cracking is not likely to be greater than 10%, and the COV is believed to be around 50%. The fact that cracks have been found in other nuclear power plants indicates that a peak value at 0 for the probability of cracking may not be appropriate. Considering all these factors, a general beta distribution defined on $[0, 0.1]$ with mean 1/97 and COV 0.5 is chosen to be the prior distribution.

A random variable Θ is said to follow a general beta distribution Gbeta$(\alpha, \beta, p_1, p_2)$ if its probability density function is

$$f(\theta) = A(\theta-p_1)^{\alpha-1}(p_2-\theta)^{\beta-1},$$

where $p_1 \leqslant \theta \leqslant p_2$, A is the normalization constant and is given by

$$A = \left[\mathrm{B}(\alpha,\beta)(p_2-p_1)^{\alpha+\beta-1}\right]^{-1},$$

where $B(\alpha,\beta)=\int_0^1 t^{\alpha-1}(1-t)^{\beta-1}dt$ is the Beta function with parameters α and β. General beta distribution can be transformed to the regular beta distribution by changing the variable θ to $x=(\theta-p_1)/(p_2-p_1)$.

The mean of general beta distribution is

$$\mathsf{E}[\Theta] = (p_2-p_1)\frac{\alpha}{\alpha+\beta}+p_1.$$

Substituting $p_1=0, p_2=0.1$, and $\mathsf{E}[\Theta]=1/97$ yields

$$\frac{1}{97} = \frac{0.1\alpha}{\alpha+\beta}. \tag{6.3.2}$$

The COV of general beta distribution is

$$\mathrm{COV}[\Theta] = \frac{(p_2-p_1)\sqrt{\alpha\beta}}{\mathsf{E}[\Theta](\alpha+\beta)\sqrt{\alpha+\beta+1}}.$$

Similarly, one gets

$$\frac{1}{2} = \frac{97\sqrt{\alpha\beta}}{10(\alpha+\beta)\sqrt{\alpha+\beta+1}}. \tag{6.3.3}$$

Solving equations (6.3.2) and (6.3.3) gives the parameters of the prior distribution as $\alpha=3.48, \beta=30.3$. The prior distribution is therefore given as

$$\pi(\theta) = A\cdot\theta^{2.48}(0.1-\theta)^{29.3}.$$

Posterior Distribution

Posterior distribution is then simply the product of the likelihood function and the prior distribution with a normalization constant c

$$\begin{aligned}\pi(\theta\,|\,x=0) &= c\cdot L(\theta\,|\,x=0)\pi(\theta)\\ &= c\cdot\theta^{\alpha-1}(0.1-\theta)^{\beta-1}(1-\theta)^{178}.\end{aligned}$$

Given $\alpha=3.48$ and $\beta=30.3$, c can be easily calculated from numerical integration. The posterior distribution is then given by

$$\pi(\theta\,|\,x=0) = 1.458\times10^{38}\cdot\theta^{2.48}(1-\theta)^{29.3}(1-\theta)^{178}.$$

Figure 6.2 shows the prior and posterior distributions. The posterior mean of cracking frequency can be calculated as 0.69% with 95% upper bound 1.55%. These numbers can then be used in the inspection and maintenance planning of the feeder fleet of the plant.

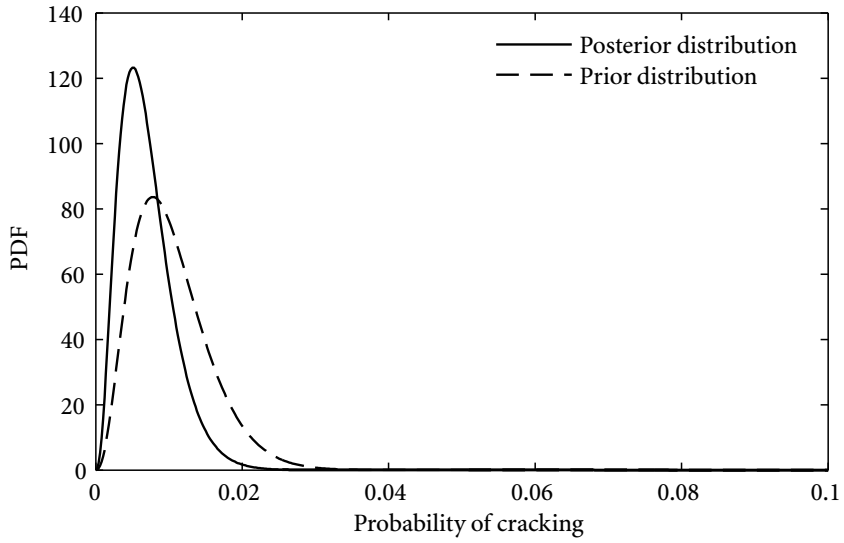

Figure 6.2 Prior and posterior distribution of the probability of feeder cracking

6.4 Example II: component specific analysis for random rate model

In previous Section 4.2, random rate model with sizing error is discussed and the ML estimate of the model parameters is obtained. The estimated model parameters can then be used to predict the flaw growth or failure time distribution of the uninspected components in the population. However, for a more refined degradation assessment, it is also important to predict the flaw growth and failure time distribution for each single inspected components, so that severe degraded components can be correctly identified and disposed through inspection and maintenance.

Unlike estimating the population flaw growth rate where the number of inspected components usually ranges from a few dozen to over hundred, providing enough data for ML analysis, the number of repeated inspections for a specific component is typically 3-4 times in the in-service inspection of nuclear power plants. With such a small data-set, the classical point estimate of the component specific rate cannot be given with high confidence. To have a better estimate, Bayesian method is employed.

6.4.1 Analysis

Zero initial degradation

First consider the random rate model with zero initial degradation. According to the model assumption, the flaw size of a specific ith component in the population at time t is given as

$$x_i(t) = r_i t,$$

where r_i is the flaw growth rate of the component. As discussed previously, r_i is a constant sampled from the population rate distribution R with PDF $f_R(r)$.

In Bayesian inference, estimate of the unknown constant r_i is treated as a random variable, denoted as R_i. Since r_i is a sample of the population rate distribution R, its prior distribution can be naturally taken the PDF of R. Therefore, the distribution of R_i, $f_{R_i}(r_i)$, is equivalent to the population rate distribution, conditioned on the component specific measurements, $\mathbf{y}_i = \{y_{i1}, y_{i2}, \cdots, y_{im_i}\}$, i.e., $R_i = R \,|\, \mathbf{y}_i$. Using Bayes' theorem, $f_{R_i}(r_i)$ can be obtained as

$$f_{R_i}(r_i) = f_{R|\mathbf{Y}_i}(r_i \,|\, \mathbf{y}_i) = C_1 f_{\mathbf{Y}_i}(\mathbf{y}_i; r_i) f_R(r_i),$$

where $C_1 = \left[\int_0^\infty f_{\mathbf{Y}_i}(\mathbf{y}_i; r_i) f_R(r_i) \mathrm{d}r_i\right]^{-1}$ is the normalization constant, $f_{\mathbf{Y}_i}(\mathbf{y}_i; r_i)$ is the joint PDF of the component specific measurements given growth rate r_i and is given by equation (4.2.7).

Given R_i, the corresponding Bayesian estimate of future flaw size $x_i(t)$, as a random variable $X_i(t)$, is

$$X_i(t) = R_i t.$$

The CDF of $X_i(t)$ is given as

$$\begin{aligned} F_{X_i(t)}(x) &= \bar{\mathcal{P}}\left[X_i(t) \leqslant x\right] = \bar{\mathcal{P}}\left[R_i \leqslant x/t\right] \\ &= F_{R_i}(x/t). \end{aligned} \tag{6.4.1}$$

Uncertain initial degradation

For the random rate model with uncertain initial degradation, the flaw size of the ith component at time t is

$$x_i(t) = a_i + r_i t,$$

where a_i is the initial degradation of the component, r_i is the component specific flaw growth rate. Similar to the case of zero initial degradation, the Bayesian estimates of a_i and r_i are probability distributions updated from the initial degradation distribution A and the population rate distribution R using the component specific measurements. Denote the estimation of a_i and r_i as A_i and R_i, respectively. From equation (4.2.10), the joint PDF of A_i and R_i is given as

$$f_{AR_i}(a_i, r_i) = C_2 f_{\mathbf{Y}_i}(\mathbf{y}_i; a_i, r_i) f_R(r_i) \phi(a_i; 0, \sigma_A), \tag{6.4.2}$$

where $C_2 = \left[\int_0^\infty \int_{-\infty}^\infty f_{\mathbf{Y}_i}(\mathbf{y}_i; a_i, r_i) f_R(r_i) \phi(a_i; 0, \sigma_A) \mathrm{d}a_i \mathrm{d}r_i\right]^{-1}$ is the normalization constant, $f_{\mathbf{Y}_i}(\mathbf{y}_i; a_i, r_i)$ is the PDF of the component specific measurements given by equation (4.2.10), and $\phi(a_i; 0, \sigma_A)$ is the assumed normal distribution of initial degradation of the components. Marginal distribution of the component specific initial degradation and flaw growth rate can be obtained by integrating equation (6.4.2) with respect to a_i and r_i respectively as (assuming R is defined on $[0, \infty)$ and A is defined on $(-\infty, \infty)$)

$$\begin{aligned} f_{A_i}(a_i) &= \int_0^\infty f_{A_i, R_i}(a_i, r_i) \mathrm{d}r_i. \\ f_{R_i}(r_i) &= \int_{-\infty}^\infty f_{A_i, R_i}(a_i, r_i) \mathrm{d}a_i, \end{aligned} \tag{6.4.3}$$

Denote the Bayesian prediction of the component's flaw size at time t as $X_i(t)$. One has

$$X_i(t) = A_i + R_i t,$$

Given the joint posterior distribution of A_i and R_i, $f_{AR_i}(a_i, r_i)$, PDF of $X_i(t)$ is

$$f_{X_i(t)}(x) = \int_0^\infty f_{AR_i}(x - r_i t, r_i) \mathrm{d}r_i. \tag{6.4.4}$$

Component specific failure time

From the distribution of $X_i(t)$, the failure time distribution for each specific component can be obtained. Suppose the maximum acceptable flaw size is x_{cr}. The CDF of the failure time of the ith component, T_i, is then

$$\begin{aligned} F_{T_i}(t) &= \mathcal{P}[T_i \leqslant t] = \mathcal{P}[X_i(t) > x_{\text{cr}}] \\ &= 1 - F_{X_i(t)}(x_{\text{cr}}), \end{aligned}$$

where $F_{X_i(t)}(x)$ is the CDF of $X_i(t)$ and can be calculate numerically from equation (6.4.1) or (6.4.4) for the case of zero initial degradation and uncertain initial degradation, respectively. The PDF of T_i can also be obtained correspondingly from numerical differentiation.

It is important to note that in a full Bayesian analysis, the parameters of the population rate distribution also need to be treated as random variables and their distributions should be estimated from some given prior distribution and the measurement data of all the inspected components using Bayes' theorem. However, when the inspection data are sufficiently large for the ML analysis, one may replace the Bayesian posterior of population rate parameter with a point estimate to simplify the component specific analysis. This type of mixed analysis method is called the empirical Bayesian method as the prior distribution used in the component specific analysis is estimated from empirical data using classical statistical method (Casella, 1985).

6.4.2 Application to the fretting wear of SG tubes

We would like revisit the fretting wear of SG tubes discussed in Section 4.2.5 and analyze the component specific wear rate of the inspected tubes using Bayesian method. The wear rate distribution of the component population is given as the estimated log-normal distribution in Section 4.2.5. The log-scale parameter of the population wear rate distribution is $\mu = -2.31$ and shape parameter is $\sigma = 0.165$. The initial wall thickness is assumed to be normally distributed with mean 6.5 mm and SD of 0.15 mm.

Two specific tubes, denoted as Tube A and B, are selected for the analysis. Measurements of the two tubes are listed in Table 6.1. The measured wear rates of the tubes are calculated as the difference between the nominal initial wall thickness and the last measured value

divided by time. As can be seen from the table, Tube A has a small measured rate of 0.046 mm/EFPY and Tube B has a larger measured rate of 0.144 mm/EFPY.

	Nominal initial thickness	17.08 EFPY	18.4 EFPY	Measured rate
Tube A	6.5 mm	5.39 mm	N.A.	0.046 mm/EFPY
Tube B	6.5 mm	3.94 mm	3.85 mm	0.144 mm/EFPY

Table 6.1 Measurements of the two selected tubes from the SG tube wear data

From equation (6.4.3), the component specific rates of the two tubes are calculated. The results are presented in Figure 6.3 along with the population rate distribution (the prior). The averages of the estimated thinning rate of Tube A and B are 0.85 mm/EFPY and 0.13 mm/EFPY, respectively. The 95th percentiles of the thinning rate of the two tubes are 0.10 mm/EFPY and 0.15 mm/EFPY. It is found that the estimated rate of Tube A using Bayesian method is significantly higher than its measured rate. This is because the measured rate of Tube A is at the far left tail of the population rate distribution, and therefore it is very likely that the small measured rate is caused by sizing error or initial uncertainty of wall thickness. Bayesian estimation considered this possibility properly.

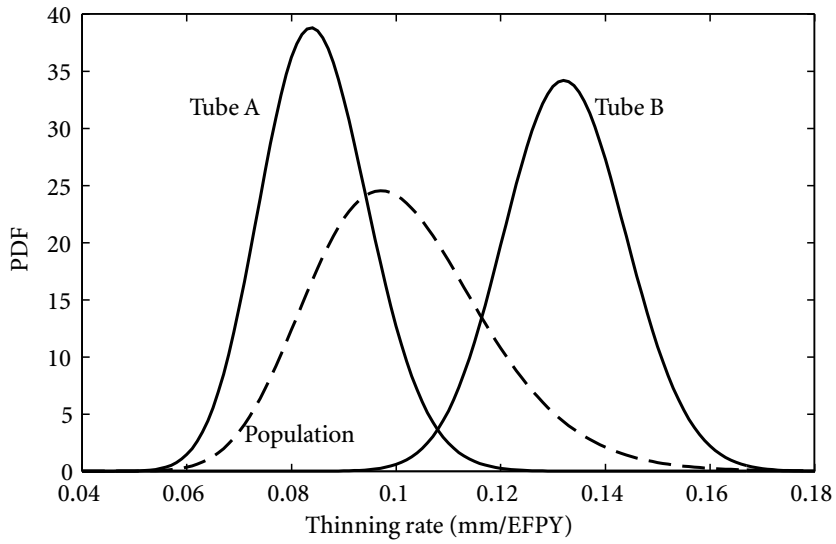

Figure 6.3 Estimated thinning rate distributions of Tube A and B using Bayesian method

Suppose the maximum acceptable wall thickness loss with respect to the nominal initial value is $x_{cr} = 3.0$ mm. The failure time distributions for Tube A and B are calculated and plotted in Figure 6.4, along with the failure time distribution of the tube population for comparison. The mean, SD and 5% lower percentile of the failure time for Tube A and B are 42.8 EFPY, 5.0 EFPY, 35.4 EFPY, and 25.8 EFPY, 1.8 EFPY, 22.9 EFPY, respectively. As Tube B is already close to its end of life, the SD of its failure time estimate is significantly smaller than that of Tube A. These results from the tube specific analyses can then be used for more refined life cycle management of the SG tubes. For example, replacement of Tube B should be planned in near term as its end of life is imminent.

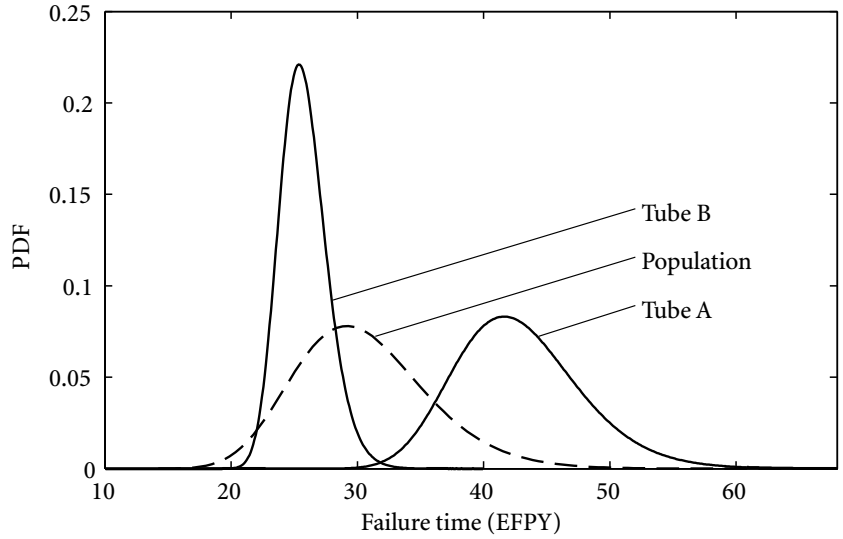

Figure 6.4 Estimated failure time distribution of Tube A and B compared with the failure time of the population

6.5 Summary

This chapter discusses the use of Bayesian inference in degradation modelling. Unlike the classical parameter inference, where the main objective is to find a point estimate of the unknown parameter, in Bayesian inference, model parameters themselves are treated

as random variables and their distributions are updated from prior distributions through Bayes' theorem as inspection data become available.

The most notable advantage of Bayesian inference over classical methods is its ability to incorporate background information in the estimation process. This ability is important for improved degradation assessment, especially when inspection data are scarce. Another advantage of Bayesian inference is that its way of presenting parameter uncertainty is more natural than the classical confidence interval method. Two practical examples, predicting the probability of feeder cracking and the component specific analysis for the random rate model, are then presented to demonstrate the application of Bayesian inference to practical degradation problems.

CHAPTER 7

Simulation-based Bayesian Computation

7.1 Introduction

This chapter discusses the computational aspects of Bayesian inference for complex stochastic models. Recall that the basic form of Bayesian inference is

$$\pi(\theta \,|\, x) = \frac{f_X(x;\theta)\pi(\theta)}{\int f_X(x;\theta)\pi(\theta)\mathrm{d}\theta} = CL(\theta \,|\, x)\pi(\theta), \tag{7.1.1}$$

where $L(x \,|\, \theta)$ is the same likelihood function used in ML analysis, $C = \left[\int f_X(x)\pi(\theta)\mathrm{d}\theta\right]^{-1}$ is the normalization constant. The objective of Bayesian inference is then to infer the posterior distribution $\pi(\theta \,|\, x)$, or alternatively, statistics such as mean and SD, of $\pi(\theta \,|\, x)$. Only for some simple probabilistic models and specially selected priors, analytic solutions of the posterior exist. For most other models, the Bayesian posterior has to be evaluated numerically.

Direct numerical evaluation of the Bayesian posterior using equation (7.1.1), however, can be quite difficult. First, for some models, such as the gamma process model and the Poisson model with inspection uncertainties, numerical evaluation of the likelihood function is extremely difficult, which makes direct calculation of posterior distribution impractical. In other cases, even if the likelihood function itself is relative easy to evaluate, calculation of the normalization constant C, which is an integral over the entire admissible region of the model parameter, can still be a time consuming step, especially when the parameter θ is of high dimension.

The computational difficulty has been a major obstacle to the application of Bayesian inference until recent years when various advanced Monte Carlo methods were developed. Instead of calculating the posterior density numerically, Monte Carlo simulation aims to draw random samples that follow the posterior distribution. These samples are then regarded as a representation of the posterior distribution of the model parameters and can be used in subsequent tasks of the probabilistic degradation assessment.

In this chapter, two particular simulation techniques, the Markov chain Monte Carlo (MCMC) and the approximate Bayesian computation (ABC), are introduced. By incorporating MCMC and ABC with some other methods, such as the auxiliary variable method or the smoothed bootstrapping, new algorithms are proposed for Bayesian inference of complicated stochastic models like the Poisson process model and the gamma process model subject to inspection uncertainties. Practical examples are presented to demonstrate the effectiveness of the proposed methods.

7.2 Markov chain Monte Carlo

7.2.1 Introduction

Drawing random samples from posterior distribution is the key step of simulation-based Bayesian inference. Numerous simulation techniques have been developed for generating random samples from uniform distribution and other common probability distributions. However, in Bayesian inference, the posterior distribution can be very non-standard. In such cases, conventional simulation methods, such as the inverse transform sampling, are not applicable.

One way to generate random samples from complicated distributions is the Markov chain Monte Carlo (MCMC) simulation, which is a general simulation technique based on drawing samples iteratively from a Markov chain with target distribution as its stationary distribution. The concepts of Markov chain and its stationary distribution are further explained below.

A random sequence, $\{X_0, X_1, X_2, \cdots\}$, is called a Markov chain if at each step t, the state of next step X_{t+1} depends only on the current state X_t and is conditionally independent of

the history of the chain $\{X_0, X_1, \cdots X_{t-1}\}$ (Roberts, 1996). Mathematically, that is

$$\mathcal{P}(X_{t+1} \,|\, X_t, X_{t-1}, \cdots, X_0) = \mathcal{P}(X_{t+1} \,|\, X_t).$$

The conditional probability $\mathcal{P}(X_{t+1} \,|\, X_t)$ is called the transition kernel of the Markov chain.

A Markov chain is said to be time-homogeneous, if its transition kernel $\mathcal{P}(X_{t+1} \,|\, X_t)$ is independent of t. An important feature of the time-homogeneous Markov chain is that the points in the chain will gradually "forget" its initial state and converge to a unique stationary distribution that does not depend on t or initial state X_0. In other words, after a sufficiently long "burn-in" step, new points generated by the time-homogeneous Markov chain are dependent samples with the same marginal distribution as the stationary distribution. Strict mathematical theory for the existence and uniqueness of the stationary distribution of Markov chain can be found at Roberts (1996) and Tierney (1996).

Thus, after, say m burn-in steps, points $\{X_{m+1}, X_{m+2}, \cdots, X_n\}$ in the Markov chain can be regarded as dependent random samples with the marginal distribution being approximately the stationary distribution. If the Markov chain is constructed in such a way that its stationary distribution is the same as the Bayesian posterior, these samples can be used for certain Bayesian analysis, such as calculating the posterior mean and standard deviation.

A number of algorithms have been developed for constructing Markov chains with stationary distributions as any given target distribution. In the next, two most common MCMC algorithms, namely, the Gibbs sampler and Metropolis-Hasting (M-H) algorithm, are introduced. Based on the M-H algorithm and a simulation technique called the auxiliary variable method, MCMC simulation for Bayesian inference of the Poisson process model with inspection uncertainties is proposed. A numerical example is presented as an illustration of the proposed method.

7.2.2 Gibbs sampler

In order to have a better understanding of the MCMC simulation, we first introduce Gibbs sampler (Geman and Geman, 1984), which is one of the simplest algorithms to construct a Markov chain with stationary distribution as a given target distribution.

Gibbs sample is suitable when drawing samples from the conditional distribution of a multivariate random variable is easier than drawing samples from its joint distribution. Consider the simple bivariate case. Suppose $\mathbf{X}=(X_1, X_2)$ is a bivariate random vector with X_1 and X_2 as its two elements. The joint distribution of $\mathbf{X}$ is $\pi(x_1, x_2)$. Denote the conditional distribution of X_1 given X_2 and X_2 given X_1 as $\pi(x_1 \,|\, x_2)$ and $\pi(x_2 \,|\, x_1)$, respectively. When drawing samples from conditional distribution $\pi(x_1 \,|\, x_2)$ and $\pi(x_2 \,|\, x_1)$ is easier than sampling directly from $\pi(x_1, x_2)$, the Gibbs sampler can be applied, as described in Algorithm 1.

Algorithm 1 Gibbs sampler

1: Select an initial point $\mathbf{x}^{(0)}=(x_1^{(0)}, x_2^{(0)})$.

2: Given the tth sample $\mathbf{x}^{(t)}=(x_1^{(t)}, x_2^{(t)})$, generate the next sample recursively according to the following conditional distributions

$$\begin{aligned} x_1^{(t+1)} &\sim \pi(x_1^{(t)} \,|\, x_2^{(t)}) \\ x_2^{(t+1)} &\sim \pi(x_2^{(t+1)} \,|\, x_1^{(t+1)}). \end{aligned}$$

3: Stop when required number of samples are generated.

It can be shown that every iteration in Gibbs sampler leaves the joint distribution invariant. That is to say, if $\mathbf{x}^{(t)}$ follows the stationary distribution of the Markov chain, so does $\mathbf{x}^{(t+1)}$. Denote the transition kernel of the Gibbs sampler in Algorithm 1 as $p(\mathbf{x}^{(t+1)} \,|\, \mathbf{x}^{(t)})$. One has

$$p(\mathbf{x}^{(t+1)} \,|\, \mathbf{x}^{(t)}) = \pi(x_2^{(t+1)} \,|\, x_1^{(t+1)}) \pi(x_1^{(t+1)} \,|\, x_2^{(t)}).$$

Suppose the joint distribution of $\mathbf{x}^{(t)}$ is the target distribution $\pi(x_1, x_2)$. Then the joint distribution of $\mathbf{x}^{(t+1)}$ is given as

$$\begin{aligned} f_{\mathbf{X}^{(t+1)}}(x_1^{(t+1)}, x_2^{(t+1)}) &= \int p(\mathbf{x}^{(t+1)} \,|\, \mathbf{x}^{(t)}) \pi(x_1^{(t)}, x_2^{(t)}) \mathrm{d}x_1^{(t)} \mathrm{d}x_2^{(t)} \\ &= \int \pi(x_2^{(t+1)} \,|\, x_1^{(t+1)}) \pi(x_1^{(t+1)} \,|\, x_2^{(t)}) \mathrm{d}x_2^{(t)} \\ &= \pi(x_2^{(t+1)} \,|\, x_1^{(t+1)}) \pi_1(x_1^{(t+1)}) = \pi(x_1^{(t+1)}, x_2^{(t+1)}), \end{aligned}$$

where $\pi_1(x_1) = \int \pi(x_1, x_2) \mathrm{d}x_2$ is the marginal distribution of X_1.

In the next, an example of Gibbs sampler is presented to illustrate the implementation of the method. Consider a bivariate normal random vector $\mathbf{X}=(X_1, X_2)$ with mean zero and covariance matrix Σ as

$$\Sigma = \begin{bmatrix} 1 & \rho \\ \rho & 1 \end{bmatrix}$$

where $\rho = 0.8$. The conditional distribution of X_1 and X_2 is then given by

$$\begin{aligned} X_2 \,|\, X_1 &\sim \mathrm{N}\left(\rho x_1, (1-\rho^2)\right) \\ X_1 \,|\, X_2 &\sim \mathrm{N}\left(\rho x_2, (1-\rho^2)\right). \end{aligned} \tag{7.2.1}$$

Starting from some initial point $(x_1^{(0)}, x_2^{(0)})$, a Markov sequence can be generated from the conditional distribution (7.2.1) using Gibbs sampler. As the iteration steps increase, the sequence gradually "forgets" its initial state $(x_1^{(0)}, x_2^{(0)})$ and converges to the target distribution, as shown in Figure 7.1 where the first 20 steps starting from two different initial points are plotted. As can be seen from figure, the sequence quickly converges to the area where higher target density locates.

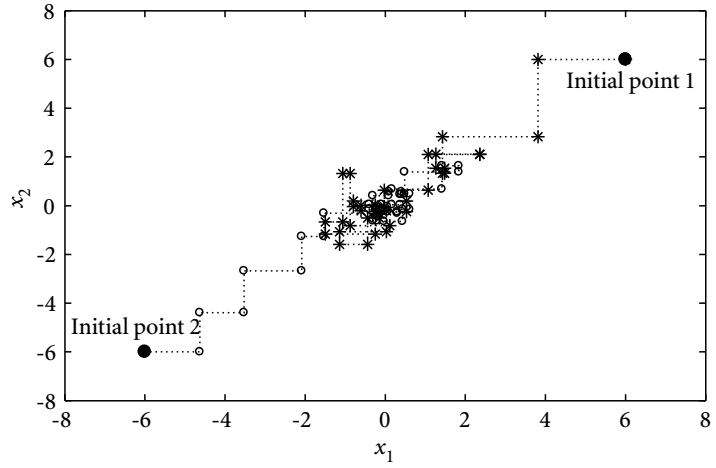

Figure 7.1 First 20 steps of the Gibbs sampler from two different initial points

Gibbs sampler is very effective when the conditional distributions are known and easy to draw samples from. However, for many practical problems, sampling from conditional

distributions is also not very easy. In those cases, Metropolis-Hastings algorithm can be used.

7.2.3 Metropolis-Hastings algorithm

Metropolis-Hastings (M-H) algorithm is a general method for constructing Markov chains targeting any arbitrary probability distribution using a prescribed transition rule. For drawing samples $\mathbf{x}^{(t)}$ from distribution $\pi(\mathbf{x})$ using the M-H algorithm, a proposal distribution function $T(\mathbf{y} \,|\, \mathbf{x})$ and an acceptance-rejection rule are needed. The basic procedures of the M-H algorithm are given in algorithm 2 (Gilks et al., 1996b).

Algorithm 2 M-H algorithm

1: Select an initial point $\mathbf{x}^{(0)}$.

2: Given $\mathbf{x}^{(t)}$, draw a sample $\mathbf{y}$ from the proposal distribution $T(\mathbf{y} \,|\, \mathbf{x}^{(t)})$.

3: The next point in the chain is given by

$$\mathbf{x}^{(t+1)} = \begin{cases} \mathbf{y}, & \text{if } U \leqslant r(\mathbf{x}^{(t)}, \mathbf{y}), \\ \mathbf{x}^{t}, & \text{otherwise,} \end{cases}$$

where

$$r(\mathbf{x}, \mathbf{y}) = \min \left\{ 1, \frac{\pi(\mathbf{y}) T(\mathbf{x} \,|\, \mathbf{y}))}{\pi(\mathbf{x}) T(\mathbf{y} \,|\, \mathbf{x})} \right\}$$

is the rejection function.

4: Stop when required number of samples are generated.

It is worth noting that in M-H algorithm the proposal function $T(\mathbf{y} \,|\, \mathbf{x})$ can be chosen as any distribution and the stationary distribution of the Markov sequence will remain $\pi(\mathbf{x})$. However, the proposal function does affect the rate of the convergence greatly. To conduct the M-H algorithm efficiently, an appropriate proposal function is crucial. For simple target distributions, the independent proposal function, i.e., $T(\mathbf{y} \,|\, \mathbf{x}^{(t)}) = T(\mathbf{y})$, can be used. When $T(\mathbf{y})$ is a good approximation of the target distribution $\pi(\mathbf{x})$, M-H algorithm usually works well (Tierney, 1994; Gilks et al., 1996b). Another common choice of the proposal function is the normal distribution $\mathrm{N}(\mathbf{y}; \mathbf{x}^{(t)}, \Sigma)$, with mean $\mathbf{x}^{(t)}$ and a properly tuned covariance

matrix Σ. For further discussion on the choice of proposal functions, refer to Tierney (1994); Gilks et al. (1996a); Rosenthal (2009).

From the procedures of the M-H algorithm, it can be seen that the target function $\pi(\mathbf{x})$ in M-H algorithm does not need not to be a normalized probability density function. That is to say, one does not need to evaluate the normalization constant C in equation (7.1.1), which simplifies the computation of Bayesian inference.

To illustrate the use of the M-H algorithm, a simple Gaussian example is presented. Suppose X is a standard normal random variable, i.e., $X \sim \mathcal{N}(0, 1^2)$. Instead of using traditional independent sampling technique, the M-H algorithm is used. The proposal distribution is chosen as $T(y|x) \sim \mathcal{N}(x, 0.6^2)$. Figure 7.2 shows a Markov sequence generated by the M-H algorithm and the corresponding histogram after 500 burn-in steps. It can seen that the result matches the theoretical density function very well.

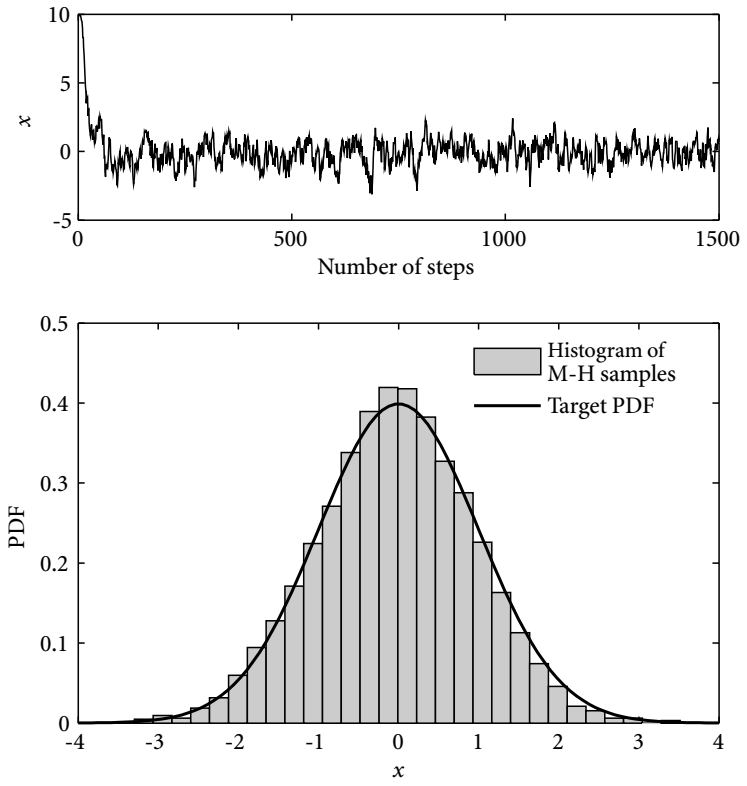

Figure 7.2 Sequence of x generated by M-H algorithm and the corresponding histogram after 500 burn-in steps

7.2.4 Application to the Poisson flaw generation model

In Chapter 5, stochastic modelling of flaw generation using the Poisson process model is discussed. When considering both sizing error and probability of detection (PoD), the likelihood function of the model parameters, i.e., equation (5.3.12) given in Section 5.3, becomes very complicated. Numerical evaluation of the model likelihood is difficult for large data-sets because of the convolution calculations involved. In this section, an MCMC simulation using the M-H algorithm and method of auxiliary variables is proposed. Using the proposed method, Bayesian inference of the Poisson flaw generation model can be conducted without doing the time-consuming convolutions.

Likelihood function

Recall that in Section 5.3, the likelihood function of the Poisson flaw generation are derived as

$$L(\lambda,\theta\,|\,\mathbf{y}_1,\mathbf{y}_2,\cdots,\mathbf{y}_n)=\prod_{i=1}^{n}L_i(\lambda,\theta\,|\,\mathbf{y}_i)=\prod_{i=1}^{n}\left[f_{D_i}(d_i)\prod_{j=1}^{d_i}f_{Y_i}(y_{ij})\right],$$

where λ is the Poisson rate of the flaw generation, θ is the parameter of the flaw size distribution, and $\mathbf{y}_i=\{y_{i1},y_{i2},\cdots,y_{id_i}\}$ are the measured size of the d_i detected flaws in the ith inspection. Due to the random sizing error, PDF of the measured flaw size Y_i is the convolution of the actual flaw size distribution and the random sizing error, i.e.,

$$f_{Y_i}(y)=\int_{-\infty}^{\infty}f_{\mathcal{D}X_i}(y-e)f_E(e)\mathrm{d}e, \tag{7.2.2}$$

where $f_{\mathcal{D}X_i}(x)$ is the actual size distribution of detected flaws in the ith inspection and is given by equation (5.3.11), $f_E(e)$ is the PDF of the sizing error. As discussed previously in Section 5.3.6, convolution (7.2.2) is the major computational difficulty in the likelihood evaluation.

Sizing error as auxiliary variables

Suppose the sizing error of the flaw measurement in the ith inspection is known as $\mathbf{e}_i=\{e_{i1},e_{i2},\cdots,e_{id_i}\}$, $i=1,2,\cdots,n$. The model likelihood function can then be formu-

lated without having any convolutions as

$$L(\lambda,\theta\,|\,\mathbf{y}_1,\mathbf{y}_2,\cdots,\mathbf{y}_n,\mathbf{e}_1,\mathbf{e}_2,\cdots,\mathbf{e}_n) = \prod_{i=1}^{n} L_i(\lambda,\theta\,|\,\mathbf{y}_i,\mathbf{e}_i) = \prod_{i=1}^{n}\left[f_{D_i}(d_i)\prod_{j=1}^{i} f_{X_i}(y_{ij}-e_{ij})\right]. \tag{7.2.3}$$

In reality, of course, sizing errors associated with the inspection data are not known and therefore equation (7.2.3) cannot be used directly for the parameter estimation.

However, when looking into equation (7.2.3) from a different perspective, sizing errors $\mathbf{e}_i$ can also be regarded as a set of hidden parameters of the flaw generation model. When so regarded, equation (7.2.3) is rewritten in the following form as

$$L(\lambda,\theta,\mathbf{e}_1,\mathbf{e}_2,\cdots,\mathbf{e}_n\,|\,\mathbf{y}_1,\mathbf{y}_2,\cdots,\mathbf{y}_n) = \prod_{i=1}^{n} L_i(\lambda,\theta\,|\,\mathbf{y}_i,\mathbf{e}_i) = \prod_{i=1}^{n}\left[f_{D_i}(d_i)\prod_{j=1}^{i} f_{X_i}(y_{ij}-e_{ij})\right], \tag{7.2.4}$$

where $\mathbf{e}_i$ are introduced as the auxiliary variables of the model. Obviously, the prior distribution of $\mathbf{e}_i$ is the density function of the sizing error of the inspection probe. Now, if the joint posterior distribution of λ, θ and $\mathbf{e}_i$ can be obtained, posterior distribution of λ and θ is then simply the marginal distribution of the joint posterior excluding the auxiliary variables $\mathbf{e}_i$. This method is called the method of auxiliary variables (Besag and Green, 1993).

The M-H algorithm is then applied to the Bayesian inference of the flaw generation model with $\mathbf{e}_i$ as auxiliary variables. Univariate normal proposal functions are used for parameter λ and θ, respectively, with properly tuned standard deviation. For the auxiliary variable $\mathbf{e}_i$, the sizing error distribution of the inspection probe is applied as the independent proposal function. For ease of presentation, let $\mathbf{s}=\{\lambda,\theta,\mathbf{e}_1,\mathbf{e}_2,\cdots,\mathbf{e}_n\}$ and $L(\mathbf{s})$ be equation (7.2.4). Given the prior distribution $\pi(\lambda,\theta)$, Markov chain Monte Carlo simulation of the Poisson flaw generation can be conducted using the procedures described in Algorithm 3.

Numerical example

An example using generated data is presented to illustrate the use of MCMC simulation and auxiliary variable method in the estimation of the Poisson flaw generation model. Suppose

Algorithm 3 M-H algorithm for Poisson flaw generation

1: Select an initial point $\lambda^{(0)}, \theta^{(0)}$ and $\mathbf{e}_i^{(0)}$ for parameters λ and θ, and the auxiliary variables $\mathbf{e}_i$, respectively. Denote the initial point as $\mathbf{s}^{(0)} = \{\lambda^{(0)}, \theta^{(0)}, \mathbf{e}_1^{(0)}, \cdots, \mathbf{e}_n^{(0)}\}$.

2: Given the tth point $\mathbf{s}^{(t)} = \{\lambda^{(t)}, \theta^{(t)}, \mathbf{e}_1^{(t)}, \cdots, \mathbf{e}_n^{(t)}\}$, draw new samples λ^* and θ^* from the proposal distribution $T(\lambda, \theta \,|\, \lambda^{(t)}, \theta^{(t)})$ and new samples of the sizing errors $\mathbf{e}_i^*$ from the sizing error distribution. Let $\mathbf{s}^* = \{\lambda^*, \theta^*, \mathbf{e}_1^*, \cdots, \mathbf{e}_n^*\}$.

3: Generate a random number u that is uniformly distributed in between 0 and 1.

4: The next point of the Markov chain is given as

$$\mathbf{s}^{(t+1)} = \begin{cases} \mathbf{s}^*, & \text{if } u \leqslant r(\mathbf{s}^{(t)}, \mathbf{s}), \\ \mathbf{s}^t, & \text{otherwise,} \end{cases}$$

where

$$r(\mathbf{s}, \mathbf{s}^*) = \min \left\{ 1, \frac{L(\mathbf{s}^*)\pi(\lambda^*, \theta^*)T(\lambda, \theta \,|\, \lambda^*, \theta^*)}{L(\mathbf{s})\pi(\lambda, \theta)T(\lambda^*, \theta^* \,|\, \lambda, \theta)} \right\}$$

is the rejection function.

5: Stop when required number of samples are generated.

the flaw generation in a structure follows a homogeneous Poisson process with rate λ. The flaw size is log-normal distributed with parameter log-scale μ and shape parameter σ. The At time zero, there are no flaws in the structure. In total, 4 inspections are conducted at 4, 8, 12 and 16 years. After each inspection, all detected flaws are eliminated. The PoD of the inspection probe is given as the log-logistic function with parameters $a = -10$ and $b = 3$ (i.e., the PoD function of the poor probe in Figure 2.1). The sizing error of the inspection probe is assumed to be normally distributed with mean zero and SD 6.

A simulated data-set including the number of detected flaws and their measured sizes are generated using the procedures described in the Appendix A.2. The true values of the model parameters are given as $\lambda = 10$, $\mu = 3.5$ and $\sigma = 0.4$. A summary of the generated data-set is presented in Figure 7.3. The data are then used to estimate the model parameters using MCMC simulation and the auxiliary variable method.

With a set of initial value $\lambda_0 = 16$, $\mu_0 = 2.5$ and $\sigma_0 = 1.5$, MCMC simulation is performed with 2×10^4 iterations using Algorithm 3. Since no convolutions are involved, the calculation

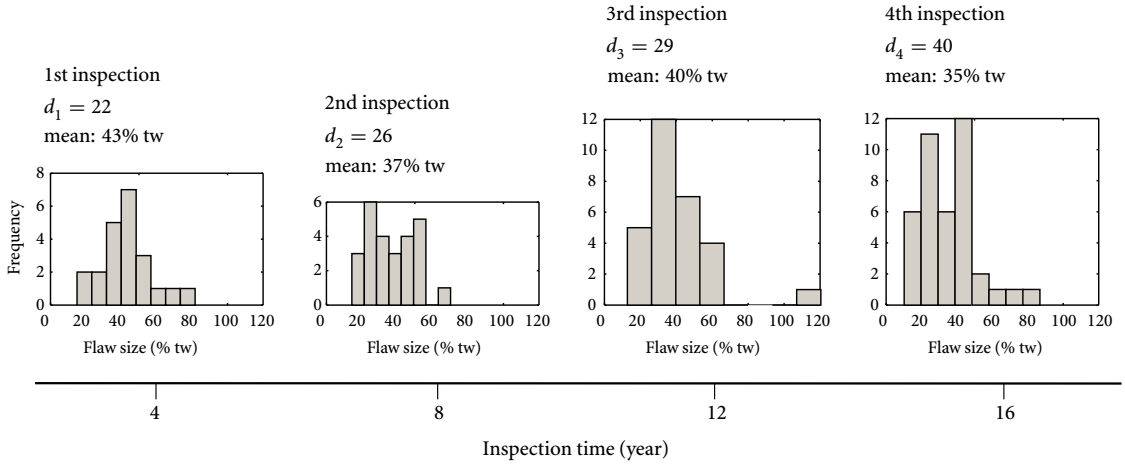

Figure 7.3 A summary of the generated flaw detection and measurement data

can be done very fast. The simulated sequences and their histograms (after 5000 burn-in steps) are plotted in Figure 7.4. From the simulated sequences, mean, SD and percentiles of the estimated parameters can be obtained easily, as given in Table 7.1. It is shown from the results that after a short burn-in stage, the MCMC sequence quickly converges to the stationary distribution with good mixing. The posterior parameters samples cover reasonable ranges near the true value of the parameters from which the data are generated, thus validate the correctness of the method. The estimated posterior distribution can then be used to predict the number of new flaws and their corresponding flaw sizes at the next inspection time.

Parameters	True value	Estimate		
		Mean	SD	95th percentile
λ	10	10.6	1.2	12.8
μ	3.5	3.36	0.07	3.47
σ	0.4	0.54	0.05	0.63

Table 7.1 Mean, SD and the 95th percentile of the estimated λ, μ and σ, compared with the true values

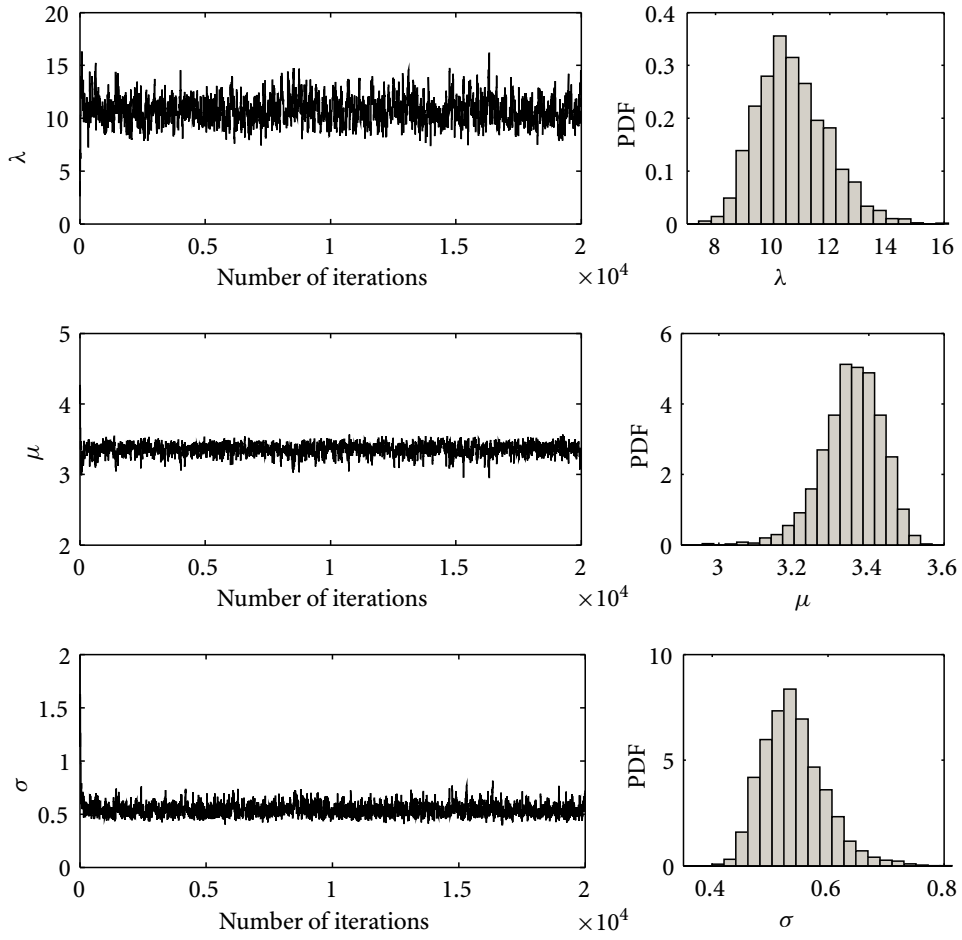

Figure 7.4 Simulated sequence of λ, μ and σ and their histograms (after 5000 burn-in steps)

7.3 Approximate Bayesian computation

7.3.1 Introduction

In the last section, MCMC simulation with auxiliary variable method is proposed for Bayesian inference of the Poisson flaw generation model subject to PoD and sizing error. By treating the sizing errors as auxiliary variables or hidden parameters, the time-consuming convolution in the model likelihood are avoided. In order to conduct the proposed MCMC method successfully, it is important to have an appropriate proposal function for the auxiliary variables. In the Poisson flaw generation model, since the sizing error are all indepen-

dent normal random variables, an independent normal proposal function performs well, as shown in the numerical example we presented. However, for the gamma process model with sizing error, as discussed in Section 4.3, the error term associated with the flaw size increments are correlated, which makes it difficult to find an appropriate proposal function that guarantees a quick convergence of the MCMC simulation. An alternative simulation method, called the approximate Bayesian computation (ABC), is applied.

Approximate Bayesian computation, also known as likelihood-free Bayesian inference, has been considered as a powerful approach in recent years for the parameter inference of complicated probabilistic models, where the likelihood functions are computationally intractable or too expensive to evaluate. The basic idea of ABC method is to replace the difficult numerical evaluation of the model likelihood by a comparison between the simulated data-sets and the actual observed data-set. If the simulated data-sets using certain values of the parameters are on average "closer" to the observed data-set, these values are conceived more likely to be the true values of the parameters.

ABC method was first applied in population genetics by Tavare et al. (1997) in its basic form as a rejection Monte Carlo sampler. Since then, various extensions of the method have been developed and applications are mainly found in fields such as bioinformatics, population genetics, ecology (Marin et al., 2011).

Suppose the joint distribution density of the observational data $\mathbf{x}$ from a statistical model is given as $f_{\mathbf{X}}(\mathbf{x};\theta)$, where θ is the model parameter. Here θ can be a vector if the model has more than one parameter. Given a set of observed data $\mathbf{x}_{\text{obs}}$ and the prior distribution $\pi(\theta)$, the aim of Bayesian inference is to infer the posterior distribution $\pi(\theta|\mathbf{x}_{\text{obs}}) \propto f_{\mathbf{X}}(\mathbf{x}_{\text{obs}};\theta)\pi(\theta)$. For many models, the direct evaluation of the model PDF $f_{\mathbf{X}}(\mathbf{x};\theta)$ could be extremely time consuming while the simulation of the data is relatively easy (e.g., the gamma process model with sizing errors). In such circumstances, ABC method can be applied, which has the following basic form as Algorithm 4 (Tavare et al., 1997).

It can be shown that output from the above basic ABC algorithm are samples from distribution $\pi(\theta \,|\, d(\mathbf{x}_{\text{obs}}, \mathbf{x}_{\text{sim}}) < \epsilon)$ (Toni et al., 2009). When ϵ is sufficiently small, the basic ABC method is able to produce a good approximation of samples from posterior distribution $\pi(\theta \,|\, \mathbf{x}_{\text{obs}})$. The disadvantages of the basic form of ABC are two-fold. First,

Algorithm 4 Basic ABC algorithm

1: Generate a candidate value of parameters θ_{sim} from prior distribution $\pi(\theta)$.

2: Generate a data-set $\mathbf{x}_{\text{sim}}$ with parameter θ_{sim} using model PDF $f_{\mathbf{X}}(\mathbf{x};\theta)$.

3: Compare the difference between the simulated data-set $\mathbf{x}_{\text{sim}}$ and the observed data $\mathbf{x}_{\text{obs}}$ using a distance function $d(\mathbf{x}_{\text{obs}}, \mathbf{x}_{\text{sim}})$. If the distance is less than a small given tolerance limit ϵ, accept θ_{sim}; otherwise reject.

4: Repeat steps 1-3 until enough number of samples of the parameters are accepted.

it is often difficult to define a suitable distance function, which is crucial to the success of the algorithm. In many applications with large data-sets, a summary statistics of the data $S(\mathbf{x})$ is often used and the distance function is defined on $S(\mathbf{x})$ as $d\left(S(\mathbf{x}_{\text{obs}}, \mathbf{x}_{\text{sim}})\right)$. Nevertheless, finding an appropriate summary statistic is still not an easy task. Second, there is no established rule for the choice of the tolerance threshold ϵ. A small ϵ gives better approximation of the posterior distribution but at the price of lower acceptance rate thus longer computation time. To improve the acceptance rate for smaller threshold, other advanced simulation techniques, such as Markov chain Monte Carlo (MCMC) and sequential Monte Carlo (SMC), are proposed to be integrated with the basic ABC algorithm (Marjoram et al., 2003; Sisson et al., 2007).

Wilkinson (2008) proposed an alternative ABC algorithm which gives exact posterior samples when observations contain independent error terms. Denote the true value of the model output as $\mathbf{X}$ and the observation as $\mathbf{Y}$, $\mathbf{Y}=\mathbf{X}+\mathbf{E}$, where $\mathbf{E}$ is the error term and is independent of $\mathbf{X}$. The probability density functions of $\mathbf{X}$ and $\mathbf{E}$ are $f_{\mathbf{X}}(\mathbf{x};\theta)$ and $f_{\mathbf{E}}(\mathbf{e})$, respectively. Given prior distribution of parameter vector $\pi(\theta)$ and the observation $\mathbf{y}_{\text{obs}}$, Wilkinson (2008) proved that Algorithm 5 gives samples following exactly the posterior distribution $\pi(\theta \,|\, \mathbf{y}_{\text{obs}})$ without explicitly calculating the PDF of $\mathbf{Y}$.

In step 3 of Algorithm 5, c is a normalization constant chosen to guarantee that $c f_{\mathbf{E}}(\mathbf{y}_{\text{obs}} - \mathbf{x}_{\text{sim}})$ defines a proper probability (i.e., defined between 0 and 1). One can take $c = 1/\max[f_{\mathbf{E}}(\mathbf{e})]$, so that the maximum possible acceptance rate can be achieved. A interesting feature of the Wilkinson's algorithm is that its efficiency improves when the error term is larger, since a more dispersed $f_{\mathbf{E}}(\mathbf{e})$ will result in a higher acceptance rate in the simulation.

Algorithm 5 Wilkinson's ABC algorithm

1: Generate a candidate value θ_{sim} from prior distribution $\pi(\theta)$.

2: Generate an error-free data-set $\mathbf{x}_{\text{sim}}$ with parameter θ_{sim} using true model PDF $f_{\mathbf{X}}(\mathbf{x};\theta)$.

3: Accept θ_{sim} with probability $cf_{\mathbf{E}}(\mathbf{y}_{\text{obs}}-\mathbf{x}_{\text{sim}})$.

4: Repeat steps 1-3 until enough number of samples are accepted.

Wilkinson's ABC algorithm was proposed mainly to understand the tolerance threshold in the basic ABC algorithm. From Wilkinson's perspective, the rejection step in the basic ABC method is equivalent to using the following acceptance probability

$$cf_{\mathbf{E}}(\mathbf{x}_{\text{obs}}-\mathbf{x}_{\text{sim}}) = \begin{cases} 1 & \text{if } d(S(\mathbf{x}_{\text{obs}}), S(\mathbf{x}_{\text{sim}})) \leqslant \epsilon, \\ 0 & \text{otherwise.} \end{cases} \tag{7.3.1}$$

That is the same as saying that the basic ABC algorithm gives the exact inference for the model that assumes an additional independent error term uniformly distributed on the region defined by the 0-1 cut-off in equation (7.3.1) (Wilkinson, 2008).

7.3.2 Sequential Bayesian updating using ABC

Direct use of Wilkinson's ABC in practical problems, however, remains very limited, despite its clear advantage of being able to give exact posterior samples. One possible reason is that in many problems, especially in bioinformatics and population genetics where ABC was originally developed, the error term is difficult to quantify, which confounds the implementation of the method. Another reason is that the acceptance rate of Wilkinson's method for large data-set can be very small, making it impractical for many problems.

In the stochastic modelling of degradation growth, these difficulties of Wilkinson's algorithm can somehow be avoided. Firstly, distribution of the measurement error of the NDE inspection can be obtained in laboratory experiments by carefully analyzing the measurements from the NDE probes with exact results from destructive metallographic examinations. Secondly, although the inspection data as a whole can consist of hundreds of data points, the number of repeated inspections for each single component is usually limited to 3 or 4 times. Using sequential Bayesian update, parameter inference given a large data-set

can be divided into a series of similar Bayesian update on smaller scales, thus improving the overall acceptance rate of the Wilkinson's ABC.

The idea of sequential Bayesian update is very simple. Suppose the degradation data are from a group of n components. If the degradation of each component is considered to be independent, the posterior distribution of the model parameters can be calculated by applying the Bayesian theorem recursively. That is, in each step only data from one component are used for Bayesian update, and the posterior obtained is then used as the prior distribution for the next update. In the next, technical details of the sequential Bayesian updating using ABC method are discussed, using the gamma process model with sizing error as an example.

Statistical data cloning

An important characteristic of ABC method is that both prior and posterior distributions are represented using samples instead of probability density functions. After each update in ABC, only a small portion of the prior samples are accepted as the posterior samples. Therefore, without generating new samples in each step, meaningful sequential Bayesian update can only be conducted for a few steps. The simulation techniques used for generating new samples from existing samples are sometimes referred as statistical data cloning techniques (Shakhnarovich et al., 2001).

One of the most widely used statistical data cloning techniques is the smoothed bootstrapping method (El-Nouty and Guillou, 2000), which is a method based on the non-parametric kernel density estimation of the existing samples. First consider the univariate case. Suppose $s_i, i=1,2,\cdots,N$, are N existing samples following some unknown distribution $f(s)$. The non-parametric kernel density estimation of $f(s)$, denoted as $\hat{f}(s)$, is given as (Silverman, 1986)

$$\hat{f}(s) = \frac{1}{Nh}\sum_{i=1}^{N} K\left(\frac{s-s_i}{h}\right), \tag{7.3.2}$$

where $K(\cdot)$ is the kernel function and h is the kernel bandwidth. The kernel function is taken such that $\hat{f}(s)$ is a proper density function. Usually one would take a symmetric probability density function as the kernel function, though any probability distribution functions can

be used. The kernel bandwidth h is a parameter which controls the smoothness of the kernel density estimation. When the number of samples N is large, kernel density estimation $\hat{f}(s)$ is able to approximate the true density $f(s)$ very accurately.

For multivariate case, the most common kernel is the product kernel, which is simply the product of same univariate kernels corresponding to each dimension. Suppose the data points are in d dimension, the product kernel is given as

$$\hat{f}(\mathbf{s}) = \frac{1}{Nh_1h_2\cdots h_d}\sum_{i=1}^{N}\left\{\prod_{j=1}^{d}K\left(\frac{s_j - s_{ij}}{h_j}\right)\right\}, \tag{7.3.3}$$

where $\mathbf{s}=\{s_1, s_2, \cdots, s_d\}$ is a d dimension vector, $\mathbf{s}_i=\{s_{i1}, s_{i2}, \cdots, s_{id}\}$, $i = 1, 2, \cdots, N$, are the N existing data points of dimension d, $K(\cdot)$ is a univariate kernel function, and h_j is the bandwidth for the jth dimension. It has been shown that, at least in two dimensional cases and when the distribution is uni-modal, product kernel is appropriate (Wand and Jones, 1993).

If one only wants to sample from the kernel estimate $\hat{f}(\mathbf{s})$, there is no need to evaluate equation (7.3.2) or equation (7.3.3). Suppose the existing N samples of dimension d are given as $\mathbf{s}_i=\{s_{i1}, s_{i2}, \cdots, s_{id}\}, i=1, 2, \cdots, N$. New samples following the kernel estimation of these samples, $\hat{f}(\mathrm{s})$, can be drawn directly from kernel function $K(\cdot)$, given $K(\cdot)$ is a proper distribution function, as described in Algorithm 6. This method of generating new samples from kernel estimates of existing samples is called the smoothed bootstrapping.

Algorithm 6 Data cloning using smoothed bootstrapping

1: Determine an appropriate kernel $K(u)$ and bandwidths for each dimension $h_1, h_2, \cdots, h_d$.

2: Randomly choose a sample $\mathbf{s}_i=\{s_{i1}, s_{i2}, \cdots, s_{id}\}$ from the given data-set $\{\mathbf{s}_1, \mathbf{s}_2, \cdots, \mathbf{s}_N\}$.

3: Draw a new sample $\mathbf{s}=\{s_1, s_2, \cdots, s_d\}$, where s_j are samples drawn from distribution $K\left(\frac{s-s_{ij}}{h_j}\right)$, $j=1, 2, \cdots, d$. $\mathbf{s}$ is then a sample from the kernel estimation of the original samples.

4: Repeat steps 2 and 3 until enough samples of $\mathbf{s}$ are generated.

Sequential ABC updating

Using the data cloning technique introduced above, sequential Bayesian updating using ABC simulation can be conducted. We will illustrate the method through the gamma process model. The Wilkinson's ABC method is used so that the sizing error in the data can be properly handled without performing the tedious calculations of the model likelihood.

From discussions in Section 4.3, in a gamma process model with normal sizing error, the error of the observed degradation growth of the ith component, $\Delta\mathbf{e}_i$, is a sample from a multivariate normal random variable with mean zero and covariance matrix

$$\Sigma_{\Delta\mathbf{E}_i} = 2\sigma_E^2 \begin{bmatrix} 1 & -1/2 & 0 & \cdots & 0 \\ -1/2 & 1 & -1/2 & \cdots & 0 \\ 0 & -1/2 & 1 & \cdots & 0 \\ \vdots & & \cdots & & \vdots \\ 0 & 0 & 0 & \cdots & 1 \end{bmatrix}_{m_i \times m_i},$$

where m_i is the number of elements in $\Delta\mathbf{y}_i$. Denote the parameter of the gamma process model as $\boldsymbol{\theta}$. $\boldsymbol{\theta}$ can be either the shape and scale parameters $\{\alpha, \beta\}$ or the mean and COV of the degradation $\{\mu, \nu\}$, with the latter pair recommended, because the posteriors of α and β are usually highly correlated. Combining the smoothed bootstrap method with Wilkinson's ABC method, the sequential ABC update for the gamma process model with sizing errors can be formulated as Algorithm 7.

The above sequential ABC method improves the overall efficiency of the Wilkinson's ABC method greatly by dividing the inference of a large data-set from a group of components into a series of Bayesian updates with smaller data-sets each from a single component. In addition, as the series updates continue, the prior distribution for each step (i.e., the posterior from last update) *in general* becomes closer to the final posterior, improving the acceptance rate in most cases. However, this feature of sequential updating becomes a major drawback when the number of components is large (for example, over 100 individual components). The reason is that as the number of sequential updates accumulates, the posterior samples tend to be concentrated in a small region where high posterior density is taken. If one of the remaining components happens to be an outlier and has a very

Algorithm 7 Sequential ABC using statistical data cloning

1: Set component index $i=0$ (meaning this is the prior). Generate N samples of parameter vector $\boldsymbol{\theta}$ from prior distribution $\pi(\boldsymbol{\theta})$. Denote these prior samples of the parameters as $\{\boldsymbol{\theta}_1^{(0)}, \boldsymbol{\theta}_2^{(0)}, \cdots, \boldsymbol{\theta}_N^{(0)}\}$.

2: Increase i by 1.

3: For the ith component, generate a new sample of parameter $\boldsymbol{\theta}^{(i)}$ from parameter samples $\{\boldsymbol{\theta}_1^{(i-1)}, \boldsymbol{\theta}_2^{(i-1)}, \cdots, \boldsymbol{\theta}_N^{(i-1)}\}$ updated from the $(i-1)$th component using the smoothed bootstrap method.

4: Simulate a set of true growth of the ith component $\Delta\mathbf{x}_i$ from the gamma process model using parameter $\boldsymbol{\theta}^{(i)}$ generated in step 3.

5: Accept $\boldsymbol{\theta}^{(i)}$ with probability $f_{\Delta\mathbf{E}_i}(\Delta\mathbf{y}_i - \Delta\mathbf{x}_i)$, where $f_{\Delta\mathbf{E}_i}$ is the multivariate normal density of the incremental sizing error and is given by equation (4.3.2). $\boldsymbol{\theta}^{(i)}$ is then a posterior sample of after Bayesian updating of the ith component.

6: Repeat steps 3-6 until N samples of parameters $\boldsymbol{\theta}^{(i)}$ are generated. Denote these samples as $\{\boldsymbol{\theta}_1^{(i)}, \boldsymbol{\theta}_2^{(i)}, \cdots, \boldsymbol{\theta}_N^{(i)}\}$.

7: If $i < n$, go to step 2 and perform the Bayesian update for the next component. Otherwise, go to the step 8.

8: After updating all the n component, samples $\{\boldsymbol{\theta}_1^{(n)}, \boldsymbol{\theta}_2^{(n)}, \cdots, \boldsymbol{\theta}_N^{(n)}\}$ are then the posterior samples of the model parameters.

dissimilar likelihood from the previously updated posterior, the sequential update can be "stuck" at this particular component for a very long time because of the low acceptance rate. Thus, for data-sets containing a large number of individual components, an alternative sequential update scheme using weighted samples (Smith and Gelfand, 1992) is proposed. The method is described in Algorithm 8.

In the sequential ABC updating with weighted samples, instead of drawing new samples in each step, the weights of the initial samples are updated sequentially. In each update, by choosing a more spread prior distribution $\pi_i(\boldsymbol{\theta})$, the issue of mismatch between prior distribution and likelihood function can be alleviated. However, the evaluation of the kernel density estimation is very time-consuming, compared to the data cloning. For example, if the kernel density estimation is calculated from N samples $\{\boldsymbol{\theta}_1^{(i)}, \boldsymbol{\theta}_2^{(i)}, \cdots, \boldsymbol{\theta}_N^{(i)}\}$ and one

Algorithm 8 Sequential ABC with weighted samples

1: Set the component index $i=0$. Generate M samples of parameter vector $\boldsymbol{\theta}$ from prior distribution $\pi(\boldsymbol{\theta})$. Denote this samples as $\{\boldsymbol{\theta}_1, \boldsymbol{\theta}_2, \cdots, \boldsymbol{\theta}_M\}$. For each $\boldsymbol{\theta}_j, j=1,2,\cdots,M$, assign an initial weight $w_j^{(0)}=1/M$.

2: Increase i by 1.

3: Generate N posterior samples for the ith component from an arbitrarily selected prior $\pi_i(\boldsymbol{\theta})$ and its component specific measured growth $\Delta\mathbf{y}_i$, using Wilkinson's ABC method. Denote these posterior samples as $\{\boldsymbol{\theta}_1^{(i)}, \boldsymbol{\theta}_2^{(i)}, \cdots, \boldsymbol{\theta}_N^{(i)}\}$.

4: Calculate the kernel density estimation of $\{\boldsymbol{\theta}_1^{(i)}, \boldsymbol{\theta}_2^{(i)}, \cdots, \boldsymbol{\theta}_N^{(i)}\}$, denoted as $\hat{f}_i(\boldsymbol{\theta})$. The likelihood function given the measured growth of the ith component is given as $L_i(\boldsymbol{\theta})=\hat{f}_i(\boldsymbol{\theta})/\pi_i(\boldsymbol{\theta})$.

5: Update the weight of initial M samples of $\boldsymbol{\theta}$ using equation $w_j^{(i)}=w_j^{(i-1)}L(\boldsymbol{\theta}_j), j=1,2,\cdots,M$. Normalize $w_j^{(i)}$ such that $\sum_{j=1}^{N} w_j^{(i)}=1$.

6: If $i<n$, go to step 2 and perform the Bayesian update on the weight for the next component. Otherwise, go to step 7.

7: Samples $\{\boldsymbol{\theta}_1, \boldsymbol{\theta}_2, \cdots, \boldsymbol{\theta}_M\}$ along with the updated weight $\{w_1^{(n)}, w_2^{(n)}, \cdots, w_M^{(n)}\}$ are then the weighted samples of the posterior distribution. The unweighted posterior sample can then be obtained simply by repeatedly sampling $\boldsymbol{\theta}$ from discrete distribution $\bar{P}(\boldsymbol{\theta}_i)=w_i^{(n)}$, $i=1,2,\cdots,M$, (Smith and Gelfand, 1992).

needs to evaluate this density estimation at M points $\{\boldsymbol{\theta}_1, \boldsymbol{\theta}_2, \cdots, \boldsymbol{\theta}_M\}$, the kernel function $K(\cdot)$ will have to be evaluated for $M\times N$ times, i.e., the computation complexity of the algorithm is $\mathcal{O}(M\times N)$. If normal product kernel is used, the computational complexity can be reduced to $\mathcal{O}(M+N)$ by applying the so called fast Gaussian transform (FGT) technique (Greengard and Sun, 1998). Nevertheless, the kernel density estimation is still a very computationally intensive step compared to the data cloning approach. Therefore, it is recommended to try the sequential update method with data cloning first, with a smaller N. If it is found that there are indeed outliers in the data-set, ABC method with weighted samples can then be applied.

7.3.3 Implementation

The proposed sequential ABC methods are implemented in C++. We use $\{\mu, \nu\}$ as the set of parameters for the gamma process model, because numerical examples show that μ and ν are less correlated than α and β are, which makes $\{\mu, \nu\}$ more suitable for the product kernel. In addition, if the uninformative prior is used, the joint posterior of μ and ν is similar to the uncorrelated bivariate normal distribution, which further improves the performance. An example of the posterior samples of $\{\mu, \nu\}$ and $\{\alpha, \beta\}$ inferred from the same data-set can be found in Figure 7.5 and 7.6 in Section 7.3.4.

It is known that the choice of the kernel function is much less important to the quality of the kernel density estimation than the choice the bandwidth value (Silverman, 1986). For the sake of simplicity, the normal kernel function is chosen. The use of normal kernel function also makes it possible to apply the fast Gaussian transform (FGT) to speed up the density estimation when using the weighted sample approach. The FGT in our implementation utilizes the FIGTree library developed by Morariu et al. (2008).

The choice of bandwidth is an important factor to successful kernel estimations and many advanced methods have been developed for determining the optimal kernel bandwidth. A brief survey of these methods can be reached at Jones et al. (1996). In our problem of Bayesian inference of the gamma process model, it is found that the following rule-of-thumb bandwidth (Scott, 1992) already gives satisfying results if μ and ν are used as the model parameters

$$h_j = \sigma_j \left[\frac{4}{(d+2)N} \right]^{1/(d+4)} \qquad j = 1, 2, \cdots, d, \tag{7.3.4}$$

where d the dimension, N is the number of data points, σ_j is the sample SD of the data-set in the jth dimension.

The number of parameter samples generated for each component, N, in the two proposed sequential ABC methods controls the accuracy of the data cloning and the kernel density estimation. In the case of the gamma process model, where there are only two parameters, $N = 10^4 \sim 10^5$ is already sufficiently large to produce very accurate kernel density results without introducing too much computational burden. The number of generated samples from prior distribution, M, in the weighted sample method controls the number of points

where posterior densities will be evaluated (i.e., resolution of the posterior evaluation). The only requirement for M is to have enough points in the region where high posterior density takes.

7.3.4 Application to the flow-accelerated corrosion of feeder pipes

We would like to revisit the problem of flow-accelerated corrosion (FAC) of feeder pipes which was previously discussed in Section 4.3.5, using the proposed sequential ABC method.

Prior distribution and posterior samples

In the ABC Bayesian simulation, mean μ and COV ν are used as the parameters of the gamma process model. For sake of simplicity, the uniform prior over a large rectangular region: $\mu \in (0, 0.4)$ and $\nu \in (0, 2)$. Considering the ML estimates of $\mu = 0.071$ and $\nu = 0.45$, this uniform prior should be able to cover all reasonable values for μ and ν.

First, the sequential ABC simulation using data cloning is tested using sample size $N = 10^4$. The sequential Bayesian update is successfully conducted for the first 41 feeders out the total 50 feeders, with computational time for each feeder only a few seconds. However, Bayesian update stayed at the 42th feeder for a very long time (over 30 minutes) due to the small acceptance rate.

ABC method with weighted samples is then applied, using $N = 10^5$ initial samples of parameters and $M = 2 \times 10^5$ samples for kernel density calculation. Gaussian product kernel and FGT are used for numerical evaluation of the kernel density. The kernel bandwidth is selected using equation (7.3.4). The overall calculation takes a little more than 40 minutes to finish (CPU: Intel E2700).

Figure 7.5 plots the posterior samples and the marginal histograms of μ and ν. Posterior samples of α and β can be calculated easily using the relation: $\alpha = 1/\nu^2$ and $\beta = \mu/\nu$. Posterior samples of α and β, and their corresponding marginal histograms are plotted in Figure 7.6. An obvious finding from Figure 7.6 is the large correlation between the posterior α and β.

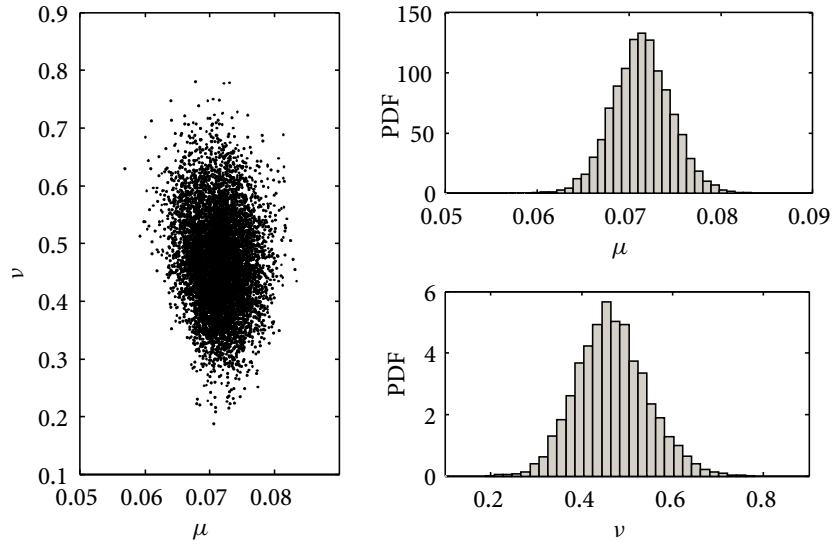

Figure 7.5 Posterior samples and marginal histograms of parameters μ and ν

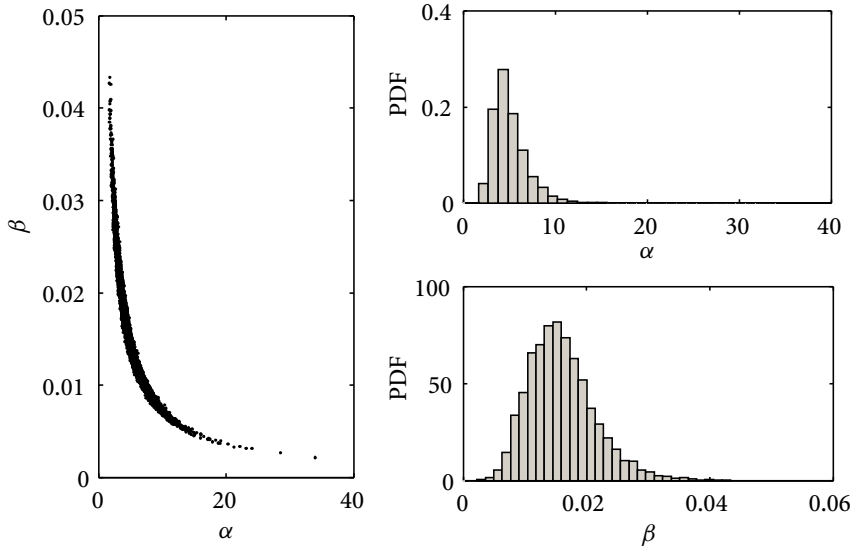

Figure 7.6 Posterior samples and marginal histograms of parameters α and β

From the posterior samples, mean and COV of the estimated parameters are obtained. The results are listed in Table 7.2 along with the results from ML estimation. Table 7.2 shows that the posterior mean of μ and ν from ABC simulation is very close to the ML estimate. This is expected since the uniform prior distribution is used. The COV of the estimated

parameters from Bayesian inference indicates the relative parameter uncertainty of the estimation, which is not provided by ML estimation. Since α and β are highly correlated, only COV of μ and ν are checked. From the table, COV of μ is very small (than 5%) and COV of ν is about 4 times larger. This indicates that the parameter uncertainty of the average flaw growth rate μ is small, but the uncertainty of the estimated COV (dispersion of the annual growth) is significant.

	α	β	μ	ν
Bayesian inference using ABC	Mean: 5.00 COV: 0.38	Mean: 0.016 COV: 0.33	Mean: 0.71 COV: 0.044	Mean: 0.47 COV: 0.166
MLE	4.89	0.015	0.071	0.45

Table 7.2 Mean and COV of the estimated parameters using Bayesian inference, compared to the MLE results

Time to failure analysis

According to previous discussions in Section 4.3.5, failure time of a specific component in the gamma process model is a random variable whose distribution depends on its current degradation and the model parameters α and β. In classical point estimation, this distribution can be calculated using equation (4.3.7) in Section 4.3.5. In Bayesian inference, the model parameters α and β themselves are also treated as random variables, which causes additional difficulties in presenting the result of failure time analysis.

One approach for easing this difficulty is to integrate out the model parameters with respect to their posterior distributions and then present the marginal distribution of the failure time. However, this method does not provide a clear distinction between the intrinsic uncertainty of the degradation growth described by the stochastic model, and the parameter uncertainty (i.e., confidence of the estimation) described by the posterior distribution. A better way is to use the probabilistic percentile (Pandey et al., 2010) which is explained below.

Denote CDF of the failure time distribution of a component as $F_T(t;\alpha,\beta)$, where α and β are random variables with joint distribution $\pi(\alpha,\beta)$. For a specific value of α and β, its lower pth percentile, T_p, can be calculated using the inverse CDF as $T_p = F_T^{-1}(p;\alpha,\beta)$, which

is a function of α and β. Since α and β are random variables, T_p is also a random variable, whose distribution can be calculated accordingly. To present the intrinsic uncertainty of degradation and the parameter uncertainty of the inference simultaneously, the probabilistic percentile $T_{p|q}$ can be used which is defined as the qth percentile of T_p. In $T_{p|q}$, p represents the percentile regarding the intrinsic uncertainty of degradation and q is the percentile regarding the parameter uncertainty. For example, the replacement time of a safety critical feeder can be determined by $T_{0.05|0.05}$, which means that there is 5% probability that the actual failure time is earlier the chosen replacement time, and the chance that this judgment is incorrect due to limited information is 5%. An illustration of the probabilistic percentile is given in Figure 7.7.

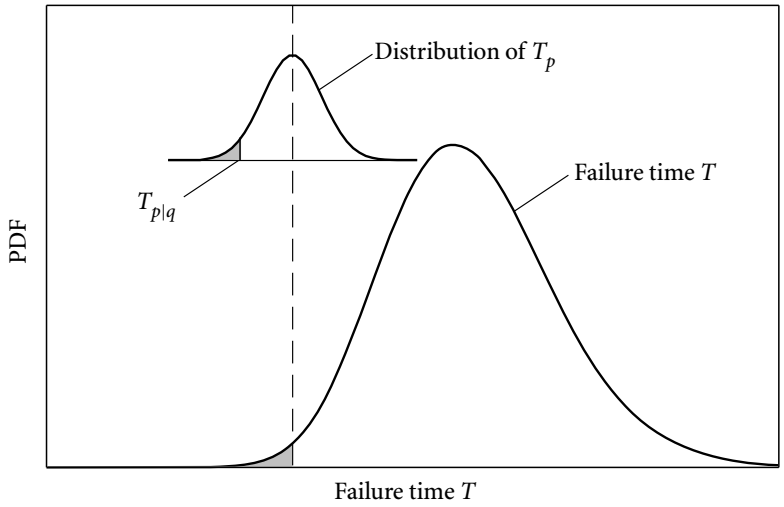

Figure 7.7 An illustration of the probabilistic percentile

Take the same feeder as in Section 4.3.5 (latest inspection at 11.5 EFPY with measured wall thickness 4.15 mm). Using posterior samples of α and β, samples of its 5% percentile of failure time $T_{0.05}$ can be calculated and the corresponding histogram is plotted in Figure 7.8. From the histogram, different probabilistic percentile of the failure time can be obtained. The results can then be used for the improved life cycle management of the feeder pipes.

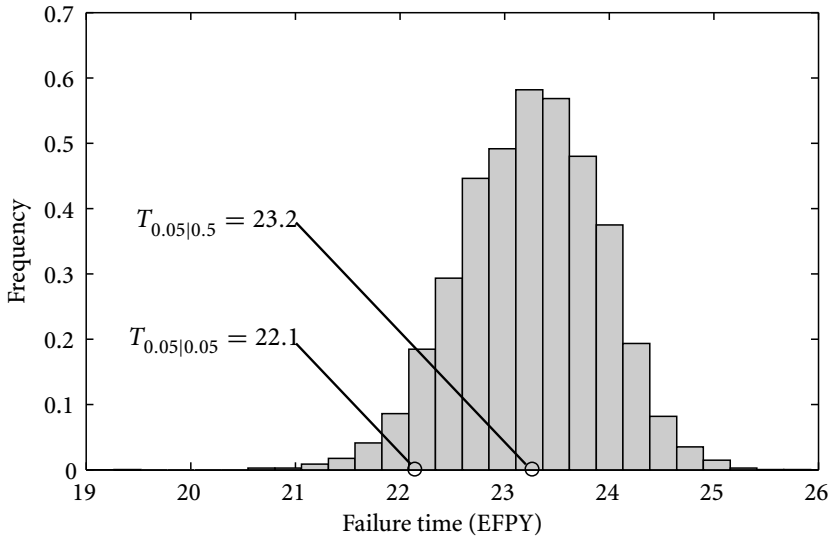

Figure 7.8 Histogram of the 5% percentile of the failure time of a selected feeder

7.4 Summary

Direct numerical evaluation of Bayesian posterior is usually very difficult, as it requires additional numerical integration and large number of likelihood evaluations. To avoid the computational difficulties, Monte Carlo simulation methods are commonly employed. Instead of calculating the value of posterior densities, Monte Carlo simulation tries to draw random samples from the posterior distribution and then use the posterior samples for subsequent probabilistic assessment.

In this chapter, two specific Monte Carlo simulation techniques, the Markov chain Monte Carlo method (MCMC) and the approximate Bayesian computation (ABC), are discussed. Based on MCMC and ABC, new algorithms for Bayesian inference of complicated stochastic degradation models, the Poisson flaw generation model with PoD and sizing error and the gamma process with sizing error, are developed. Using the proposed methods, parameter uncertainty of the estimates of these complicated stochastic models, which is not discussed in previous chapters due to numerical difficulties, can be obtained.

CHAPTER 8

Conclusions and Recommendations

8.1 Summary of results

This thesis discusses various issues arising from the parameter estimation of stochastic degradation models using uncertain inspection data. We start with the introduction of two typical inspection uncertainties, the probability of detection (PoD) and the sizing error. Probabilistic models of these two inspection uncertainties and their effects on degradation modelling are discussed briefly. Then, in Chapter 3, three common stochastic models for flaw growth and flaw generation, including the random rate model, the gamma process model and the Poisson process model, are introduced. Their definitions, properties and likelihood functions given accurate inspection data are presented.

Following that, Chapter 4 discusses the estimation of flaw growth from noisy inspection data. The random rate model and the gamma process model are considered. For the random rate model, an ML estimate of the model parameter is derived in the setting of a two-stage hierarchical model. The proposed ML method can be applied to random rate model with both zero initial degradation and uncertain initial degradation. For the gamma process model, the complete likelihood function given data with normally distributed sizing error are derived. An efficient numerical method using the Genz's transform and quasi-Monte Carlo simulation is developed for the ML estimation of the parameters. Chapter 5 discusses the estimation of Poisson flaw generation model, under the "repair-on-detection"

maintenance strategy. A simple case with only PoD included and a complete case considering both PoD and sizing error are discussed. It is found that the likelihood function for the complete case is very complicated and direct ML estimation of the model parameters is only possible for small data-sets. This computational difficulty is resolved later using an MCMC simulation method in Chapter 7.

Chapter 6 discusses the application of Bayesian inference to stochastic degradation models. The most important advantage of Bayesian inference is its ability to incorporate subjective information other than inspection data in the parameter estimation process. In addition, Bayesian method also provides a more natural way for presenting the parameter uncertainty associated with an estimate. Applications of Bayesian inference in degradation assessment are then illustrated through two practical examples. Chapter 7 investigates the computational aspects of Bayesian inference. Two simulation methods, the Markov chain Monte Carlo method (MCMC) and the approximate Bayesian computation (ABC), are introduced. Based on MCMC and ABC, new algorithms are developed for Bayesian inference of complicated stochastic models, such as the Poisson flaw generation model and the gamma process model subject to inspection uncertainties. Using Bayesian method, parameter uncertainty of the estimates, which is not discussed in previous chapters due to computational difficulties, is obtained.

Some key research contribution of the thesis are as follows:

- A statistically sound method is developed for the estimation of the random rate model from noisy measurement. The proposed method is able to handle arbitrary rate distributions and repeated inspection data properly, and can be applied to analyze flaw growth data with either zero or uncertain initial degradation

- An effective numerical method using Genz's transform and quasi-Monte Carlo simulation is developed for the ML estimate of the gamma process model using data with normally distributed sizing errors.

- Under the "repair-on-detection" maintenance strategy, likelihood function of the Poisson flaw generation model given data from repeated inspections with both PoD and

sizing error is firstly derived. An MCMC simulation using auxiliary variable method is developed for efficient parameter estimation of the model.

- First introduces the approximate Bayesian computation (ABC) to the estimation of stochastic degradation models. Using a proposed sequential ABC updating method, Bayesian inference of the gamma process model with sizing error can now be conducted efficiently.

8.2 Recommendations for future research

This thesis mainly discusses likelihood formulation and parameter estimation of stochastic degradation models using data with large inspection uncertainties. To better focus on the main objective, some simplifications are made. For example, the stochastic models discussed in the thesis do not consider the effect of exploratory variables (e.g. pressure or temperature) on the degradation. Another example is that the sizing errors in this study are all assumed to be normally distributed, which may not be realistic in some cases. Generalization of the methods developed in the thesis to more realistic stochastic models should be investigated in future.

In the stochastic modelling of flaw generation, dealing with the repeated inspections is a major difficulty for the likelihood formulation, as many details, such as whether the flaws are being tracked across inspections, or whether a previously undetected flaw will be detected in the next inspection, need to be considered. In this thesis, a relatively simple case is considered by assuming the "repair-on-detection" maintenance strategy, in which all previously detected flaws are removed or repaired. The stochastic modelling of flaw generation in various other inspection and maintenance strategies remains open.

Another promising work based on the results of this study is the model selection and validation using uncertain field data. Due to the large inspection uncertainties, specific features of degradation process can be heavily masked in field degradation data. Model selection and validation are thus difficult, especially when the model parameters are estimated using approximate methods. With the accurate ML and Bayesian estimates developed in the thesis, it is now possible to apply some sophisticated methods, such as the likelihood ratio

test, methods based on Akaike information criterion (AIC), or Bayesian factor method, to the model selection and validation using uncertain field data.

Bibliography

Mohamed Abdel-Hameed. A gamma wear process. *IEEE Transactions on Reliability*, R-24 (2):152–153, 1975.

Giorgio G. J. Achterbosch and Lech A. Grzelak. Determination of the corrosion rate of a MIC influenced pipeline using four consecutive pig runs. *ASME Conference Proceedings*, 2006(42622):209–217, January 2006.

Alfredo H-S. Ang and Wilson H. Tang. *Probability Concepts in Engineering Planning and Design*. Wiley, New York, 1975.

ASM and American Society for Metals. *ASM Handbook Volume 18: Friction, Lubrication, and Wear Technology*. ASM International, 10th edition edition, 1992.

ASTM. Guide for applying statistics to analysis of corrosion data. Standards ASTM G16-95, ASTM International, West Conshohocken, PA, 2010.

P. M Aziz. Application of the statistical theory of extreme values to the analysis of maximum pit depth data for aluminum. *Corrosion*, 12:495, 1956.

M. Beckers and A. Haegemans. Transformation of integrands for lattice rules. *Numerical Integration*, pages 329–340, 1992.

Jack R. Benjamin and Carl Allin Cornell. *Probability, Statistics, and Decision for Civil Engineers*. McGraw-Hill, New York, 1970.

Jose M. Bernardo. Reference posterior distributions for bayesian inference. *Journal of the Royal Statistical Society. Series B (Methodological)*, 41(2):113–147, 1979.

Julian Besag and Peter J. Green. Spatial statistics and bayesian computation. *Journal of the Royal Statistical Society. Series B (Methodological)*, 55(1):25–37, 1993.

Z. W. Birnbaum and S. C. Saunders. A statistical model for Life-Length of materials. *Journal of the American Statistical Association*, 53(281):151–160, 1958.

Åke Björck. *Numerical methods for least squares problems*. SIAM, 1996.

J. L. Bogdanoff and Frank Kozin. *Probabilistic Models of Cumulative Damage*. Wiley, New York, 1985.

George E. P Box and George C Tiao. *Bayesian Inference in Statistical Analysis*. Wiley, New York, 1992.

K. A. Burrill and E. L. Cheluget. Corrosion of candu outlet feeder pipes. Technical Report AECL-11965, COG-98-292-1, Atomic Energy of Canada Limited, AECL, Reactor Chemistry Branch, Chalk River Laboratories, Chalk River, Ontario, 1999.

Russel E. Caflisch. Monte carlo and Quasi-Monte carlo methods. *Acta Numerica*, 7:1–49, 1998.

Fernanado Camacho. Statistical methods for darlington steam generator tube fitness-for-service assessments. In *5th CNS International Steam Generator Conference*, Toronto, ON, Canada, November 2006.

M. B Carey and R. H Koenig. Reliability assessment based on accelerated degradation: a case study. *IEEE Transactions on Reliability*, 40(5):499–506, 1991.

R. J. Carroll. *Measurement Error in Nonlinear Models: A Modern Perspective*. Chapman & Hall/CRC, Boca Raton, FL, 2006.

George Casella. An introduction to empirical bayes data analysis. *The American Statistician*, 39(2):83–87, 1985.

G. Celeux, M. Persoz, J. N. Wandji, and F. Perrot. Using markov chain monte carlo methods to solve full bayesian modeling of PWR vessel flaw distributions. *Reliability Engineering & System Safety*, 66(3):243–252, 1999.

T. Cheng and M. D. Pandey. An accurate analysis of maintenance cost of structures experiencing stochastic degradation. *Structure and Infrastructure Engineering*, pages 1–11, 2011.

Léon Cohen. *Time-frequency Analysis*. Prentice Hall PTR, 1995.

V. Crk. Reliability assessment from degradation data. In *Reliability and Maintainability Symposium, 2000. Proceedi gs. Annual*, pages 155–161. IEEE, 2000.

Suresh V. Datla, Mikko I. Jyrkama, and Mahesh D. Pandey. Probabilistic modelling of steam generator tube pitting corrosion. *Nuclear Engineering and Design*, 238(7):1771–1778, July 2008.

Philip J. Davis and Philip Rabinowitz. *Methods of Numerical Integration: Second Edition*. Dover Publications, 2nd edition, October 2007.

Eugene Demidenko. *Mixed Models: Theory and Applications*. Wiley-IEEE, July 2004.

R.B Dooley and V.K Chexal. Flow-accelerated corrosion of pressure vessels in fossil plants. *International Journal of Pressure Vessels and Piping*, 77(2-3):85–90, February 2000.

Daniel Dufresne. Algebraic properties of beta and gamma distributions, and applications. *Advances in Applied Mathematics*, 20(3):285–299, April 1998.

Charles El-Nouty and Armelle Guillou. On the smoothed bootstrap. *Journal of Statistical Planning and Inference*, 83(1):203–220, January 2000.

GG Eldredge. Analysis of corrosion pitting by extreme value statistics and its application to oil well tubing caliper surveys. *Corrosion*, 13(1):67–76, 1957.

EPRI. Steam generator integrity assessment guidelines: revision 2. Technical Report TR-1012987, EPRI, Palo Alto, CA, 2006a.

EPRI. Technical basis for steam generator tube integrity performance acceptance standards. Technical Report 1012984, EPRI, Palo Alto, CA, 2006b.

EPRI. Least squares methods for evaluating inspection data. Technical Report 1018456, EPRI, Palo Alto, CA, 2008.

EPRI. Statistical methods for the analysis of Multiple-Inspection Flow-Accelerated corrosion data. Technical Report 1019175, EPRI, Palo Alto, CA, 2009.

ERPI. Risk informed inspection for steam generators volume 1 deterministic performance based criteria. Technical Report TR-114736, EPRI, Palo Alto, CA, 2000.

L. Fenyvesi, H. Lu, and TR Jack. Prediction of corrosion defect growth on operating pipelines. In *2004 International Pipeline Conference (IPC2004)*, Calgary, Alberta, Canada, November 2004.

Wayne A Fuller. *Measurement Error Models*. Wiley, New York, 1987.

Luca Gandossi and Charles Annis. Probability of detection curves: Statistical Best-Practices. Technical report, the European Network for Inspection and Qualification (ENIQ), 2010.

R Ganesan. A stochastic modelling and analysis methodology for quantification of fatigue damage. *Computer Methods in Applied Mechanics and Engineering*, 190(8-10):1005–1019, November 2000.

Andrew Gelman. *Bayesian Data Analysis*. Chapman & Hall/CRC, 2004.

Stuart Geman and Donald Geman. Stochastic relaxation, gibbs distributions, and the bayesian restoration of images. *IEEE Transactions on Pattern Analysis and Machine Intelligence*, PAMI(6):721–741, November 1984.

Alan Genz. Numerical computation of multivariate normal probabilities. *Journal of Computational and Graphical Statistics*, 1(2):141–149, June 1992.

I.B. Gertsbakh and Kordonskiy. *Models of Failure*. Springer, June 1969.

W. R. Gilks, S. Richardson, and D. J. Spiegelhalter. *Markov Chain Monte Carlo in Practice*. Chapman & Hall/CRC, 1996a.

W.R. Gilks, S. Richardson, and D.J. Spiegelhalter. Introducing markov chain monte carlo. *Markov chain Monte Carlo in practice*, pages 1–19, 1996b.

J.E. Gray and S.R. Addison. Characteristic functions in radar and sonar. In *System Theory, 2002. Proceedings of the Thirty-Fourth Southeastern Symposium on*, pages 31–35, 2002.

L. Greengard and X. Sun. A new version of the fast gauss transform. *Documenta Mathematica*, 3:575–584, 1998.

E.J. Gumbel and J. Lieblein. *Statistical Theory of Extreme Values and Some Practical Applications-A Series of Lectures.* Govt. Print. Off., 1954.

Arjun K. Gupta, Wei-Bin Zeng, and Yanhong Wu. *Probability and Statistical Models: Foundations for Problems in Reliability and Financial Mathematics*. Springer, New York, August 2010.

J. H Halton. Radical-inverse quasi-random point sequence. *Commun. ACM*, 7(12):701–702, December 1964. ACM ID: 365104.

H. P. Hong. Application of the stochastic process to pitting corrosion. *Corrosion*, 55(01), 1999.

HSE. RR454 -Probability of detection (PoD) curves derivation, applications and limitations. Report, Health and Safety Executive, 2006.

L. Huyse and A. van Roodselaar. Effects of inline inspection sizing uncertainties on the accuracy of the largest features and corrosion rate statistics. In *2010 8th International Pipeline Conference (IPC2010)*, Calgary, Alberta, Canada, September 2010.

E. T Jaynes. Prior probabilities. *IEEE Transactions on Systems Science and Cybernetics*, 4(3): 227–241, September 1968.

H. Jeffreys. *Theory of Probability*. Oxford University Press, 1961.

Jiming Jiang. *Linear and Generalized Linear Mixed Models and Their Applications*. Springer, 1 edition, March 2007.

M. C. Jones, J. S. Marron, and S. J. Sheather. A brief survey of bandwidth selection for density estimation. *Journal of the American Statistical Association*, 91(433):401–407, March 1996.

M. J. Kallen and J. M. van Noortwijk. Optimal maintenance decisions under imperfect inspection. *Reliability Engineering and System Safety*, 90(2-3):177–185, 2005.

R.E. Kass and L. Wasserman. Formal rules for selecting prior distributions: A review and annotated bibliography. *J. Amer. Statist. Assoc*, 91:343–1370, 1996.

Dong-Goo Kim and Young-Ze Lee. Experimental investigation on sliding and fretting wear of steam generator tube materials. *Wear*, 250(1-12):673–680, October 2001.

Armen Der Kiureghian and Ove Ditlevsen. Aleatory or epistemic? does it matter? *Structural Safety*, 31(2):105–112, 2009.

S. P. Kuniewski and J. M. van Noortwijk. Sampling inspection for the evaluation of time-dependent reliability of deteriorating structures. *Reliability Engineering and System Safety*, 2009.

R. J. Kurtz, R. A. Clark, E. R. Bradley, W. M. Bowen, P. G. Doctor, R. H. Ferris, and F. A. Simonen. Steam generator tube integrity Program/Steam generator group project. Technical report, Nuclear Regulatory Commission, Washington DC, 1990.

R. J Kurtz, P. G Heasler, and C. M Anderson. Performance demonstration tests for eddy current inspection of steam generator tubing. Technical report, US NRC, May 1996.

Jerry Lawless and Martin Crowder. Covariates and random effects in a gamma process model with application to degradation and failure. *Lifetime Data Analysis*, 10(3):213–227, 2004.

D. V. Lindley. *Introduction to Probability and Statistics from a Bayesian Viewpoint*. University Press, 1965.

C. Joseph Lu and William Q. Meeker. Using degradation measures to estimate a Time-to-Failure distribution. *Technometrics*, 35(2):161–174, May 1993.

S. Madanat and W.H.W. Ibrahim. Poisson regression models of infrastructure transition probabilities. *Journal of Transportation Engineering*, 121:267, 1995.

S. Madanat, R. Mishalani, and W. H. W. Ibrahim. Estimation of infrastructure transition probabilities from condition rating data. *Journal of Infrastructure Systems*, 1(2):120–125, 1995.

Jean-Michel Marin, Pierre Pudlo, Christian P Robert, and Robin Ryder. Approximate bayesian computational methods. *1101.0955*, January 2011.

Paul Marjoram, John Molitor, Vincent Plagnol, and Simon TavarÃ©. Markov chain monte carlo without likelihoods. *Proceedings of the National Academy of Sciences*, 100(26):15324 –15328, December 2003.

AT Martinsek. Reliable inference for the maximum pit depth within pitting colonies on long pipelines. *Corrosion*, 59(12), 2003.

T.P. McAllister and B.R. Ellingwood. Reliability-based condition assessment of welded miter gate structures. *Journal of Infrastructure Systems*, 7:95, 2001.

T. Micevski, G. Kuczera, and P. Coombes. Markov model for storm water pipe deterioration. *Journal of Infrastructure Systems*, 8:49, 2002.

V. I Morariu, B. V Srinivasan, V. C Raykar, R. Duraiswami, and L. Davis. Automatic online tuning for fast gaussian summation. *Advances in Neural Information Processing Systems*, 2008.

J.A. Nelder and R. Mead. A simplex method for function minimization. *The computer journal*, 7(4):308, 1965.

M. Nessim, J. Dawson, R. Mora, and S. Hassanein. Obtaining corrosion growth rates from repeat In-Line inspection runs and dealing with the measurement uncertainties. In *2008 7th International Pipeline Conference (IPC2008)*, Calgary, Alberta, Canada, September 2008.

Robin P. Nicolai, Rommert Dekker, and Jan M. van Noortwijk. A comparison of models for measurable deterioration: An application to coatings on steel structures. *Reliability Engineering & System Safety*, 92(12):1635–1650, December 2007.

H. Niederreiter. *Random Number Generation and Quasi-Monte Carlo Methods*. Society for Industrial and Applied Mathematics, Philadelphia, Pennsylvania, 1992.

L. Obrutsky, J. Renaud, and R. Lakhan. Steam generator inspections: Faster, cheaper and better, are we there yet? In *IV Conferencia Panamericana de END Buenos Aires*, Buenos Aires, Argentina, October 2007.

L. Obrutsky, J. Renaud, and R. Lakhan. Overview of steam generator Tube-Inspection technology. In *NDT in Canada 2009 National Conference*, London, ON, Canada, 2009.

M. D. Pandey, X. X. Yuan, and J. M. van Noortwijk. The influence of temporal uncertainty of deterioration in life-cycle management of structures. *Structure and Infrastructure Engineering*, 5(2), 2006.

M. D. Pandey, D. Lu, and D. Komljenovic. The impact of probabilistic modeling in Life-Cycle management of nuclear piping systems. *Journal of Engineering for Gas Turbines and Power*, 133(1):012901–7, January 2011.

M.D. Pandey, M. Wang, and G.A. Bickel. A probabilistic approach to update lower bound threshold stress intensity factor (KIH) for delayed hydride cracking. *Nuclear Engineering and Design*, 240(10):2682–2690, October 2010.

P.C. Paris, M.P. Gomez, and W.E. Anderson. A rational analytic theory of fatigue. *Trend Engng*, page 13, 1961.

Emanuel Parzen. *Stochastic processes*. Holden-Day, 1967.

N. U Prabhu. *Stochastic Processes: Basic Theory and Its Applications*. World Scientific, Hackensack, NJ, 2007.

Singiresu S. Rao and S. S. Rao. *Engineering Optimization: Theory and Practice*. John Wiley and Sons, Hoboken, NJ, July 2009.

Christian P Robert. *The Bayesian Choice: A Decision-Theoretic Motivation*. Springer texts in statistics. Springer-Verlag, New York, 1994.

G.O. Roberts. Markov chain concepts related to sampling algorithms. *Markov Chain Monte Carlo in Practice*, 57, 1996.

ES Rodriguez. Part II: development of a general failure control system for estimating the reliability of deteriorating structures. *Corrosion*, 45(3):193–206, 1989.

Jeffrey S Rosenthal. Optimal proposal distributions and adaptive MCMC. In *MCMC Handbook*. Chapman and Hall/CRC Press, 2009.

L. J. Savage. *The Foundations of Statistics*. Dover Publications, 1972.

P. A. Scarf, R. A. Cottis, and P. J. Laycock. Extrapolation of extreme pit depths in space and time using the r deepest pit depths. *Journal of The Electrochemical Society*, 139(9): 2621–2627, 1992.

David W. Scott. *Multivariate Density Estimation: Theory, Practice, and Visualization*. Wiley-Interscience, 1992.

G. Shakhnarovich, R. El-Yaniv, and Y. Baram. Smoothed bootstrap and statistical data cloning for classifier evaluation. In *Machine Learning-International Workshop and Conference*, pages 521–528, 2001.

T. Shibata. Whitney award lecture: Statistical and stochastic approaches to localized corrosion. *Corrosion Science*, 52:813–830, 1996.

Bernard. W. Silverman. *Density Estimation for Statistics and Data Analysis*. Chapman and Hall/CRC, 1 edition, April 1986.

Kaisa Simola and Urho Pulkkinen. Models for non-destructive inspection data. *Reliability Engineering & System Safety*, 60(1):1–12, April 1998.

N. Singpurwalla. Gamma processes and their generalizations: an overview. *Engineering Probabilistic Design and Maintenance for Flood Protection*, page 67–75, 1997.

S. A. Sisson, Y. Fan, and Mark M. Tanaka. Sequential monte carlo without likelihoods. *Proceedings of the National Academy of Sciences*, 104(6):1760 –1765, February 2007.

Nathan O. Siu and Dana L. Kelly. Bayesian parameter estimation in probabilistic risk assessment. *Reliability Engineering & System Safety*, 62(1-2):89–116, October 1998.

A. F. M. Smith and A. E. Gelfand. Bayesian statistics without tears: A Sampling-Resampling perspective. *The American Statistician*, 46(2):84–88, May 1992.

I. M Sobol. On the distribution of points in a cube and the approximate evaluation of integrals. *Zhurnal Vychislitelnoi Matematiki i Matematicheskoi Fiziki*, 7(4):784–802, 1967.

S. P. Sullivan, V. S. Cecco, L. S. Obrutsky, J. R. Lakhan, and A. H. Park. Validating eddy current array probes for inspecting steam generator tubes. In *Proceedings of the Joint EC OECD IAEA Specialists Meeting*, Petten, 1997.

S. Tavare, D. J Balding, R. C. Griffiths, and P. Donnelly. Inferring coalescence times from DNA sequence data. *Genetics*, 145(2):505, 1997.

L. Tierney. Introduction to general state-space markov chain theory. *Markov Chain Monte Carlo in Practice*, pages 59–74, 1996.

Luke Tierney. Markov chains for exploring posterior distributions. *The Annals of Statistics*, 22(4):1701–1728, December 1994.

Tina Toni, David Welch, Natalja Strelkowa, Andreas Ipsen, and Michael P.H Stumpf. Approximate bayesian computation scheme for parameter inference and model selection in dynamical systems. *Journal of The Royal Society Interface*, 6(31):187 –202, February 2009.

A. Valor, F. Caleyo, L. Alfonso, D. Rivas, and J.M. Hallen. Stochastic modeling of pitting corrosion: A new model for initiation and growth of multiple corrosion pits. *Corrosion Science*, 49(2):559–579, February 2007.

J.M. van Noortwijk. A survey of the application of gamma processes in maintenance. *Reliability Engineering & System Safety*, 94(1):2–21, January 2009.

J.M van Noortwijk and H.E Klatter. Optimal inspection decisions for the block mats of the Eastern-Scheldt barrier. *Reliability Engineering & System Safety*, 65(3):203–211, September 1999.

J.M. Van Noortwijk, R.M. Cooke, and M. Kok. A Bayesian failure model based on isotropic deterioration. *European Journal of Operational Research*, 82(2):270–282, 1995.

M. P. Wand and M. C. Jones. Comparison of smoothing parameterizations in bivariate kernel density estimation. *Journal of the American Statistical Association*, 88(422):520–528, June 1993.

Sanford Weisberg. *Applied Linear Regression*. John Wiley and Sons, 2005.

G. A. Whitmore. Estimating degradation by a wiener diffusion process subject to measurement error. *Lifetime Data Analysis*, 1(3):307–319, 1995.

Richard D Wilkinson. Approximate bayesian computation (ABC) gives exact results under the assumption of model error. *0811.3355*, November 2008.

D. E. Williams, C. Westcott, and M. Fleischmann. Stochastic models of pitting corrosion of stainless steels. *Journal of The Electrochemical Society*, 132(8):1804–1811, 1985.

WF Wu and CC Ni. A study of stochastic fatigue crack growth modeling through experimental data. *Probabilistic Engineering Mechanics*, 18(2):107–118, 2003.

Wei-Chau Xie. *Dynamic Stability of Structures*. Cambridge University Press, New York, 2006.

JN Yang and SD Manning. A simple second order approximation for stochastic crack growth analysis. *Engineering Fracture Mechanics*, 53(5):677–686, 1996.

X. X. Yuan. *Stochastic Modeling of Deterioration in Nuclear Power Plant Components*. Ph.D. thesis, University of Waterloo, Waterloo, Ont., 2007.

X. X. Yuan, M. D. Pandey, and G. A. Bickel. A probabilistic model of wall thinning in CANDU feeders due to flow-accelerated corrosion. *Nuclear Engineering and Design*, 238(1):16–24, 2008.

X.-X. Yuan, D. Mao, and M.D. Pandey. A bayesian approach to modeling and predicting pitting flaws in steam generator tubes. *Reliability Engineering & System Safety*, 94(11): 1838–1847, November 2009.

APPENDIX A

A.1 Genz's transform

Likelihood function of the gamma process model subject to normally distributed sizing error can be transformed into an integral over a hyper-cubic region using a series of transforms proposed by Genz (1992). Take the 2-dimension case as an example. Without causing confusion, we omit the symbol Δ and the subscript i in the equations. The likelihood function is then written

$$\begin{aligned} f_{\mathbf{Y}}(\mathbf{y}) &= \int_D f_{\mathbf{X}}(\mathbf{y}-\mathbf{e}) f_{\mathbf{E}}(\mathbf{e}) \mathrm{d}\mathbf{e} \\ &= \int_{-\infty}^{y_2}\int_{-\infty}^{y_1} f_{X_1}(y_1-e_1) f_{X_2}(y_2-e_2) f_{\mathbf{E}}(e_1,e_2)\mathrm{d}e_1\mathrm{d}e_2, \end{aligned} \tag{A.1.1}$$

where X_1 and X_2 are independent and gamma distributed random variables. Here the model parameters α and β in f_{X_1} and f_{X_2} are omitted, $\mathbf{y}=\{y_1,y_2\}^T$ is the measured growth with sizing errors and $\mathbf{e}=\{e_1,e_2\}^T$ is the sizing error associated with $\mathbf{y}$. Let $\mathbf{E}=\{E_1,E_2\}^T$ be the joint distribution for the sizing error $\mathbf{e}$. The mean of $\mathbf{E}$ is zero and its covariance matrix is

$$\Sigma_{\mathbf{E}} = 2\sigma_E^2 \begin{bmatrix} 1 & -1/2 \\ -1/2 & 1 \end{bmatrix}.$$

The likelihood function is then given as

$$f_{\mathbf{Y}}(\mathbf{y}) = \int_{-\infty}^{y_2}\int_{-\infty}^{y_1} f_{X_1}(y_1-e_1) f_{X_2}(y_2-e_2) \frac{1}{2\pi\sqrt{|\Sigma_{\mathbf{E}}|}} \exp\left(-\mathbf{e}\Sigma_{\mathbf{E}}^{-1}\mathbf{e}^T\right) \mathrm{d}e_1\mathrm{d}e_2.$$

Then Genz's transform can be conducted using following steps

- Calculate the Cholesky decomposition of $\Sigma_{\mathbf{E}}$, i.e., find a lower triangular matrix C such that $\Sigma_{\mathbf{E}_i} = CC^T$. This can be done easily using routines provided in many numerical packages. For the 2-dimension case, C is calculated as

$$C = \sqrt{2}\sigma_E \begin{bmatrix} 1 & 0 \\ -0.5 & 0.86 \end{bmatrix}.$$

- Apply the first transform $\mathbf{e} = \mathbf{p}C^T$ to equation (A.1.1), where $\mathbf{p} = \{p_1, p_2\}^T$ is a 2-dimension vector. Expanding $\mathbf{e} = \mathbf{p}C^T$ gives $e_1 = \sqrt{2}\sigma_E p_1$ and $e_2 = \sqrt{2}\sigma_E(-0.5p_1 + 0.86p_2)$. Also according to the definition of Cholesky decomposition, one has

$$\mathbf{e}\Sigma_{\mathbf{E}}^{-1}\mathbf{e}^T = \mathbf{p}C^T C^{T^{-1}} C^{-1} C\mathbf{p}^T = \mathbf{p}\mathbf{p}^T.$$

Thus, after applying the first transform, the equation (A.1.1) becomes

$$\begin{aligned} f_{\mathbf{Y}}(\mathbf{y}) &= \int_{-\infty}^{a_2}\int_{-\infty}^{a_1} f_{X_1}(y_1 - \sqrt{2}\sigma_E p_1) f_{X_2}\left(y_2 - \sqrt{2}\sigma_E(0.5p_1 - 0.86p_2)\right) \\ &\qquad \frac{1}{2\pi\sqrt{|\Sigma_{\mathbf{E}}|}} \exp\left(-\frac{1}{2}\mathbf{p}\mathbf{p}^T\right)\left|\frac{\partial \mathbf{e}}{\partial \mathbf{p}}\right| \mathrm{d}p_1 \mathrm{d}p_2 \\ &= \int_{-\infty}^{a_2}\int_{-\infty}^{a_1} f_{X_1}(y_1 - \sqrt{2}\sigma_E p_1) f_{X_2}\left(y_2 - \sqrt{2}\sigma_E(0.5p_1 - 0.86p_2)\right) \\ &\qquad \frac{1}{2\pi|C|} \exp\left(-\frac{1}{2}(p_1^2 + p_2^2)\right)|C|\mathrm{d}p_1\mathrm{d}p_2 \\ &= \frac{1}{2\pi}\int_{-\infty}^{a_2}\int_{-\infty}^{a_1} m(p_1, p_2)\mathrm{d}p_1\mathrm{d}p_2, \end{aligned} \tag{A.1.2}$$

where $m(p_1, p_2)$ is a function of p_1 and p_2 given by

$$\begin{aligned} m(p_1, p_2) = f_{X_1}(y_1 - \sqrt{2}\sigma_E p_1) f_{X_2}\left(y_2 - \sqrt{2}\sigma_E(0.5p_1 - 0.86p_2)\right) \\ \exp\left(-\frac{1}{2}(p_1^2 + p_2^2)\right), \end{aligned}$$

$\mathbf{a} = \{a_1, a_2\}$ is the integration upper bound and is a function of p_1 and p_2. $\mathbf{a}$ can be obtained by letting the two integration regions $\mathbf{e} \leqslant \mathbf{y}$ and $\mathbf{p} \leqslant \mathbf{a}$ identical. Because C is a triangular matrix, $\mathbf{a}$ be calculated recursively starting from a_1. The result is given as $a_1 = y_1/(\sqrt{2}\sigma_E)$ and $a_2 = (y_2 + 0.5p_1)/(0.86\sqrt{2}\sigma_E)$.

- The next step is to apply transform $p_i = \Phi^{-1}(q_i)$, $i = 1, 2$, to equation (A.1.2), where $\Phi^{-1}(q_i)$ is the inverse cumulative density function of the standard normal distribution, i.e., $\Phi(q_i) = \frac{1}{\sqrt{2\pi}} \int_{-\infty}^{q_i} \exp(-u^2/2)\mathrm{d}u$. After applying inserting $p_i = \Phi^{-1}(q_i)$, equation (A.1.2) becomes

$$\begin{aligned} f_{\mathbf{Y}}(\mathbf{y}) &= \frac{1}{2\pi} \int_0^{b_2} \int_0^{b_1} m\left[\Phi^{-1}(q_1), \Phi^{-1}(q_2)\right] \mathrm{d}\Phi^{-1}(q_1)\mathrm{d}\Phi^{-1}(q_2) \\ &= \int_0^{b_2} \int_0^{b_1} n(q_1, q_2)\mathrm{d}q_1\mathrm{d}q_2, \end{aligned} \tag{A.1.3}$$

  where $n(q_1, q_2) = \frac{1}{2\pi} m\left[\Phi^{-1}(q_1), \Phi^{-1}(q_2)\right] \Phi^{-1'}(q_1)\Phi^{-1'}(q_2)$, b_1 and b_2 are the integration upper bound given as (note that b_2 is a function of q_1)

$$\begin{aligned} b_1 &= \Phi(a_1) = \Phi(y_1) \\ b_2 &= \Phi(a_2) = \Phi((y_2 + 0.5p_1)/(0.86\sqrt{2}\sigma_E)) \\ &= \Phi((y_2 + 0.5\Phi^{-1}(q_1))/(0.86\sqrt{2}\sigma_E)). \end{aligned}$$

- Finally, let $q_i = b_i s_i$, $i = 1, 2$. Since b_2 is a function of q_1, it is needed to express b_2 in terms of s_1 and s_2, so that the integral after transform can be evaluated. From relation $q_1 = b_1 s_1$, one has

$$\begin{aligned} b_2 &= \Phi((y_2 + 0.5\Phi^{-1}(q_1))/(0.86\sqrt{2}\sigma_E)) \\ &= \Phi((y_2 + 0.5\Phi^{-1}(b_1 s_1))/(0.86\sqrt{2}\sigma_E)) \\ &= \Phi((y_2 + 0.5\Phi^{-1}(\Phi(y_1)s_1))/(0.86\sqrt{2}\sigma_E)). \end{aligned}$$

  Equation (A.1.3) is then transformed into an integral over a unit region as

$$f_{\mathbf{Y}}(\mathbf{y}) = \int_0^1 \int_0^1 n(b_1 s_1, b_2 s_2) b_1 b_2 \mathrm{d}s_1 \mathrm{d}s_2,$$

  where $b_1 = \Phi(y_1)$ and $b_2 = \Phi((y_2 + 0.5\Phi^{-1}(\Phi(y_1)s_1))/(0.86\sqrt{2}\sigma_E))$.

Using the above Genz's transform, the original likelihood function, which is an integral over an infinite region, is converted into an equivalent integral over a unit rectangular. Denote the converted integrand as $p(s_1, s_2)$, $p(s_1, s_2) = n(b_1 s_1, b_2 s_2) b_1 b_2$. To evaluate equation A.1 using QMC simulation, one first generates a 2-dimension LDS of s_1 and s_2,

denoted as $\{s_1^{(1)}, s_1^{(2)}, \cdots, s_1^{(N)}\}$ and $\{s_2^{(1)}, s_2^{(2)}, \cdots, s_2^{(N)}\}$, over the unit integration region. Equation A.1 can then be calculated as the following average as

$$f_{\mathbf{Y}}(\mathbf{y}) \approx \frac{1}{N} \sum_{i=1}^{N} p(s_1^{(i)}, s_2^{(i)}).$$

When conducting the maximum likelihood estimation of the model, equation A.1 needs to be calculated repeatedly with respect to different values of model parameters α and β. As can be observed from the above procedures, the converted integrand after Genz's transform is very complicated and involves large number of numerically expensive calculations such as the inverse normal CDF Φ^{-1} and its derivative $\Phi^{-1'}$. Since in QMC simulation the generated sequences are identical for each evaluation, much of these difficult calculations only need to be conducted once and the results can be stored for later use.

A.2 Simulating flaw generation data

Suppose the flaw initiation in a component follows a homogeneous Poisson process with rate λ. The flaw sizes are assumed to be *i.i.d.* distributed with PDF $f_X(x;\theta)$. The flaws are considered to be stable. That is the flaw size does not grow with time. n inspections are conducted at time $t_1, t_2, \cdots, t_n$ using inspection probe with PoD $p(x)$ and sizing error with PDF $f_E(e)$. After each inspection, all the detected flaws are removed to mimic a "repair-on-detection" maintenance strategy. The number of detected flaws and their measured flaw sizes can be simulated using the following procedures iteratively.

- At time $t_0 = 0$, there are no flaws in the component.
- Suppose at the $(i-1)$th inspection at time t_{i-1}, there are s_{i-1} flaws left after the repair with true flaw size $\{u_1^{(i-1)}, u_2^{(i-1)}, \cdots, u_{s_{i-1}}^{(i-1)}\}$.
- Simulate k_i new generated flaws with size $\{x_1^{(i)}, x_2^{(i)}, \cdots, x_{k_i}^{(i)}\}$, where k_i is a sample from Poisson random variable with rate $\lambda(t_i - t_{i-1})$, $\{x_1^{(i)}, x_2^{(i)}, \cdots, x_{k_i}^{(i)}\}$ are samples drawn from PDF $f_X(x;\theta)$. Then, $\{u_1^{(i-1)}, u_2^{(i-1)}, \cdots, u_{s_{i-1}}^{(i-1)}, x_1^{(i)}, x_2^{(i)}, \cdots, x_{k_i}^{(i)}\}$ are the size of the flaws before the ith inspection.
- For each flaw in $\{u_1^{(i-1)}, u_2^{(i-1)}, \cdots, u_{s_{i-1}}^{(i-1)}, x_1^{(i)}, x_2^{(i)}, \cdots, x_{k_i}^{(i)}\}$, simulate a random number q from uniform distribution on 0 and 1 $U(0,1)$. If $q \leqslant p(x)$, where x is its size,

the flaw is regarded as detected. Otherwise, the flaw is not detected. Denote the detected flaws as $\{d_1^{(i)}, d_2, \cdots, d_{r_i}^{(i)}\}$ and the undetected flaws as $\{u_1^{(i)}, u_2^{(i)}, \cdots, u_{s_i}^{(i)}\}$. $r_i + s_i = s_{i-1} + k_i$. $\{u_1^{(i)}, x_2^{(i)}, \cdots, u_{s_i}^{(i)}\}$ are then the undetected flaws in the ith inspection.

- For the r_i detected flaws, simulate r_i sizing errors from $f_E(e)$ as $\{e_1^{(i)}, e_2^{(i)}, \cdots, e_{r_i}^{(i)}\}$. The measured flaw sizes are then $y_j^{(i)} = d_j^{(i)} + e_j^{(i)}$. r_i and $\{y_1^{(i)}, y_2^{(i)}, \cdots, y_{r_i}^{(i)}\}$ are then the simulated number and size of the detected flaws in the ith inspection.